



OSLO METROPOLITAN UNIVERSITY
STORBYUNIVERSITETET

OsloMet – Oslo Metropolitan University
Department of Civil Engineering and Energy Technology
Energy and Environment in buildings
Mailing address: PB 4 St. Olavs plass, N-0130 Oslo, Norway
Street address: Pilestredet 35, Oslo

Phone: 67 23 50 00
www.oslomet.no

| |
|---------------------------|
| Group/Candidate No. 13 |
|---------------------------|

| |
|----------------------|
| AVAILABILITY Open |
|----------------------|

MASTER'S THESIS

| | |
|--|--|
| TITLE Experimental and numerical studies on thermal performance and optimization of night ventilation strategies for improvement of cooling energy performance in office cubicles with PCM-enhanced spackling | DATE 15.06.2020 |
| | NUMBER OF PAGES/ATTACHEMENTS 80 / 2 |
| AUTHOR Andreas Aamodt | SUPERVISOR Tor Arvid Vik Habtamu Bayera Madessa Arnab Chaudhuri |
| DONE IN COLLABORATION WITH Gyproc Saint-Gobain, Sweden AB | CONTACT +47 99 39 63 66 |

ABSTRACT
PCM enhanced wallboards on internal surfaces of building spaces is an attractive solution for improvement of thermal performance in buildings. This work deals with using a novel spackling compound as a primer coating material, from Gyproc Saint-Gobain, Sweden AB, in the inner walls of building envelopes for passive cooling and thermal comfort management. Experimental studies in an office cubicle showed the material to increase the thermal inertia of the environment and cause for a reduction in the indoor air temperature development throughout the hot period of the day. An office building with multiple single celled cubicles was modelled to investigate the PCM spackle in a larger scale environment with dynamic climate during the summer season in Oslo. A natural and a hybrid night night ventilation strategy was designed and optimal air flow rates was determined to ensure good performance with the PCM spackle to provide passive cooling. It was found that the night ventilation strategies were effective and the PCM spackle further improved the thermal behaviour of the building to significantly reduce the cooling load and energy consumption needed for cooling to meet thermal comfort criterias.

| |
|---------------------|
| 3 KEYWORDS |
| PCM |
| Cooling performance |
| Energy reduction |

Project description

Today, we are faced with an acute climate crisis due to global warming. Most countries have committed to the Paris Agreement by UN to pursue efforts to limit the extent of global average temperature rise.

Buildings and the building sector as a whole are today responsible for over 30% of the worlds total energy demand, and 40% of direct and indirect CO₂ emissions. The International Energy Agency (IEA) describes this sector to be a source of enormous untapped potential of energy efficiency. The energy demand of the building sector is swiftly rising as growth in living standards around the world leads to an increase and development of new and existing building mass. In buildings, heating and cooling measures expends 60% of the total energy consumption, where energy usage for cooling is the sole area of most rapid development as the demand increases. The IEA concludes that *"Growing demand for air conditioners is one of the most critical blind spots in today's energy debate. Setting higher efficiency standards for cooling is one of the easiest steps governments can take to reduce the need for new power plants, cut emissions and reduce costs at the same time."*

Gyproc Saint-Gobain, Sweden AB has developed a new building material in which a spackle compound composed of different binding materials and microencapsulated PCM (phase changing materials) can increase the thermal inertia of a building by a relatively substantial amount. By increasing the thermal inertia, the building becomes more resistant to changes in indoor temperatures, which in turn can reduce the need and energy required to cool the indoor environment for better thermal comfort. Recent years advancements in material sciences have excited an interest for further study and development of PCM applied in building materials, as they can prove to be an auspicious contributor to the solutions needed to improve energy efficiency of buildings and reduce the worlds energy consumption.

Problem statement

In collaboration with Gyproc, OsloMet is supplied with the material which we are to study and analyze. This thesis will explore the following research questions:

1. How does the PCM spackle affect the indoor temperature in a realistic summer environment?
2. What is the PCM spackles thermal conductivity, and are there issues in achieving full phase change cycles with the material?
3. How can the PCM spackle be most efficiently utilized in a large scale building, and how much energy savings potential can be expected?

Summary

This study set out to investigate how a novel spackle material enhanced with microencapsulated PCM could improve thermal behaviour and cooling energy performance in office buildings in Oslo during the summer season. This was analyzed both experimentally and with numerical simulations. The studied application of the material was in the range of 2 – 4 mm on walls and ceiling surfaces in office cubicles. The results showed that although being applied only in thin layers it gave a significant boost to the thermal inertia of the environment, slowing down and reducing the indoor temperature development throughout the hot period of the day. This leads to better thermal comfort of the occupants by reducing the operative temperature, and also benefits the cooling load and energy consumption needed to maintain thermal comfort requirements.

In the experiment, the PCM spackle was applied at $\approx 2\text{mm}$ in an emulated office cubicle. A peak air temperature reduction of 1.1 K, and a maximum reduction of 1.3 K occurring early afternoon was observed. It was observed that melting of the PCM started at surface temperatures of $\approx 19.5^\circ\text{C}$ and had a peak performance between $\approx 23.5 - 24.5^\circ\text{C}$.

The numerical model was validated with $CV_{RMSE} = 1.12\%$. An office building with multiple single celled cubicles was simulated to analyze the PCM spackle in a larger scale environment and dynamic climate conditions. A natural and a hybrid night ventilation strategy was designed and optimized for energy savings potential. The PCM spackle at 2 mm and 4 mm application in each cubicle could contribute to 14% and 21% additional energy savings for local cooling, respectively. These numbers were in addition to the very effective night ventilation strategies which boosted the total energy savings to 25–95% at air flow rates during night ventilation of 0.5 – 5 ACH. However, going beyond 3 ACH gave diminishing returns in energy savings and it was determined to be the optimal air flow rate. Considering the total change in delivered energy to the building, it was found that energy savings started to decrease from 3 ACH and on wards for the hybrid night ventilation due to increasing energy consumption by fans. Moreover, the PCM spackle could also cause for a $\approx 1.1 - 1.9\text{K}$ reduction in the operative temperature, and ≈ 1 hour delay of the peak temperature in comparison to the night ventilation alone. This effect showed potential for the PCM spackle to significantly reduce the cooling power load needed to maintain thermal comfort criteria. Furthermore, by investigating the solidification on a monthly average ratio it was found the PCM spackle spent approximately the same amount of time solidified at 2 mm and 4 mm, indicating that reaching solidification was not an issue at double the amount.

Overall, this study found that both PCM technology and night ventilation strategies can contribute significantly to lessen the cooling demand for buildings with office cubicles environments in Norway.

Preface

This thesis was written during the spring of 2020 for the Department of Civil Engineering and Energy Technology at Oslo Metropolitan University. The work was made possible by Gyproc Saint-Gobain, Sweden AB.

I want to especially thank my three supervisors, Tor Arvid Vik, Habtamu Bayera Madessa and Arnab Chaudhuri. You have provided excellent guidance and support for the whole project. You show remarkable care for your students, and I am grateful for the encouragement and motivation you have continuously provided me. Equally important for this work have been the collaboration with my lab partner and good friend, Chakkrit Phengphan. We have solved countless problems together and motivated each other the entire way. I will truly miss the experience and teamwork we shared this final semester.

I also want to thank Mehrdad Rabani for assisting me in the work with numerical simulations, Øystein Andersen for providing invaluable help and advice with laboratory equipment and experiment setup and Gyproc Sweden for providing an exciting topic for my thesis.

I am also grateful to my friends and family for all encouragement and support. Most of all I would like to express my gratitude to my dear fiancée, Yessenia, for your endless support and cheering me on. Not only for my very last semester, but for the whole span of my degree starting 5 years ago. I could not have done this without your love and care.



Andreas Aamodt

Asker, 13th June 2020

Contents

| | | |
|----------|---|-----------|
| 1 | Introduction | 1 |
| 1.1 | Background | 1 |
| 1.2 | Phase change materials | 2 |
| 1.3 | A view on the material in study in light of research | 3 |
| 1.4 | Formulation of research questions | 6 |
| 1.5 | Scope | 6 |
| 2 | Methodology | 7 |
| 2.1 | Climate room experiment | 9 |
| | Experimental design | 10 |
| | Further setup and execution of experiment | 21 |
| 2.2 | Determination of thermal conductivity | 24 |
| | Theory | 25 |
| | Design of a guarded hot box system | 28 |
| | Instrumentation and measurements | 31 |
| | Challenges with heat transfer with specimen | 33 |
| | Execution of the experiment | 36 |
| 2.3 | Numerical simulations | 37 |
| | Simulation tool | 37 |
| | Validation | 38 |
| | Optimization of night ventilation strategies for energy savings potential | 43 |
| | Analysis | 56 |
| 3 | Results and discussion | 61 |
| 3.1 | Climate room experiment | 61 |
| 3.2 | Determination of thermal conductivity | 64 |
| 3.3 | Numerical simulations | 68 |
| | Validation | 68 |
| | Optimization of night ventilation strategies for energy savings potential | 69 |
| 4 | Conclusion | 79 |
| A | Experiment | a |
| | Sensor placements and details: climate room experiment | a |
| | Sensor placements and details: guarded hot box experiment | f |
| B | Simulations | i |

Chapter 1

Introduction

1.1 Background

Today, we are faced with an acute climate crisis due to global warming. Most countries have committed to the Paris Agreement by UN to pursue efforts to limit the extent of global average temperature rise [1]. EU aims to achieve climate-neutrality by 2050 and wants to lead global efforts to this way. A key part of the strategy is to maximize the energy efficiency of its building mass [2]. This is a colossal target and focus are directed towards increasing public research and deployment of technologies which can immediately have an impact on emissions. Research is advised to prioritize the reduction of energy demand and not only focus on replacement of fossil fuels [3].

Buildings and the building sector as a whole are today responsible for over 30% of the worlds total energy demand, and 40% of direct and indirect CO₂ emissions. The International Energy Agency (IEA) describes this sector to be a source of enormous untapped potential of energy efficiency [4]. The energy demand of the building sector is swiftly rising as growth in living standards around the world leads to an increase and development of new and existing building mass. In buildings, heating and cooling measures expends 60% of the total energy consumption, where energy usage for cooling is the sole area of most rapid development as the demand increases [5]. The IEA concludes that *"Growing demand for air conditioners is one of the most critical blind spots in today's energy debate. Setting higher efficiency standards for cooling is one of the easiest steps governments can take to reduce the need for new power plants, cut emissions and reduce costs at the same time."* [6].

Gyproc Saint-Gobain, Sweden AB, is in the development of a novel building material in which a spackle compound composed of different binding materials and micro-encapsulated PCM (phase changing materials) can increase the thermal inertia of a building by a relatively substantial amount. By increasing the thermal inertia, the building becomes more resistant to changes in indoor temperatures, which in turn reduces the need and energy required to cool the indoor environment for better thermal comfort [7]. Recent years advancements in material sciences have excited an interest for further study and development of PCM applied in building materials, as they can prove to be an auspicious contributor to the solutions urgently needed to reduce the worlds energy consumption [8].

1.2 Phase change materials

PCM's are a promising passive cooling technology which can increase a buildings thermal mass in an effective way [8]. Thermal mass in the context of building applications normally means high density materials, like e.g. concrete and bricks in which large amounts of heat (energy) is required to change the temperature. When describing thermal properties of buildings, an often used categorization is based on the buildings total mass ranging from light to heavy weight constructions. A light weight building is usually of a wooden construction and low in thermal mass, and a heavy weight building has extensive use of thermal mass in the building body, floor separators, internal partitioning walls and et cetera.

The use of thermal mass in the building envelope have been widely used historically as a thermal energy storage system (TES), and when utilized correctly it can reduce heating and cooling loads, shift peak load hours as well as dampen the diurnal indoor temperature swings throughout the day [9]. This is no less true when utilizing thermal mass potential of PCM's [10]. The indoor temperature is affected by the building envelope, climatic conditions, solar gain and internal heat loads. During the summer when solar load and outdoor temperatures are at its highest, rapid rise in the indoor temperatures bring needs for systems that can remove all excess energy from the indoor environment to maintain thermal comfort. If outdoor air temperatures are high, simple passive solutions like opening windows will be of limited effect. Removing energy solely by mechanical solutions leads to high energy usage and oversized systems that can handle the short peak hours of intense cooling load. Thermal mass can absorb and store high amounts of energy during the day and slowly release it back to the space later, and is therefore an attractive passive solution for energy savings and improvement of thermal comfort [9]. However, the building industry have shifted focus towards lighter buildings and there is interest in regaining the thermal benefits traditionally found in heavy weight buildings.

The energy storage capabilities of ordinary materials used for TES like e.g. concrete is related to the sensible heat needed to change the materials temperature. PCM's have a much higher potential for energy storage due to the latent heat storage capabilities when the materials phase change is utilized [11]. PCM's for building applications are designed to melt or solidify during temperatures that can be expected in indoor environments. The chemical composition of the PCM can be tailored to have melting temperatures suit a wide range of climates and environments, and this has been identified by numerous studies as the key design parameter for successful application of the material [11],[12],[13],[14].

Although PCM's great potential for sustainable cooling is firmly entrenched in literature, some significant downsides with the material pose challenges for employment in buildings. The major issue of risk is the inability to complete the solidification process. Often called to charge the PCM, meaning to build up the heat storage potential by releasing stored heat. It is a vital process to make the material ready for the next day when heat needs to be absorbed from the building spaces all over again. The benefits of heat storage in the PCM can be completely lost if incomplete charging occurs repeatedly [11],[15]. The problem is mainly due to PCM's having low thermal conductivity which cause heat to propagate slowly through the material, and in turn serves for low rate of heat exchange with its environment [13]. This makes exposure of the material, amount of PCM and convective heat transfer with

PCM surfaces some of the most important parameters in achieving complete phase change cycles [16].

The solidifying process can be assisted with enhanced convection, and a commonly proposed strategy is night ventilation (NV) where air change rates are increased during night time to remove heat from the building. There is great interest in coupling NV with free cooling by letting cool ambient air into the building, which can enhance the heat transfer with the PCM considerably [12],[13]. This is dependent on climatic conditions, and works best in locations with diurnal temperature variations of 12 - 15K [17]. NV strategies utilizing free cooling can consist of mechanical solutions with the ventilation system, natural solutions with window openings or hybrid systems which is a combination of both. While all variations can be equally adequate in priming the PCM for good performance, the highest energy savings benefit can be achieved in the natural strategy as ventilation fans can be shut off [16]. Of course, not all buildings are suited for a natural NV strategy where just the means of window openings can provide sufficient air flow rates. Mechanical strategies involves letting the ventilation system of the building provide high air flow rates during night with the cool outdoor air, but are known to quickly become disadvantageous as the fans consume more energy with increasing air flow rates. Hybrid systems are therefore an interesting alternative as it can reduce the energy consumption by having only one of the fans run while air is either let in or expelled through window openings. However, most studies indicate that the energy usage in hybrid systems still becomes an issue if too large air flow rates are used [18].

Several experimental and numerical studies have investigated thermal comfort and energy savings potential with PCM's. The results are most often positive, but still wide ranging to every extent of the word. This is however not unexpected given the number of parameters which influence the effectiveness of the material. Also, PCM's are developed in numerous different configurations, with different approaches to building implementation. It's evident that results are reliant on the PCM material in study, chosen design parameters for experiments and input data in the numerical models.

1.3 A view on the material in study in light of research

The PCM enhanced spackle material is a compound consisting of fillers, microencapsulated PCM, rheological additives and binding agents. Microencapsulation of PCM is one of the most promising ways of incorporating PCM into building elements [10]. It consists of packing the PCM in encapsulating organic or silica material, where the size of the capsules are in the scale of micrometers. The capsules can then be dispersed into various composite materials, as for this instance a spackling mixture. Other benefits include low risk of leakage and reactivity with other materials in the compound due to the encapsulating shell and higher heat transfer rate with the PCM as the surface area of each PCM capsule is large compared to its volume. A disadvantage is that PCM's suited for microencapsulation is usually on the low-end scale of thermal conductivity amongst different chemical categorizes of PCM [19]. The mentioned benefit of each capsules large surface area for heat transfer does entail high energy storage and release capacity of the PCM if the low thermal con-

ductivity characteristics can be combated. The ingenuity with the PCM spackling in this study is it's aptness for thin layer applications in the range of 1 – 4 *mm* at internal wall and ceiling surfaces. This makes it possible to expose a large surface area of the material directly with the air inside the building spaces. The low conductivity problems is an issue propagating with increasing layer thickness, so this intended usage of the material might be suitable to combat the issue.

No tests have been done on the PCM spackling's thermal conductivity, all though Gyproc expects the value to be around $\approx 0.1 W/(m \cdot K)$ based on composition of the compound. A differential scanning calorimetry (DSC) test has been performed in 2019 for Gyproc by KTH labs in Sweden to determine the heat capacity of the material during phase change. The test consists of heating a small sample of material, and is a standard way of investigating energy storage and release characteristics. Results from heating the sample is shown in figure 1.1.

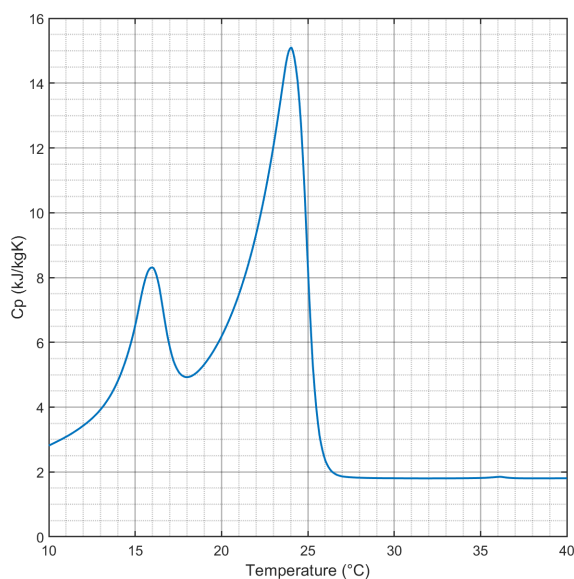


Figure 1.1: Output curve of DSC for heating of PCM spackle.

The curve shows that the PCM spackle has high capacity to quickly store and release large amounts of energy, illustrated by the high peak of heat capacity and rapid increase and decrease of the curve over a short temperature range. The two bumps in the curve are typical of microencapsulated PCM where the phase change of the pure PCM would only have one peak, but when the PCM is encapsulated and dispersed into a compound mixture the phase change is not occurring at a single temperature but rather over a temperature range [20],[21]. The larger bump represents the melting of the PCM, and KTH labs have provided $20^{\circ}C$ as the onset melt temperature, a peak melt temperature of $24^{\circ}C$ and a latent heat of fusion of $88kJ/kg$. The onset melt temperature is a reliable value for when melting starts to occur in the PCM derived from the methodology in the DSC testing, but the peak melt temperature is not a property inherent to the material itself but rather affected by sample size and heat rate of the test. The peak performance of the material can in reality be slightly shifted from the peak at $24^{\circ}C$ seen in the curve. It can further be seen in the figure that the phase change seems to be completed around $\approx 27^{\circ}C$.

Several studies mentioned the melting temperature to be the most significant design parameter for PCM to function well, and the optimal melting temperature

varies with the climate and application the PCM is intended for [13]. A good measure is to have the melting temperature in between diurnal ambient temperature variations and also close to the thermal comfort range. The PCM spackle fits both criteria well, as the climate here in Oslo in which the material is to be studied have high diurnal temperature variations during the summer with highs up to $\approx 25-30^{\circ}C$ and the thermal comfort range posed by national standards is an operative temperature between $19-26^{\circ}C$ for light activity situations.

The novelty of the PCM spackle in study makes it so no other research have been found of matching PCM's in a spackling composition. Two studies on similar materials in Germany have been found where microencapsulated PCM was rather dispersed into plaster based compounds instead of spackle. Although other structural agents are used in the compound, the use of the material is similar to the PCM spackle in that it's applied directly on to internal surfaces in thin layers. Schossig et al. [22] investigated two different microencapsulated PCM's applied at 6 and 15mm at interior walls in small office rooms experimentally. A temperature reduction of 2K and 4K for the respective thicknesses was observed, when the temperature of the reference experiment reached $28^{\circ}C$. Night ventilation of 4 ACH was insufficient to consistently cool the material, and extra measures to improve ventilation was needed. Voelker et. al [23] tested microencapsulated PCM applied to internal walls at 3cm. It had a melting temperature of $28^{\circ}C$, and the testing conditions were extreme in comparison with realistic indoor environments for buildings in Norway. The indoor air temperatures fluctuated between $15-35^{\circ}C$ when ambient diurnal temperature fluctuations were only that of $5-20^{\circ}C$ at the same time. A temperature reduction due to the PCM was usually around 3K under those conditions while a maximum of 3.8K was reported, but room temperatures were sometimes as high as $45^{\circ}C$.

An interesting quality about the PCM spackle in study is its state of readiness for direct applications in the market. It's apt for certain climatic conditions, and the application solution certifies necessary standards for building materials. The incorporation of microencapsulated PCM into a suitable spackling mixture is an interesting cost effective alternative to other alternatives of PCM enhanced materials, like MPCM incorporated gypsum boards which incurs high production costs. Spackling can easily be retrofitted into existing building mass as it can be applied to gypsum boards, plaster boards, concrete or bricks. It will therefore be interesting to research how the PCM spackle will behave in realistic environments and conditions.

1.4 Formulation of research questions

It has been found that the literature mainly focuses on issues in solidifying the PCM, and analysis with this in regard can be valuable. Many studies also encourage more research to investigate how PCM's can positively improve thermal behaviour in buildings and benefit in energy usage needed to be spent for cooling. There is also interest in investigating ways to assist effective utilization of PCM's with night ventilation strategies.

Based on how the material is intended to be used by Gyproc and the available opportunities in research facilities allocated by the faculty, the following questions will be studied in this report:

1. How does the PCM spackle affect the indoor temperature in a realistic summer environment?
2. What is the PCM spackles thermal conductivity, and are there issues in achieving full phase change cycles with the material?
3. How can the PCM spackle be most efficiently utilized in a large scale building, and how much energy savings potential can be expected?

1.5 Scope

In this study, a specific spackling material enhanced with microencapsulated PCM will be studied under summer conditions in the climate of Oslo, Norway. The focus will be realistic usage of the material in office environments, complying with the current Norwegian building code, TEK-17.

Chapter 2

Methodology

To answer the research questions, both experimental and numerical approaches were used. An experiment was set up to investigate the material under realistic conditions. Experimental results are valuable as they can provide solid evidence to back up claims about how the PCM spackle will function in real applications. It was also chosen to use numerical simulations to investigate night ventilation strategies and the use of the material in a larger scale environment. Measurements of the thermal conductivity were performed as this property had never been tested in prior to this research. This was implemented into the model which was later validated against the experimental result to check its accuracy and predictive capabilities.

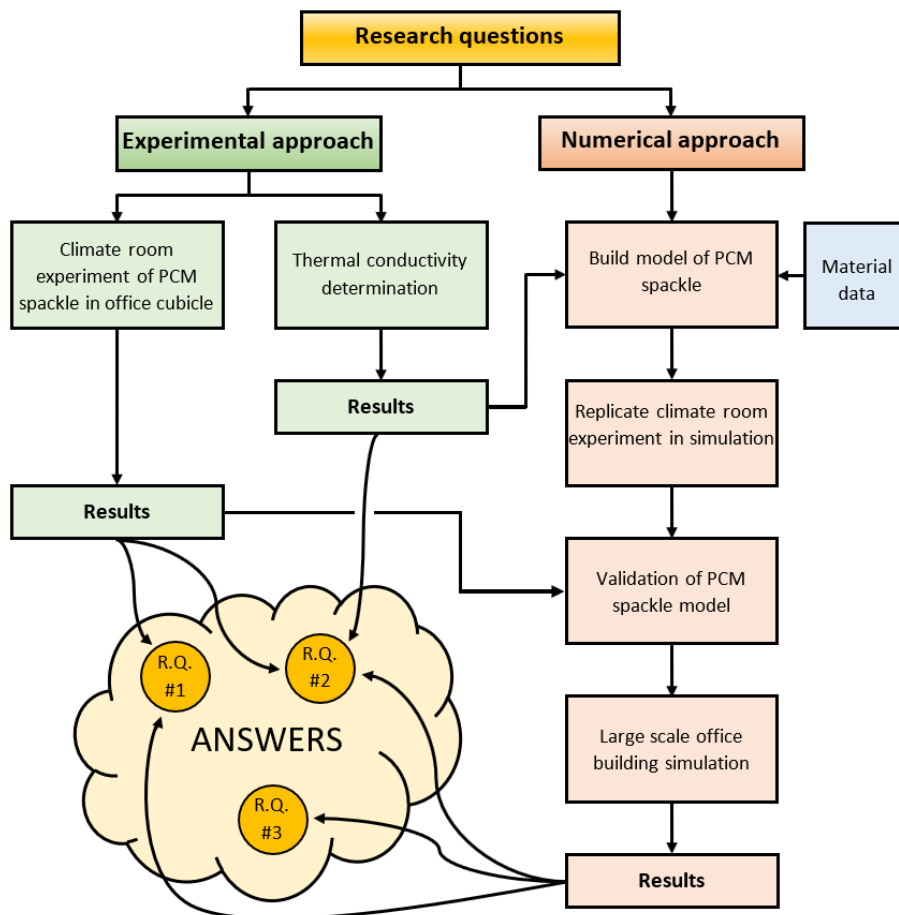


Figure 2.1: Chosen methods to answer research questions.

The tools that were used are summed up in table 2.1 along with the reasons and purposes motivating each choice of tool.

Table 2.1: Choice of tools for methodology.

| Method | | | |
|---------------------------------|---|--|---|
| | Experimental approach: Climate room experiment | Experimental approach: Thermal conductivity measurement | Numerical approach |
| Tools | Climate room | Guarded hot box | IDA Indoor Climate and Energy 4.8 |
| Reason | <ul style="list-style-type: none"> • Can design controlled environment with heat loads and ventilation system • Experimental results are of high value as effect of material can be directly observed | <ul style="list-style-type: none"> • Standardized method to measure thermal conductivity | <ul style="list-style-type: none"> • Advanced building simulation tool • Validated by numerous studies to be very precise • Has mathematical PCM model • Advanced control over all building parameters • Can design custom NV controls |
| Purpose | <ul style="list-style-type: none"> • To analyze effect of material in real case scenario • To have results to validate numerical model | <ul style="list-style-type: none"> • To assist in evaluation of potential solidification issues in the other methods • Thermal conductivity data will be applied to simulation model | <ul style="list-style-type: none"> • To analyze use of material in a larger environment • To optimize NV strategies for efficient usage of material and energy savings |
| Parameters / topics of analysis | <ul style="list-style-type: none"> • Air temperature • Surface temperature • Phase change behaviour of material | <ul style="list-style-type: none"> • Surface temperatures • Thermal conductivity | <ul style="list-style-type: none"> • Air and operative temperatures • Different NV strategies • Varying air flow rates • Varying amounts of material • Energy usage w/ and without material • PCM efficiency |

2.1 Climate room experiment

A laboratory experiment was conducted where the PCM spackle was tested in a climate room. An office cubicle environment was built where typical summer conditions in Oslo was emulated. The purpose of the experiment was to study the material in an environment close to it's actual intended usage, and also to have the measurements and results serve as a reference case to validate a numerical simulation model.

To have the PCM spackle operate to its full potential, it was decided to enhance the night time ventilation rate. The reason for this was to ensure that the latent heat stored in the PCM spackle during day time could be fully released by night time, i.e. to achieve full solidification of the PCM spackle. A common problem reported in experimental studies of PCM is to underestimate the amount of cooling needed to reach solidification, and the results can consequently turn out difficult to analyze and draw conclusions from. It was therefore decided to be on the safe side in regards to the cooling load applied during night time. Apart from this, having realistic values and design of heat gains and day time ventilation representative for normal office cubicle situations was the main priority.

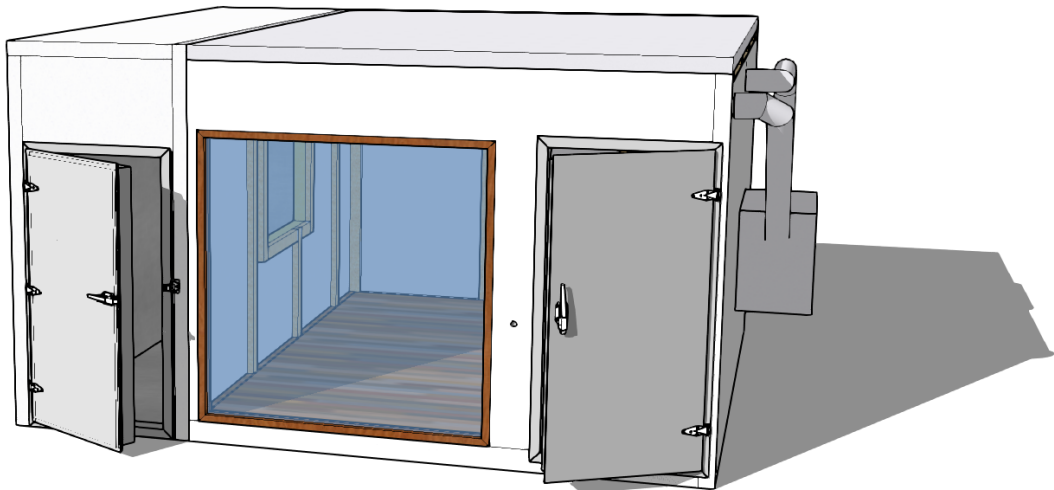


Figure 2.2: 3D rendering of the climate room where the experiment was conducted.

Experimental design

Description of the climate room:

Building body

The climate room is an insulated cubicle situated in a normal indoor environment in OsloMet faculty. The ventilation system works independently from the rest of the building. It has a floor area of $14m^2$ and room height of $2.34m$, with the layout and composition of the building body shown in figure 2.3. The orientation denoted in the figure does not represent true compass directions, but is a local system to easier refer to the different parts of the room. This will be consistent for the rest of the report. On the south wall there is a $(2 \times 2)m^2$ window and a $(1 \times 2)m^2$ door facing the surrounding laboratory room.

A difference between the floor plan and the 3D rendered model in figure 2.2 is the exclusion of a cooling chamber used for special purposes adjacent to the west wall of the climate room. This chamber is not included in the definition of the climate room, as its not in use during the experiment. The door of the cooling chamber was held opened at all times to obtain room conditions similar to that of the surroundings. The partition wall between the two rooms are of the same kind as the rest of the walls in the climate room.

The room height is lower than that of a normal office cubicle in Norway which is often $2.7m$. This can lead to a slightly different stratification profile of the air temperature compared to a real cubicle.

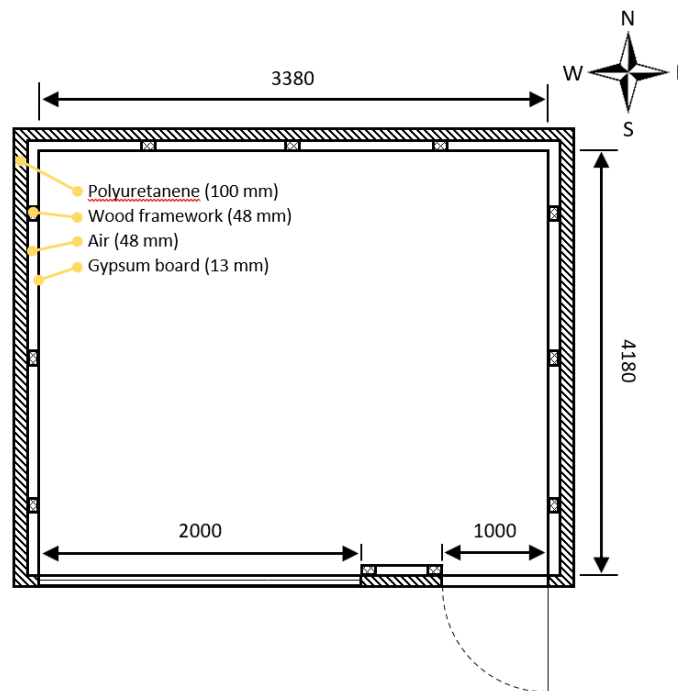


Figure 2.3: Floor plan of the climate room

The different components of the building body are described in table 2.2. The U-values are based on initial hand calculations from the construction layers, and was later fine tuned through validation of the climate room model in IDA-ICE to compensate for unknown faults in the construction and thermal bridges.

Table 2.2: Components of the building body.

| Component | Surface area [m^2] | U-value [W/m^2K] |
|-----------|---------------------------|-------------------------|
| Walls | 28.7 | 0.22 |
| Ceiling | 14.1 | 0.22 |
| Floor | 14.1 | 0.24 |
| Window | 4 | 0.78 |
| Door | 2.1 | 0.64 |

Ventilation system

A dedicated air handling unit (AHU) placed outside of the climate room on the east side supplies the room with fresh air. Air flow rates and supply air temperature can be scheduled by user inputs on the AHU. The AHU is equipped with a rotary heat exchanger and heating and cooling batteries. The AHU's intake and exhaust is connected to the outdoor through the building complex facade. The ventilation is set up as a mechanically balanced constant air volume (CAV) system.

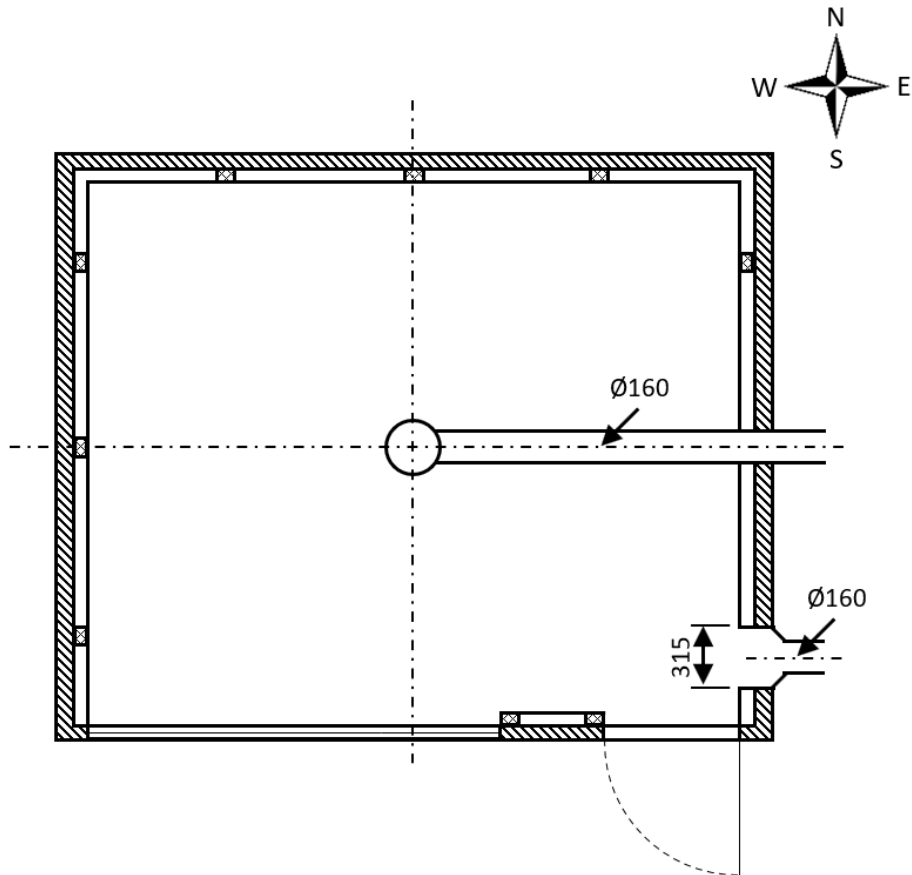


Figure 2.4: Ventilation layout in the climate room.

The air enters the climate room through an insulated duct and a centrally placed circular diffuser, as shown in figure 2.4. The diffuser has a perforated face plate and spreads the air horizontally in 360° approximately $30cm$ from the ceiling. The air is extracted from the room through an outlet in the top S.E. corner.

Design of office cubicle conditions

Even though the climate room is situated indoors and the heat exchanged with its environment will differ by some degree from a building exposed to the outside climate, a realistic indoor temperature development is still possible to achieve with use of the ventilation system and artificial heat gains.

The goal was to emulate a situation which produced a realistic day-by-day indoor air temperature development for a typical summer situation in Oslo climate, without needing to resort to unrealistic sizing of the heat gains and the ventilation parameters. This was achieved in situ by simulating a simplistic model of the climate room in IDA-ICE. Simulated results were continuously compared to live temperature measurements from the climate room. Heat gains and ventilation parameters in the climate room were changed on site to correspond with simulation input.

The resulting decision was to emulate an office cubicle environment for two persons with a south facing window with external venetian blinds for solar shading. The Norwegian building code (TEK-17) requirements were followed in regards to ventilation rates.

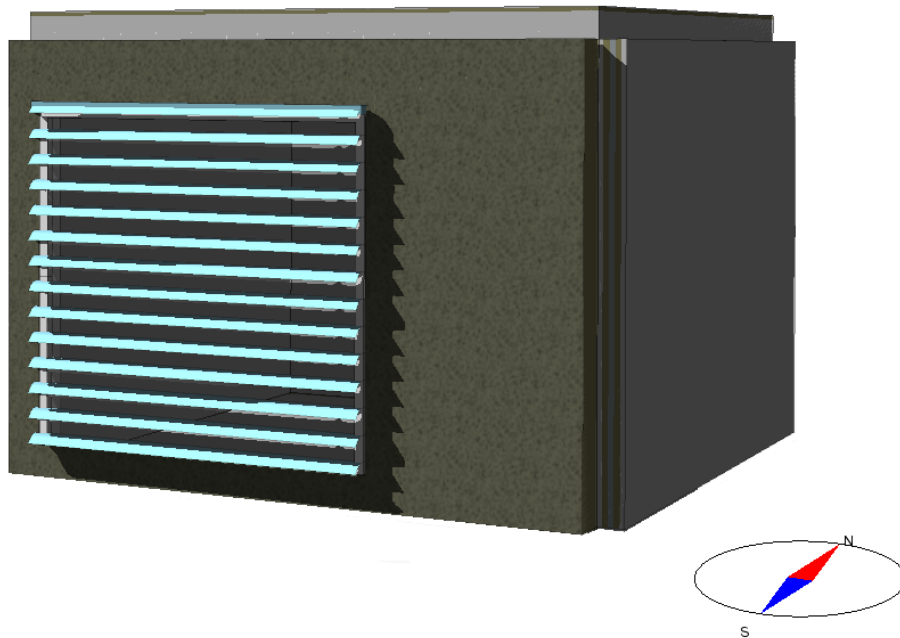


Figure 2.5: Simple IDA-ICE model used to determine a suitable scenario.

Heat gain design

This chapter explains how the different heat gains were sized and built in the climate room to model its real counterparts.

The Norwegian labor inspection agency enforces requirements to the office environment through the working environment act. The minimum allowed floor area per worker is $6m^2$ for cubicles and open working landscapes. The climate room, having $14m^2$ of floor area is therefore suited to model a cubicle intended for two persons. Suggested values from ASHRAE [24] were used as guidelines in determining the size of each internal heat gain.

A total heat gain of $556W$, all running on the same schedule was applied during the experiment. The resulting heat gains and its schedules are summed up in table 2.3, and the placement of them can be seen in figure 2.6.



Figure 2.6: The climate room with the heat gains.

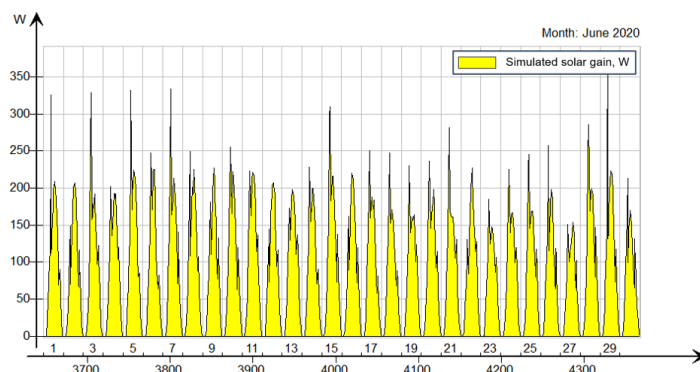
Table 2.3: Schedule of the heat gains in the climate room

| Heat gain | Size [W] | Schedule | Design |
|------------|----------|---------------|--------------------------------------|
| Occupants | 2x 90 | 08:00 - 18:00 | Light bulbs in matte black tubes |
| Computers | 2x 60 | 08:00 - 18:00 | Light bulbs in matte black tubes |
| Lights | 2x 28 | 08:00 - 18:00 | Fluorescent lights in ceiling |
| Solar gain | 200 | 08:00 - 18:00 | Electric heat foils placed at window |

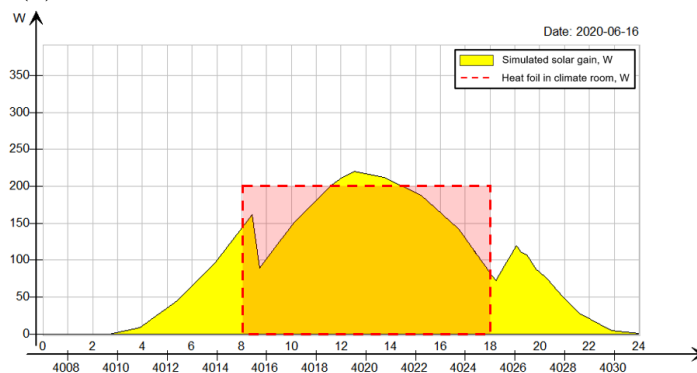
Solar heat gain

In IDA-ICE, the climate room was given an external south facing facade as shown in figure 2.5, and an EnergyPlus Weather (EPW) file containing climate data from Gardermoen in Oslo was applied to the model. The window in the climate room was remodelled as a typical external window with adjustable venetian blinds mounted on the outside. It was decided to have 80mm wide slats with 80mm spacing in between. The slat angle was set to 20°. This would block most of the direct solar beam from entering through the glazing pane, while still allowing for good view and daylight inside the cubicle. Still, diffusive solar radiation could contribute distinctly to the heat gain inside of the room, which is a realistic scenario. The solar heat gain coefficient (g-value) for the window was 0.69 and the total g-value with the solar shades drawn was 0.48.

The month of June was simulated with the external blinds being drawn when solar flux on the facade exceeded $100W/m^2$. The solar gain inside the cubicle is shown in figure 2.7a. The sharp spikes that can be seen each day is due to systems smoothing in IDA-ICE, having the shades not being drawn abruptly at the activation signal. Figure 2.7b shows the gain during a typical day in the simulations, and how the heat gain was applied in the real climate room. Practical limitations necessitated the heat gain to be distributed with constant power. The best match with available equipment was to use electrical heat foils of 200W activated from 08:00 - 18:00. Although not matching the length of the solar gain, approximately the same total amount of energy would be supplied to the room in that $\int Q_{\text{solar}} dt \approx \int Q_{\text{heat foil}} dt$.



(a) Simulated solar heat gain in the cubicle for June.



(b) Simulated solar heat gain for one day, and how the heat gain was applied in the experiment.

Figure 2.7: Sizing of the heat foil in regards to simulations of solar heat gain.

The heating foil was fastened to the inside of the window frame in the climate room, hanging a couple of centimeters from the glazing pane. The inside of the glass was covered with aluminium foil to limit heat loss by radiation out of the window and to the surrounding room.

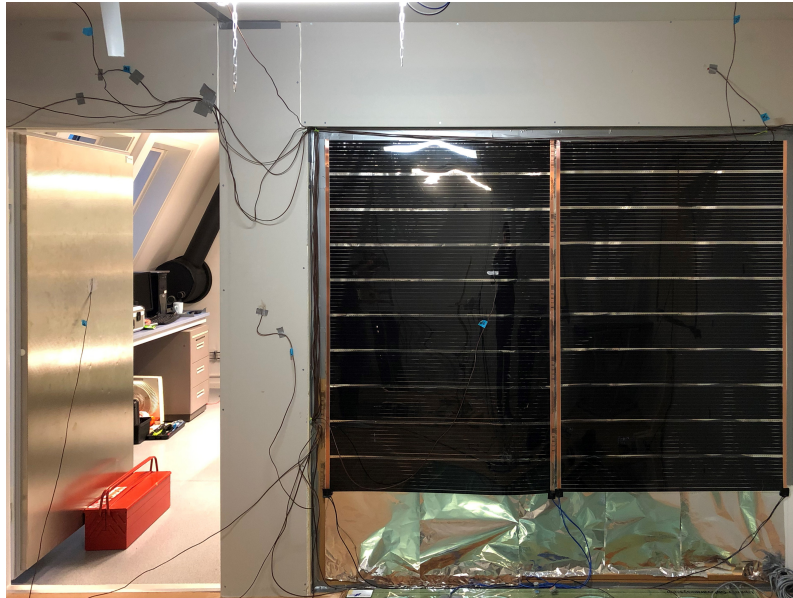


Figure 2.8: The solar heat gain emulated with heat foils in the climate room.

An analog timer switch was used to control the time schedule. The power drawn by the foil was verified through an electrical power meter.



(a) Heat foil sizing verified with an electrical power meter.



(b) Thermal image of the heating foil activated.

Figure 2.9: Heating foil.

Internal heat gains

It was decided to place two workers in the climate room, each equipped with a personal computer. Incandescent light bulbs were used as heat ballasts. Due to limited availability of bulbs, it was chosen to use two light bulbs for each occupant of 30W and 60W totalling 90W per occupant. The computers each had one light bulb of 60W. Two fluorescent lamps, totalling 56W, were hanged from the ceiling in the climate room. The internal heat gains amounted to 356W or 25W/m².

Incandescent light bulbs works well as heat ballasts, as through the effect of incandescence over 90% of the power supplied to a light bulb is emitted as heat through black body radiation [25]. However, placing them directly in the climate room as a heat source is not a good representation of how heat is emitted from the heat gains to be modelled. Not only having a high radiative fraction of the heat emitted, the small surface area of the bulbs can run well over 120°C, creating a concentrated and intense convective heat source [25][26].

To model the occupants and computers more realistically, the light bulbs were placed inside partitioned ventilation ducts of metal which were painted with a matte black spray coating. This is shown in figure 2.10a. By painting the metal surface, the effective emissivity of the surface can be increased by a considerable amount [27]. This means that the surface can efficiently emit thermal radiation. For this reason, and in combination with the larger surface area of the heat gains due to the ducts, the surface temperature of the heat gains is lowered so it's closer to the black body radiation of its real counterparts. Figure 2.10c shows the surface temperature of the occupant. It can be seen that the surface temperature is a little higher than that of a real human body, meaning that the models are not completely realistic. This could have been modelled better by having larger ducts, but only tools available on hand could be used. However, it was reasoned that a good representation of the heat gains were modelled, and the deviation shown would be of minuscule effect to the results.

It was also decided to not cover the duct for the computers entirely to allow for more convection with the light bulb, as real computers have a low radiative fraction of its heat emissions due to the computer fan doing most of the heat transfer by forced convection [24]. This is shown in figure 2.10b.

The internal gain from lights could be modelled realistically as fluorescent lights were installed in the climate room. The lights were of type T5 IP20, and two diffusers with 28W of lights in each were hanged from the ceiling. Table 2.4 shows the total power load from the internal heat gains. This was verified to 349W, as shown in figure 2.10d.

Table 2.4: Internal gains

| Internal gain | Power[W] |
|---------------|----------|
| Occupants | 2 x 90 |
| Computers | 2 x 60 |
| Lights | 2 x 28 |
| Total | 356 |

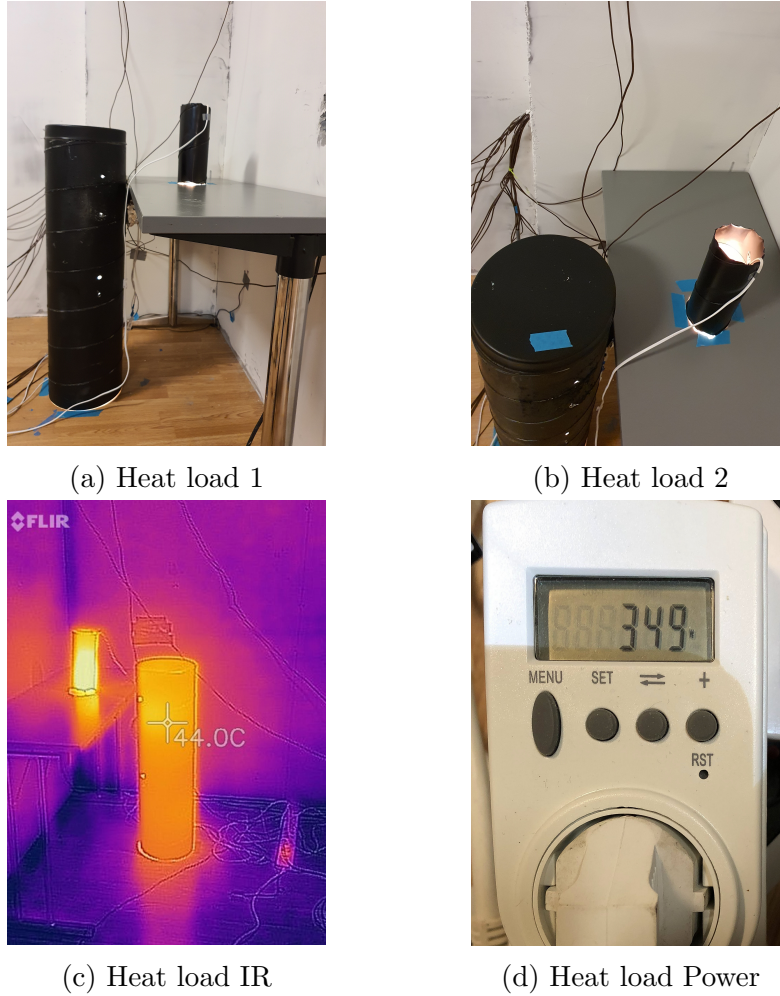


Figure 2.10: Heat loads

Ventilation

Two ventilation settings were scheduled, a day setting and a night setting as detailed in table 2.5. In the night setting, the goal was to supply a high air flow rate with low temperature to enhance the cooling load to ensure solidification of the PCM spackle.

The day setting was sized in regards to the minimum requirements for ventilation rates in TEK-17, but the AHU was unable to provide this low air flow rate while simultaneously have high air flow rates during the night. The air flow rate was therefore a little higher than the minimum requirements.

Table 2.5: Ventilation settings

| Setting | Air flow rate [m^3/h] | Supply air temperature [$^{\circ}C$] | Schedule |
|---------|------------------------------|---|---------------|
| Day | 135 | 19 | 08:00 - 18:00 |
| Night | 230 | 14 | 18:00 - 08:00 |

Instrumentation and measurements

For this report, air and surface temperatures at different positions would serve as the main parameters for analysis of the experiment and validation of the IDA-ICE model. The detailed positioning of each sensor can be found in appendix A.

Figure 2.11 shows an overview of the climate room after measuring equipment and sensors were placed. The red and blue circles indicates some of the positions for surface and air temperatures, respectively. Between the desktops for the occupants, a measuring jig for air temperatures and other thermal comfort properties can be seen. Several thermal comfort linked parameters were measured but as it would be of focus in another study, they will not be given much details in this report. The placement of all sensors were however positioned to suit both studies.

Thermocouples of type T were used as temperature sensors. The air temperatures were measured at 0.1, 0.6, 1.1 and 2.2m height from floor level, where the first three heights mentioned were positioned by the measuring jig and the last one was placed inside the exhaust air duct. All heights were used to calculate the average air temperature in the room, where each sensor was given a weight ratio in accordance to their relative height in the room. Five thermocouples were placed in a symmetric grid at all surfaces to have a representative average temperature of each surface. Air temperatures were also recorded outside of the room, at the south and northern side of the climate room to record the surrounding conditions.

Air velocity sensors were placed at center of the west and east wall surfaces, and could assist in analysis if any problems with solidifying the PCM spackle would occur. Lastly, a white box on the floor indicates the position of the dataloggers and power supplies that needed to be placed inside the room during the experiments. Dataloggers for all of the thermocouples were placed outside the climate room, so that data could be monitored during the experiments without intervention.

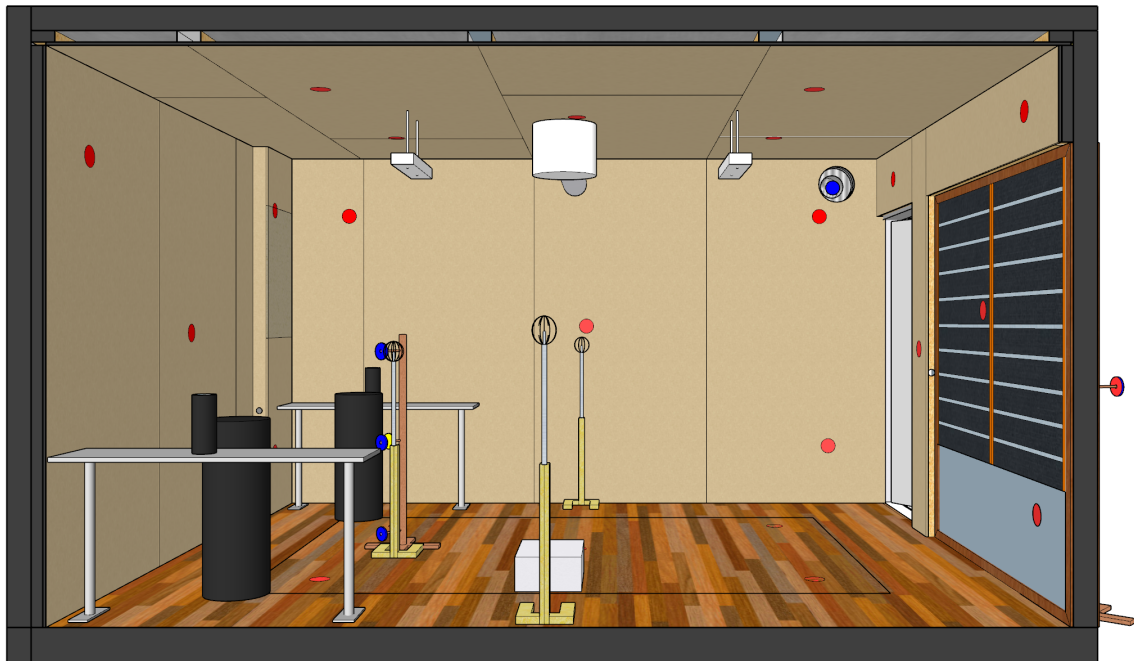


Figure 2.11: Set up of sensors in the climate room.

Table 2.6 shows a complete list over all sensors used in the experiment, as well as the purpose behind each of them and which parameter they were linked to. The abbreviation "TC" means thermocouple and a naming system was created to separate them.

Table 2.6: Measurement plan for the experiment.

| Room sensors | | | | | |
|------------------------|---------|-------------------------|----------------------|------------------------------|-------------------|
| Position | Sensor | Purpose | Parameter | Equipment / tools | Time schedule |
| Jig, 0.1 m | TC 1-18 | Average air temperature | Tavg,air | Thermocouples | During experiment |
| | | Experiment analysis | T0.1 | Intab PC-Logger 3100i | |
| | | IDA-ICE validation | | EasyView Pro 10 | |
| Jig, 0.6 m | TC 1-19 | Thermal comfort | | Innova 1221 | |
| | | Average air temperature | Tavg,air | Thermal Comfort Manager 7701 | |
| | | Experiment analysis | T0.6 | Swema 3000 | |
| Jig, 1.1 m | TC 1-20 | IDA-ICE validation | | Swema Terminal 3.0 | |
| | | Thermal comfort | Tglobe | | |
| | | Thermal comfort | Tavg,air | | |
| Supply air | MM0060 | Thermal comfort | T1.1 | | |
| | | Thermal comfort | Top | | |
| | | Thermal comfort | Humidity | | |
| Exhaust air | MM0037 | Thermal comfort | | | |
| | | Thermal comfort | Air velocity | | |
| | | Thermal comfort | Air velocity | | |
| Outside, north side | SWA 03 | Thermal comfort | Tsupply | | |
| | | Input for IDA-ICE model | Tavg,air | | |
| | | Input for IDA-ICE model | | | |
| Outside, south side | TC 2-14 | Average air temperature | | | |
| | | Experiment analysis | | | |
| | | IDA-ICE validation | | | |
| Outside, north side | TC 2-15 | Input for IDA-ICE model | Tair | | |
| | | Input for IDA-ICE model | | | |
| | | Input for IDA-ICE model | | | |
| Outside, south side | TC 2-16 | Input for IDA-ICE model | | | |
| | | Input for IDA-ICE model | | | |
| | | Input for IDA-ICE model | | | |
| Surface sensors | | | | | |
| Position | Sensor | Purpose | Parameter | Equipment | Time schedule |
| All | TC | Experiment analysis | Tavg,surface | Thermocouples | During experiment |
| | | Thermal comfort | Top | Intab PC-Logger 3100i | |
| | | Experiment analysis | Air velocity | EasyView Pro 10 | |
| All | SWA 03 | Air flow over surface | | Swema 3000 | |
| | | Air flow over surface | | Swema Terminal 3.0 | |
| | | Air flow over surface | | | |
| North surface | | | South surface | | |
| Position | Sensor | | Position | Sensor | |
| Top W | TC 1-1 | | Top W | TC 2-9 | |
| Top E | TC 1-2 | | Top E | TC 2-10 | |
| Center | TC 1-3 | | Middle | TC 2-11 | |
| Btm W | TC 1-4 | | Door | TC 2-8 | |
| Btm E | TC 1-5 | | Heat foil | TC 2-7 | |
| West surface | | | East surface | | |
| Position | Sensor | | Position | Sensor | |
| Top N | TC 1-6 | | Top N | TC 1-10 | |
| Top S | TC 2-1 | | Top S | TC 2-6 | |
| Center | TC 1-8 | | Center | TC 1-11 | |
| | SWA 03 | | | SWA 03 | |
| Btm N | TC 1-7 | | Btm N | TC 1-9 | |
| Btm S | TC 2-2 | | Btm S | TC 2-5 | |
| Ceiling | | | Floor | | |
| Position | Sensor | | Position | Sensor | |
| NW | TC 1-15 | | NW | TC 1-12 | |
| NE | TC 1-16 | | NE | TC 1-13 | |
| Center | TC 1-17 | | Center | TC 1-14 | |
| SW | TC 2-12 | | SW | TC 2-3 | |
| SE | TC 2-13 | | SE | TC 2-4 | |

Equipment, calibration and accuracy

Table 2.7 shows an overview of all measuring devices and sensor types used during the experiment, as well as the manufacturer listed accuracy. The sampling time is the chosen time steps for the experiments. The long duration of the experiment necessitated some of the time steps to be a little higher than desired due to fear of filling the internal memory for some of the data loggers completely.

Table 2.7: Equipment used during the experiment.

| Equipment / sensor | Calibration | Parameter | Range | Resolution | Accuracy | Instantaneous sampling time | Average sampling time |
|----------------------|-------------|------------------------------|-----------------------------------|-----------------|--------------------------|-----------------------------|-----------------------|
| PC-Logger 3100i #1 | 2018 | Thermoelectric voltage | $\pm 50mV$ | $\pm 2\mu V$ | max 50ppm/ $^{\circ}C$ | 1 min | - |
| PC-Logger 3100i #2 | 2019 | Thermoelectric voltage | $\pm 50mV$ | $\pm 2\mu V$ | max 50ppm/ $^{\circ}C$ | 1 min | - |
| Thermocouple: Type T | - | Temperature | $-270^{\circ}C$ to $370^{\circ}C$ | $0.1^{\circ}C$ | $\pm 0.5K$ | - | - |
| Innova 1221 UA 1276 | 2019 | - | $-20^{\circ}C$ to $100^{\circ}C$ | $0.1^{\circ}C$ | - | 10 min | 3 min |
| MM0060 | - | Operative temperature | $-20^{\circ}C$ to $100^{\circ}C$ | $0.1^{\circ}C$ | $\pm 0.3K$ | - | - |
| MM038 | - | Omnidirectional air velocity | $0m/s$ to $10m/s$ | $0.01m/s$ | $\pm 0.05m/s$ | - | - |
| MM037 | - | Absolute humidity | $-20^{\circ}C$ to $100^{\circ}C$ | $0.1K$ | $\pm 0.5K / \pm 0.05kPa$ | - | - |
| SWEMA 3000 | 2019 | - | - | - | - | 5 min | - |
| SWA03 | - | Omnidirectional air velocity | $0.05m/s$ to $3m/s$ | $0.001m/s$ | $\pm 0.03m/s$ | - | - |
| | - | Temperature | $10^{\circ}C$ to $40^{\circ}C$ | $0.01^{\circ}C$ | $\pm 0.1K$ | - | - |

An ice water test was performed to validate the accuracy of each datalogger with the thermocouples in use. The thermocouples were placed in a bucket with a liquid water-ice mixture, as shown in figure 2.13a. It was strived to keep them approximately at the same level and towards the center of the bucket, while at the same time not in contact with each other. When most of the ice had melted, the water temperature was measured to $0.1^{\circ}C$ as shown in figure 2.13b.

Figure 2.12 shows temperature readings for all thermocouples, where every channel except for four outliers were in the range of $\pm 0.5^{\circ}C$. The four outliers were thermocouple channel 1-1, 1-2, 1-3 and 1-4, and had a deviation of $+0.6 - 0.9^{\circ}C$.

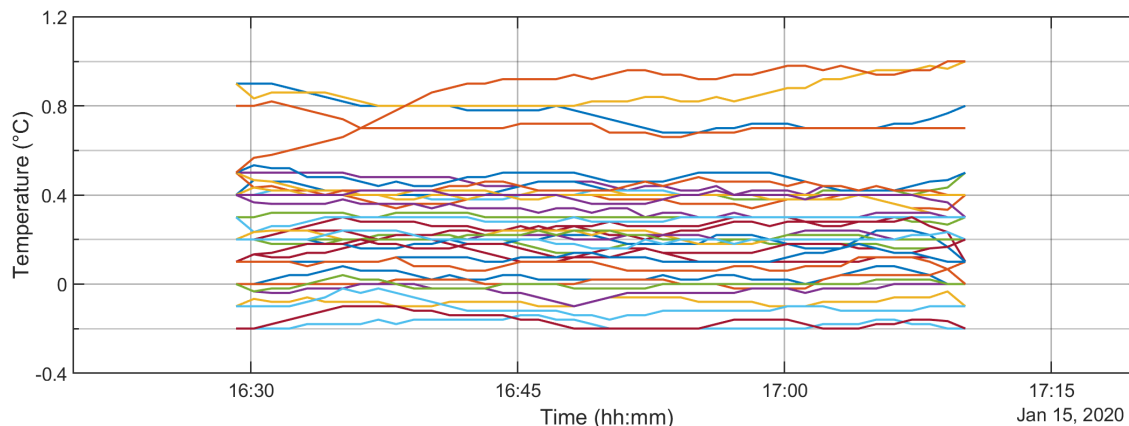


Figure 2.12: Ice water test: thermocouple readings.

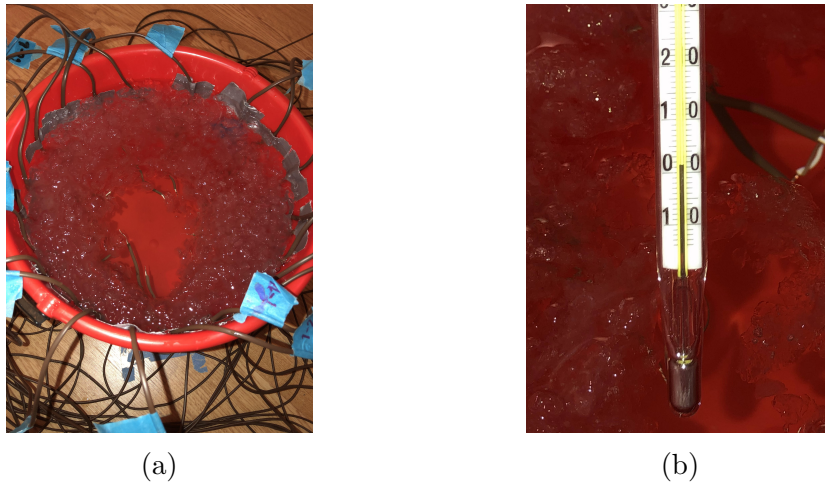


Figure 2.13: Ice water test.

Further setup and execution of experiment

Experiment setup

An important focus was to achieve identical setups of the reference and the PCM spackle experiment. Both setups can be seen in figure 2.14, where it also can be seen in 2.14b that blue tape on the floor marked the location of all heat loads and measurement equipment. No changes were made to the heat gains and ventilation schedule.

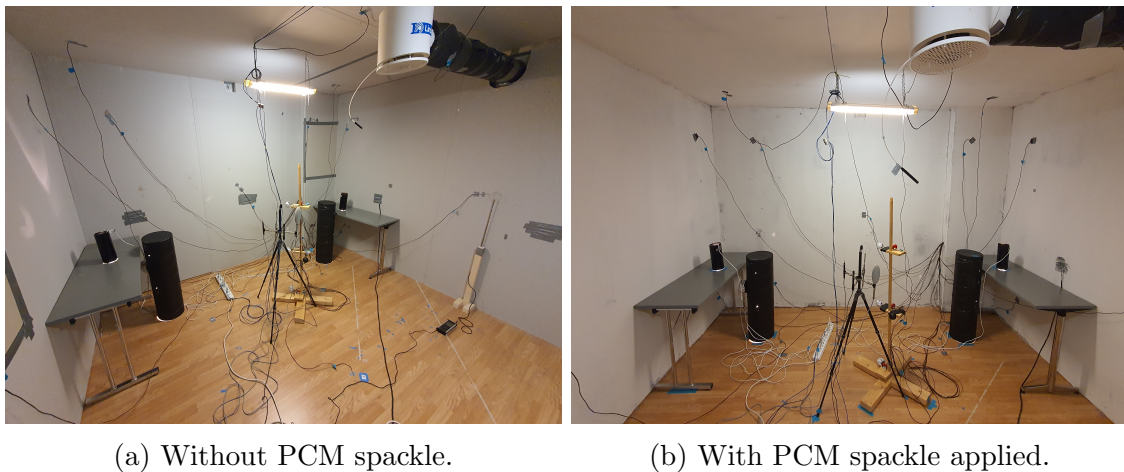


Figure 2.14: Setup of both experiments, focusing on having the PCM spackle be the only differing factor.

Applying the PCM spackle

After the reference experiment was finished, the PCM spackle was applied to the inner surfaces as shown in figure 2.15a. Also, the gypsum boards on the southern surface had the PCM spackle applied. Two strokes of PCM spackle was applied before a final stroke of thin paint coating was applied in the end. After the experiment was concluded, a total of 45 samples were cut out from the ceiling and all walls to measure the layer thickness of the PCM spackle. Figure 2.15c shows a sample, where the individual layers can be seen. On an area weighted average, $1.7mm$ and $2.1mm$ of the PCM spackle was applied to the walls and the ceiling, respectively.



(a) PCM spackle applied to the inner surfaces of the climate room.



(b) Samples cut out of the walls after experiments.

(c) Gypsum, PCM and coating layers of a sample.

Figure 2.15: PCM spackle applied to the surfaces, and layer thickness was measured afterwards.

Execution of the experiment

The experiment was conducted in the following sequence:

1. Heat gains and ventilation schedule ran for 5 days while parameters were measured to record a reference experiment.
2. Equipment and sensors were dismantled to apply PCM spackle to all gypsum boards.
3. Equipment and sensors were placed in the same position as before. No changes were made to the ventilation or the heat loads.
4. The schedule of heat loads and ventilation was restarted, and the parameters were recorded for another 5 days.

2.2 Determination of thermal conductivity

An experiment was conducted, aimed at characterizing the PCM spackle's thermal conductivity. The purpose of measuring the thermal conductivity was to use the value in IDA-ICE simulations as it's an important parameter to model the heat transfer interactions between the PCM spackle and its environment. Also, knowing the value could give insight and assist in analysis if any troubles with solidifying the PCM would occur in the experiment.

A specimen of the PCM spackle was studied in a controlled thermal environment under steady-state conditions, following a standardised set up for determination of thermal transmission properties in materials. The material was tested during three temperature ranges associated with the different phases of matter for the PCM to see if any changes in thermal conductivity could be observed.

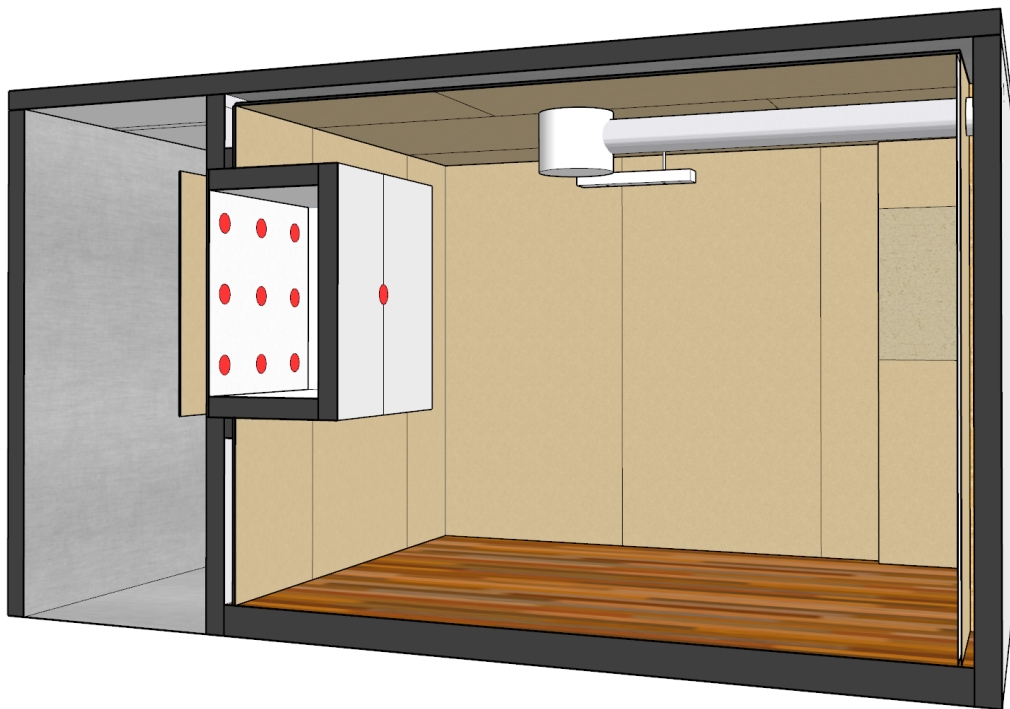


Figure 2.16: An adaptation of a guarded hot box system set up between the climate room and the cooling chamber.

Theory

The method was planned according to ISO 8990:1994, which is an European standard that describes methods for determining thermal transmission properties of materials during steady-state conditions. A guarded hot box system was modelled after the recommendations defined in the standard. The ideal system detailed in the standard was not possible to build due to limitations in available equipment, resources and time. The standard declares that as different materials to be tested and necessary thermal conditions varies greatly, the standard does not mandate a specific design. Many different designs and variations of the systems exists conforming to national standards and specific testing conditions and purposes [28].

The essence of the experiment is to surround a specimen of the material to be tested with insulated boxes on both sides of the specimen. Inside the boxes, a hot and a cold environment is maintained by supplying heat to one side, and removing heat on the other. By establishing a temperature difference across the material, a heat flux is forced through the material. By measuring the power supplied to the hot side and the surface temperatures on both sides of the specimen, the thermal conductivity of the material can be derived by Fourier's law of heat conduction when steady-state conditions are established (equation 2.1).

$$\Phi = -kA \frac{dT}{dx} \quad (2.1)$$

where Φ is the rate of heat transfer by conduction, k is the conductivity coefficient, and dT/dx is the differential temperature over the length (thickness) of the specimen.

As commented in the standard, it's difficult in practice to exclude heat losses during testing. In figure 2.17, these heat losses are depicted as Φ_3 and Φ_5 . Φ_1 is the heat flux through the specimen from the hot to the cold side. Φ_p is the supplied heat to the metering box. Φ_2 is heat transfer in the lateral direction inside the specimen due to temperature variations and the thermal bridges where the specimen is connected to other surfaces.

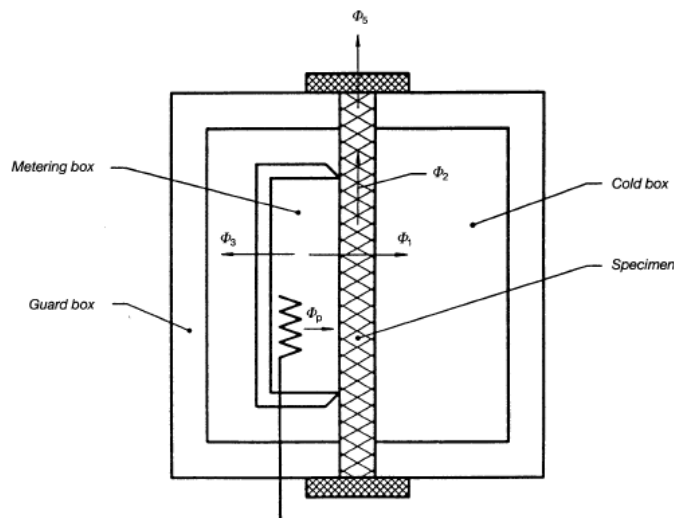


Figure 2.17: A guarded hot box system described by ISO 8990 [28].

As Φ_p is the only heat flux being measured during the experiment, the heat conductivity of the material can not be derived from equation 2.1, as Φ_p is not equal to Φ_1 . As described in the standard, a preliminary calibration test of a specimen with known heat conductivity, k_{ref} , should be performed to establish a calibration constant which will counterbalance the heat losses. Later, when the material with unknown heat conductivity is to be measured, the same calibration constant can be applied if the same boundary conditions are maintained. This assumes that the heat losses are the same for both tests.

A gypsum board from Gyproc was chosen as the reference sample, as the heat conductivity have been measured to be $k_{\text{ref}} = 0.25 \text{ W}/(\text{m} \cdot \text{K})$ by the manufacturer at 23°C and 50% RF.

The calibration constant was calculated by equation 2.2, where D is the calibration constant, k_0 is the measured conductivity of the reference sample and k_{ref} is the known conductivity of the reference sample.

$$D = \frac{\sqrt{k_0 k_{\text{ref}}} - k_{\text{ref}}}{2} \quad (2.2)$$

For the next test with the PCM spackle, the calibration constant could be applied to calculate the thermal conductivity by equation 2.3, where k_0 now is the measured conductivity of the PCM spackle instead.

$$k = \frac{k_0 - 2D + \sqrt{k_0^2 - 4Dk_0}}{2} \quad (2.3)$$

Furthermore, as the PCM spackle to be tested must be applied to a surface as support for the material, it was chosen to use the same type of gypsum board that served as a reference sample. This induced a thermal resistance network as shown in figure 2.18. Here, k_{pcm} will be k_0 to be used in equation 2.3 and k_{ref} was substituted for k_{gyp} .

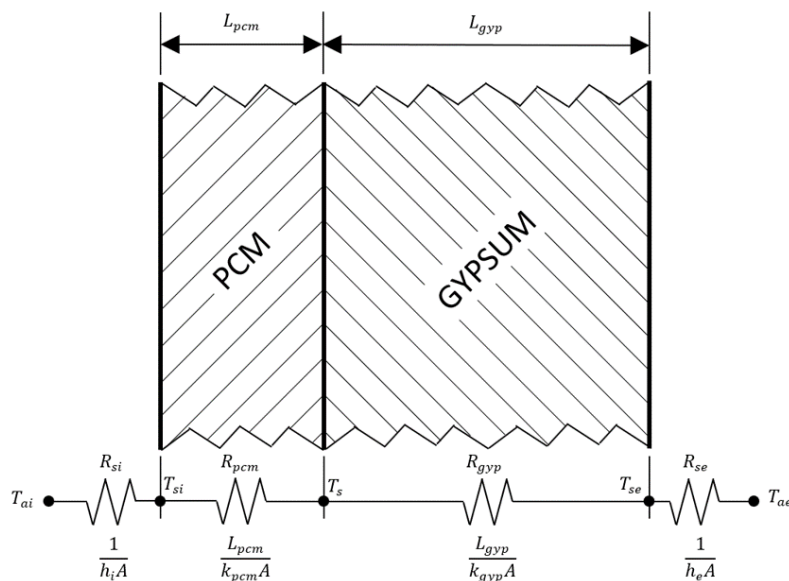


Figure 2.18: Thermal resistance network.

The measured thermal conductivity coefficient, k_0 , could be calculated by the 1D steady-state equation for heat transfer

$$\Phi_p = \frac{\Delta T}{R_{\text{total}}} \quad (2.4)$$

Where R is the thermal resistance, and the total resistance is defined by $1/R_{\text{total}} = 1/R_i + \dots + 1/R_n$

From figure 2.18, it can be seen that R_{total} can be defined in different ways. The measurements performed in the experiments allowed two ways to calculate the thermal conductivity.

The simplest way is to hold the surface temperatures on both sides of the specimen as boundary conditions, such that the total thermal resistance will be $1/R_{\text{total}} = 1/R_{\text{pcm}} + 1/R_{\text{gyp}}$. In this case, k_{pcm} will be the only unknown parameter in equation 2.4. This would be the primary calculations performed to calculate the thermal conductivity of the PCM spackle.

Another possibility is to hold the air temperatures at each side of the specimen as boundary conditions, such that $1/R_{\text{total}} = 1/R_{\text{si}} + 1/R_{\text{pcm}} + 1/R_{\text{gyp}} + 1/R_{\text{se}}$. Here, R_{si} and R_{se} are the surface resistances on each side of the specimen. The surface resistance is a combined effect of convective and radiative heat transfer at the surface, and the combined heat transfer coefficient is defined as $h = h_c + h_r$. The surface resistance on the interior side of the specimen is therefore $R_{\text{si}} = 1/h_i = 1/(h_{c,i} + h_{r,i})$, and on the exterior side; $R_{\text{se}} = 1/h_e = 1/(h_{c,e} + h_{r,e})$. This method is much more sensitive to errors in measurements and calculations, as especially convection is a complex mechanism due to effects such as turbulent air flows.

Nonetheless, the measurements were performed in the experiment so that the surface resistances could be estimated. It was reasoned that it could be of assistance in case insight was needed in explaining unexpected results from the experiment.

Design of a guarded hot box system

Adjacent to the west side of the climate room is another insulated room with a cooling unit installed. An opening of $(1.2 \times 1.2)m^2$ was cut out in the partitioning wall between the rooms, where the specimen would be mounted. Figure 2.19 show how the climate room and the cooling chamber were adopted as the guarded hot box system described ISO:8990 in figure 2.17.

The cooling unit had a powerful fan, allowing for good air circulation in the cold box. In the guard box, the ventilation system maintained a stable temperature with a high air flow rate. It was aimed at maintaining the same air temperature in the guard box as in the metering box, as this would limit the heat transfer between the two.

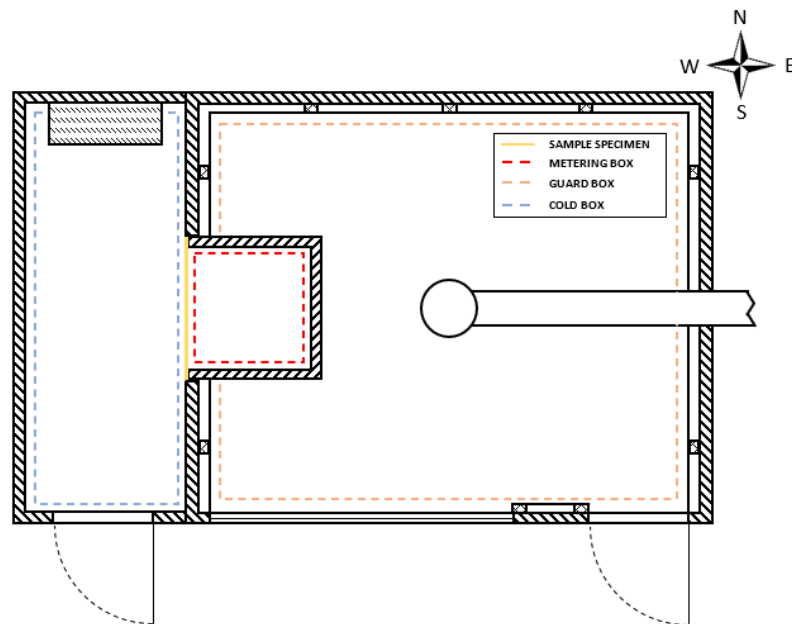


Figure 2.19: Design of the guarded hotbox system. Plan view.

The metering box was built with walls of $100mm$ plates of EPS material with low thermal conductivity. The box was built to dimensions as shown in figure 2.20. All EPS plate connections were sealed with Tec7 sealant both on the inside and the outside. Inside the metering box, two electrical fans were used to create a forced convection flow across the specimen surface. The placement and angling of the fans were adjusted several times to find the set up that provided the highest air flow rate across the specimen. Four incandescent light bulbs were placed in aluminium ducts as heat sources. Both the fans and the bulbs were connected to separate dimmers so the power output could be adjusted.

On both sides of the specimen, guard plates were placed close to the specimen to guide the airflows across the surface and to shield the specimen from thermal radiation from electrical equipment. Both plates can be seen in figure 2.21g and 2.21i. The guard plate in the cold box room was a large gypsum board of $(1.2 \times 2.4)m^2$, placed approximately $15cm$ from the specimen surface. The guard plate in the meter box was made of cardboard, cut to fit the entire length of the meter box, but allow space for air flow at the top and bottom. This plate was placed approximately $10cm$ from the specimen surface. Furthermore, this guard plate was

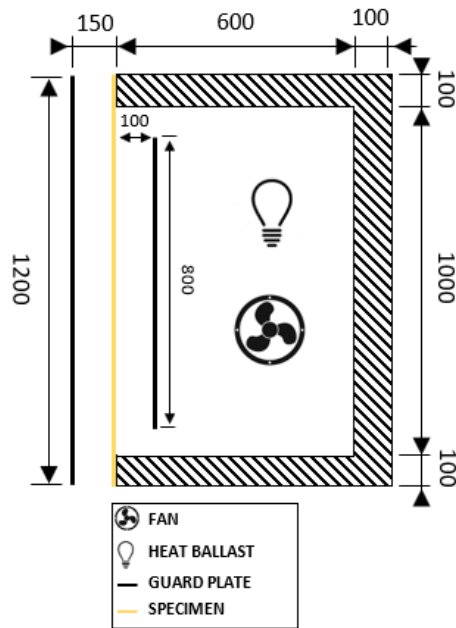


Figure 2.20: Metering box setup. Section view.

covered by aluminium foil. The purpose of this was to shield the specimen and its thermocouples and the guard plate it self due to excessive radiation from the light bulbs.

As shown in figure 2.21a, b and c, the metering box was pushed against the specimen and held tight by a strong tape which was fixed to the wall with metal plates. Gaps between the metering box and the wall were air tightened with tape, and rubber window gaskets were used to seal the connection with the specimen surface. Wires for electrical equipment entered the box by a hole in the back which was sealed with mineral wool insulation.

In figure 2.21d, e and f, the space between the guard plates and the specimen surface is shown, and it can be seen how thermocouples and anemometers are placed. Also, thermal covers are applied to the thermocouples that are exposed to the radiation from the light bulbs.

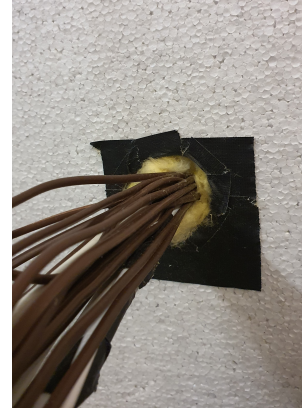
In figure 2.21g, h and i, 3D views are used to show an overview of the setup in the cold box, metering box and a sectioned view of the entire test setup.



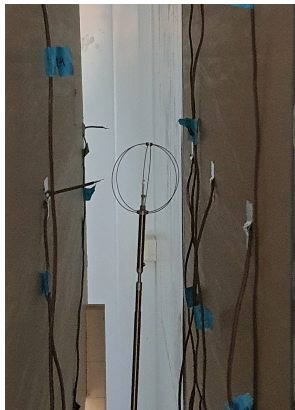
(a)



(b)



(c)



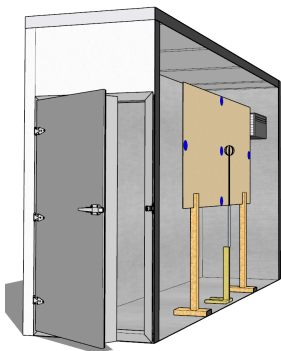
(d)



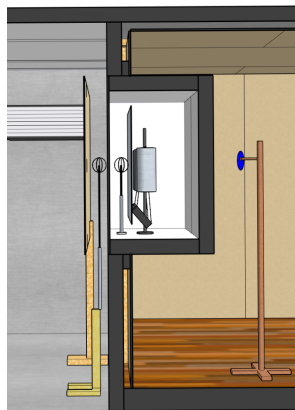
(e)



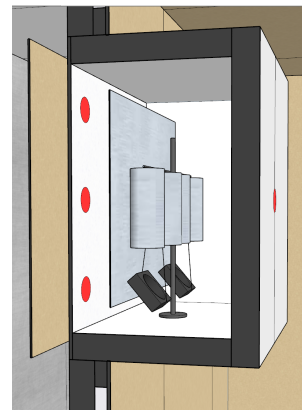
(f)



(g)



(h)



(i)

Figure 2.21: Details of the guarded hot box design.

Instrumentation and measurements

Thermocouples were used to measure surface and air temperatures, and omnidirectional anemometers were used to measure air velocity over the surface of the specimen. The exact positioning and further explanations of each sensor is detailed in appendix A. The main parameters measured to calculate the thermal conductivity were surface temperatures at each sides of the specimen and the electric power applied to the lights and fans inside the metering box. The purpose of all remaining parameters that were measured were only to assist in the analysis and included air temperatures in each box, surface temperatures of the metering box and air velocity across the specimen.

ISO:8990 comments that uniform heat flux across the specimen is difficult to achieve in practice due to the nature of the heat losses along the perimeter of the specimen, temperature stratification and material imperfections. This results in varying temperature differences between the hot and the cold side of the specimen. For that reason, average surface temperatures on both sides of the specimen should be used. In order to calculate a representative average, it was chosen to use a total of eighteen thermocouples, where nine thermocouples on each side of the specimen were placed in a symmetric grid directly adjacent to each other. Figure 2.22 show the thermocouple placements for one of the sides.

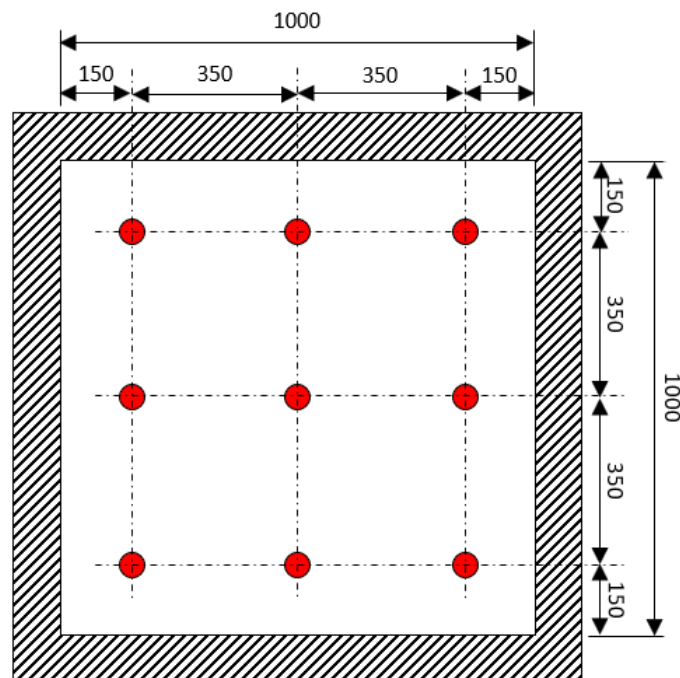


Figure 2.22: Placement of thermocouples on the specimen surface. Section view.

Measurement plan

Table 2.8 shows a complete list of all measurements that were performed during the experiment. As for accuracy of equipment, table 2.7 is also valid for this experiment.

Table 2.8: Measurement plan of the guarded hot box experiment.

| Surface temp, specimen | | | | Surface temp, metering box | | | | | |
|---------------------------------|--|--|---|---|--------------|---|--|--|-----------|
| Position | Thermocouple hot side | Thermocouple cold side | Purpose | Parameter | Position | Thermocouple inside | Thermocouple outside | Purpose | Parameter |
| Top Sth | 2-17 | 1-18 | Calculate heat transfer by conduction through specimen. | Φ_{cond} k_0 $h_{r,i}$ $h_{r,e}$ | South | 2-11 | 2-23 | Calculate heat loss by conduction through metering box | Φ_3 |
| Top Cnt | 2-12 | 1-17 | | | North | 2-7 | 2-22 | | |
| Top Nrth | 2-10 | 1-8 | | | East | 2-4 | 2-20 | | |
| Mid Sth | 2-14 | 1-24 | | | Bottom | 2-5 | 2-21 | | |
| Mid Cnt | 2-1 | 1-20 | | | Top | 2-18 | 2-19 | | |
| Mid Nrth | 2-6 | 1-15 | | | | | | | |
| Btm Sth | 2-8 | 1-9 | | | | | | | |
| Btm Cnt | 2-9 | 1-13 | | | | | | | |
| Btm Nrth | 2-3 | 1-19 | | | | | | | |
| | | | | | | | | | |
| Air temp and velocity, cold box | | | | Air temp and velocity, metering box | | | | | |
| Position | Thermocouple | Purpose | Parameter | Position | Thermocouple | Purpose | Parameter | | |
| North | 1-6 | Assistive calculation of heat transfer by convection and radiation on cold side of specimen. | $\Phi_{\text{conv,e}}$ $h_{c,e}$ $h_{r,e}$ | Center high | 2-13 | Assistive calculation of heat transfer by convection and radiation on hot side of specimen. | $\Phi_{\text{conv,i}}$ $h_{c,i}$ $h_{r,i}$ | | |
| Center high | 1-11 | | | Center mid | 2-2 | | | | |
| Center mid | 1-16 Anemometer | | | Center low | 2-15 | | | | |
| Center low | 1-12 | | | | | | | | |
| South | 1-2 | | | | | | | | |
| Air temp, guard box | | | | | | | | | |
| Position | Thermocouple | Purpose | Parameter | | | | | | |
| Center mid | 2-16 | Maintain stable and equal air temperature as in metering box | None | | | | | | |
| Power | | | | | | | | | |
| Equipment | Measuring device | Purpose | Parameter | | | | | | |
| Lights, fans | Digital power meter Digital clamp meter Analog ohm meter | Measure supplied power to the metering box | Φ_p | | | | | | |

Challenges with heat transfer with specimen

While setting up the experiment, some problems occurred with achieving good heat transfer between the circulating air inside the metering box and the specimen. By applying some solutions on the spot and observing test runs of the experiment, it was reasoned that it would still be possible to achieve valid results in spite of some conditions being subpar and not in strict accordance with the standard. This chapter contains an assessment of the problem and its potential impact on the results. Data from the results are used to calculate heat transfer coefficients.

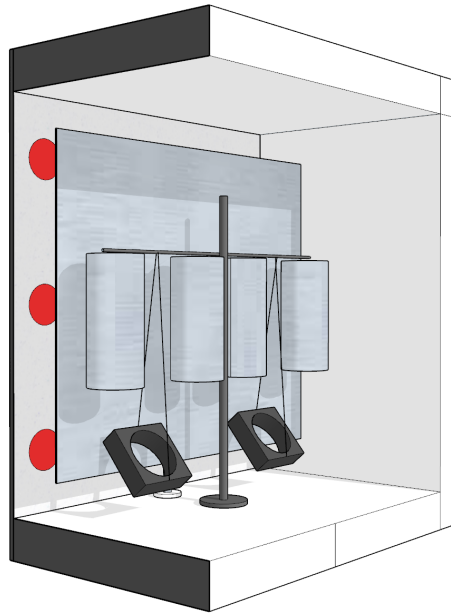


Figure 2.23: The final setup of equipment inside the metering box.

A limiting factor in finding a satisfying solution was the available equipment on hand and the very porous material of the meter box walls, not being able to support any fastening mechanism for equipment. The main problem seemed to be the electric fan which proved insufficient to create good air circulation inside the box. When setting up the experiment, a very low air velocity of $0.1m/s$ was measured which indicated poor convective heat transfer with the specimen. This led to a high temperature difference between the top and bottom surface of the specimen, as well as making it difficult to maintain equal air temperatures inside the metering box and the outside room (guard box) to limit the heat loss in this direction, and still achieve the desired surface temperature to be tested. The standard does not mandate any lower limit to the convection rate, but poses some requirements to the heat loss in this direction and the temperature variation across the surface.

In trying to improve the convection heat transfer rate, one more fan of the same size was added and different positions were tested, improving the air velocity to $0.3m/s$. The best position was found by trial and error is depicted in figure 2.23, but the standard recommends a much higher fidelity in guiding the air flow over the specimen surface than this.

The setup in figure 2.24 show that the fans were placed low at an angle to pull air out from the opening beneath the guard plate. The sides of the guard plate were sealed against the walls of the box with tape. The idea was that extracting air from underneath the guard plate would in turn create a low pressure area around the opening above the guard plate, forcing the air to circulate over the specimen. This worked better than the initial setup which had one fan in the middle of the box.

A problem with this setup was that natural convection would counteract the flow over the specimen surface to some degree. It was desired to try to reverse the flow by placing the fans at the top instead, but no solutions were found to mounting the fans in this position. It must also be realised that the air flow inside the box is most likely of a highly complex mixed laminar and turbulent regime, where the effect of vorticies would limit the air flow in going uniformly in the desired directions. A better setup would be to have larger fans, and a proper enclosure between the guard plate and the fans such that all the air pushed by the fan would be forced to flow over the surface.

The convective h.t. coefficient was calculated using a correlation which takes into account the interplay of forced and natural convective flow in a mixed laminar and turbulent regime. D.Damien et. al [29] developed the equation in a study of the effect of convective heat transfer over vertical PCM walls.

$$h = \left\{ \left[\left(4.54 \left(\frac{|V|}{H} \right)^{1/2} \right)^3 \pm \left(1.335 \left(\frac{|\Delta T|}{H} \right)^{1/4} \right)^3 \right]^2 + \left[\left(5.41 \left(\frac{|V|^4}{H} \right)^{1/5} \right)^3 \pm \left(1.293 (|\Delta T|)^{1/3} \right)^3 \right]^2 \right\}^{1/6}$$

where V is the mean vertical air velocity in front of the wall, H is the height of the vertical wall and ΔT is the average temperature difference between the air and the surface. The \pm signs will turn positive if the forced flow is in the same direction as the natural convection, and negative if otherwise.

As necessary measurements were in place for the experiment, the convective h.t. coefficient could be calculated to be $h_c = 2.5W/(m^2 \cdot K)$ for this case, where it could have been improved to $h_c = 3.4W/(m^2 \cdot K)$ if the flow could be reversed to have assist from natural convection. Still, an increase in $0.9W/(m^2 \cdot K)$ would probably not have made a large difference altogheter.

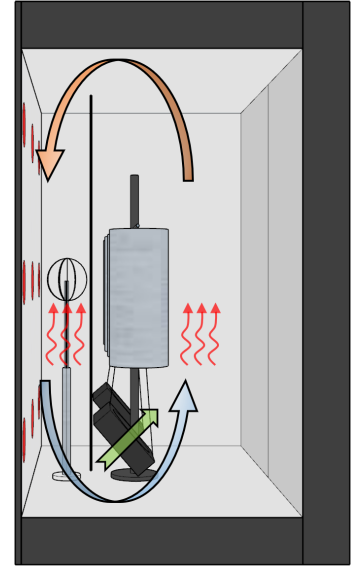


Figure 2.24: Direction of forced air circulation inside the box. Red arrows indicates direction of natural convection.

A realization was made in hindsight that could have proved a larger effect on the heat transfer. The standard recommended electrical resistance devices as heat gain mechanism, and to cover them thoroughly with insulated reflective shields to protect both the specimen surface and the guard plate from thermal radiation. As light bulbs were used as heat ballasts in this case, they could not be covered sufficiently due to risk of fire, so it was instead decided to cover the guard plate with aluminium foil as the light spread inside the box was immense. In effect, the radiative share of the heat transfer with the specimen was significantly reduced. It could have assisted considerably in the total heat transfer due to the problems with convection that occurred.

Assuming the guard plate to have approximately the same surface temperature as the surrounding air, emissivity of aluminium foil of $\epsilon = 0.04$ and a viewfactor of 1 due to the large size and close placement of the plate, the radiative h.t. coefficient was only that of $h_r = 0.2W/(m^2 \cdot K)$. If the guard plate instead was painted matte black, and assuming the emissivity could be raised to at least $\epsilon = 0.90$, the h.t. coefficient could be raised to $h_r = 4.2W/(m^2 \cdot K)$. In reality it would be a little less due to the air and surface temperature being lowered with more heat transfer. However, as both radiative and convective heat transfer are weighted equally in the total heat transfer coefficient, as $h_{tot} = h_r + h_c$, this solution could have made for a significant improvement.

Impact on the experiment

Although the problems aforementioned was not amended, it was still possible to achieve the desired surface temperatures for the three cases presented earlier in table 3.1, but higher temperatures inside the metering box was needed. The problem lead to a temperature difference of $10K$ between the air in the metering box and the guard box (surrounding room) for the worst case. Also, the problem with high surface temperature variance between top and bottom of the specimen was still the case.

However, there was always expected to be a significant heat loss due to thermal bridges in the system after all. This was depicted in figure 2.17. It was reasoned that as long as a good replication of thermal conditions could be achieved, this additional heat loss would just add to the bulk of heat losses which the calibration constant would compensate for. Moreover, thermocouples were placed both on the inside and the outside at each of the metering box walls, which could make it possible to analyse the heat losses further if needed. Lastly, having nine thermocouples on each side of the specimen, it was reason that a representative average surface temperature could be calculated.

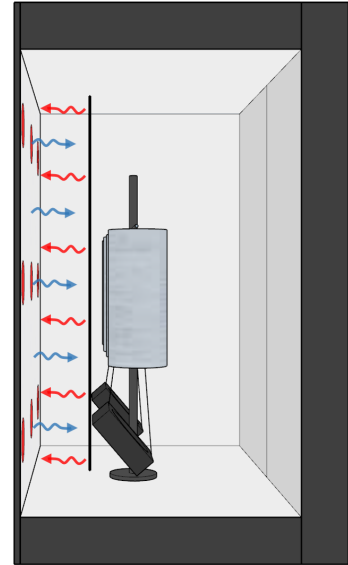


Figure 2.25: Radiative heat exchange between specimen and guard plate was not utilized. Section view.

Execution of the experiment

The PCM spackle was tested during three temperature ranges associated with the different states of matter for the PCM to see if any changes in thermal conductivity could be observed. These cases are listed in table 3.1.

Table 2.9: Experiment cases to be performed of the PCM spackle.

| # | Case | Temperature range |
|---|---------------|-------------------|
| 1 | Solidified | <20 C |
| 2 | In transition | 20 - 24 C |
| 3 | Melted | >24 C |

As each case needed an accompanied reference test to calibrate heat losses, a total of 6 test runs would be performed. The main priority of the experiment was to achieve replication of thermal conditions for each pair of cases, as this would be key for the calibration constant to be valid. To achieve this, the following conditions were determined to be held constant during each pair of cases:

- The set point temperature for the guard box room and the cold box room.
- The surface temperature on the hot side of the specimen.

This would lead the varying parameters to be the power supplied to the metering box and the temperature difference between the hot and cold surface of the specimen. By trial, this was found to be the best parameters to vary as if any of these were tried to be held constant, a mismatch between the desired surface temperature and the actual surface temperature could occur.

Furthermore, care was taken to achieve stable conditions for each configuration, meaning to find a balance between the power supplied and desired surface temperature without having the temperatures continue to develop in one direction. In practice, each run took in the order of 3 hours or more as a small incremental adjustment to the supplied heat would lead the surface temperatures to develop very slowly before landing on a balance point. When stable conditions were achieved, measurements were logged for another 30 minutes.

The experiment was carried out in the following sequence:

1. The reference specimen of known thermal conductivity was mounted in the guarded hot box system to calibrate heat losses.
2. For each of the reference cases, a critical measuring point on the hot side of the specimen surface was determined. For example; for case 1, the critical point would be the thermocouple being closest to 20°C. The power supplied to the metering box was logged after thermal stability was achieved for each of the cases.
3. The reference specimen was replaced by the PCM spackle specimen. The same tests were performed, and the temperature reading for the critical point were matched with the reference experiment for each case. The power supplied to the metering box was logged after thermal stability was achieved.

2.3 Numerical simulations

IDA Indoor Climate and Energy (IDA-ICE) 4.8 software was used to build a numerical simulation of an office building with a model of the PCM spackle that was validated against experimental results. This study will focus on how night ventilation (NV) strategies best can utilize the energy savings potential of the PCM spackle. This chapter will first focus on the validation of the PCM spackle model, and then describe the method for the energy analysis.

Simulation tool

IDA-ICE was chosen as a simulation tool as it fits all criteria for the topics under investigation in this study. It is a multi-zone building simulation software where all building parameters can be controlled through intuitive menus, making it easy to formulate a numerical simulation model through the graphical interface. A comparison between capabilities in different simulation tools showed IDA-ICE to have a comprehensive tool-box of models for all important parameters needed for complete energy assessment of building performance [30].

Most importantly, it has a partial enthalpy mathematical model for PCM inclusion in the building envelope and internal constructions. Not many studies have validated this model but two have been found, although not being of peer-reviewed published work. Cornaro et al. [31] validated the model to be accurate with a RMSE and NRMSE of $1.57 - 1.83^{\circ}C$ and $5.0 - 5.1\%$, respectively, in an validation of experimental results from PCM incorporated solar test boxes for a conference paper. S.Wirak [32] validated the model to be very accurate with a RMSE and NRMSE of $0.41^{\circ}C$ and 1.80% , respectively, in a hot box experiment for his MSc thesis.

For the design of NV strategies, advanced custom control schemes of e.g. window openings and mechanical ventilation systems can be created with macros. IDA-ICE can model dynamic flow rates through window openings based on the differential in ambient and internal air pressures, calculated from data of temperatures, wind over the facia and moisture contents from energy plus climate files (EPW). This makes it possible to couple the inclusion of PCM spackle with realistic NV strategies. More comparisons of PCM coupled with natural, mechanical or natural-mechanical hybrid strategies are of high interest in the field. From an extensive overview by E.Solgi in his doctorate thesis of studies on this particular topic, it has been noted that none studies have explored the topic with IDA-ICE whenever building simulation tools are used [18]. A tendency is to use TRNSYS, EnergyPlus and ESP-R but IDA-ICE have the same capabilities as these with more advanced design of natural and hybrid systems as of comparisons made in Crawley's study [30]. Modelling natural NV systems are a complex issue as the influential parameters are of such dynamic behaviour. Pfafferott et al. commented in a thorough study on validating experimental results of NV in an office building with both parametric and ESP-R simulation models that *"Surely, even more design tools are available. Self-evident, building simulation programmes can be used favourably for the design of free and mechanical night ventilation."* [33].

An investigation with IDA-ICE on this topic can be an interesting addition to the field as most studies have used parametric models or other simulation tools.

Validation

Modelling the climate room experiment in IDA-ICE

The climate room was modelled in IDA ICE with emphasis on designing the thermal environment as close to the real scenario as possible. The goal was to build a realistic model of the climate room which could accurately simulate the reference experiment, i.e. before the PCM spackle was applied to the room. Then without changing any parameters, the PCM spackle would be applied to the model at the same amounts as in the real experiment to validate the PCM spackle model.

All parameters that were measured in the climate room experiment were implemented in the model. This includes the ventilation schedule and actual supply temperatures, internal heat loads and the surrounding temperatures outside of the climate room. Some parameters contributing to the energy balance of the model were not measured and the true value was not strictly known. This was accounted for by putting in an expected value, and slightly adjust the values so the simulation would match the reference experiment. This included the true ventilation air flow rate, radiative emissivity of the internal heat loads and the overall U-value due to the effects of thermal bridges and impurities in the building construction. However, it was found that the ventilation air flow rate was the most uncertain parameter, and expected values for the other parameters yielded accurate results.

Adjusting the parameters to achieve a good replication of the thermal behaviour is a common method in retrofitting energy analysis with simulation tools, described by ASHRAE as the "Calibrated simulation approach" [24],[34].



Figure 2.26: 3D rendering of the climate room model in IDA-ICE.

Building body and ventilation

All components of the building body are based on the true layer composition of the construction parts, and are listed in table 2.10. The ventilation air flow rates was adjusted to match the experimental results.

It was found after the experiments that the air handling unit did not provide the initial set up air flow rates, but deviated by approximately $\pm 20\%$ whenever measurements were taken. This was likely due to effects such as low fan speeds, imbalance when night/day settings switched and outdoor wind through the ducts. A resulting inaccuracy in the IDA-ICE model can be seen in figure 2.27 where the night ventilation flow rate provided slightly more cooling of the room. The air flow rates was therefore adjusted in IDA-ICE so that the temperature development inside the room would match better with the experimental results. The resulting values are shown in table 2.11.

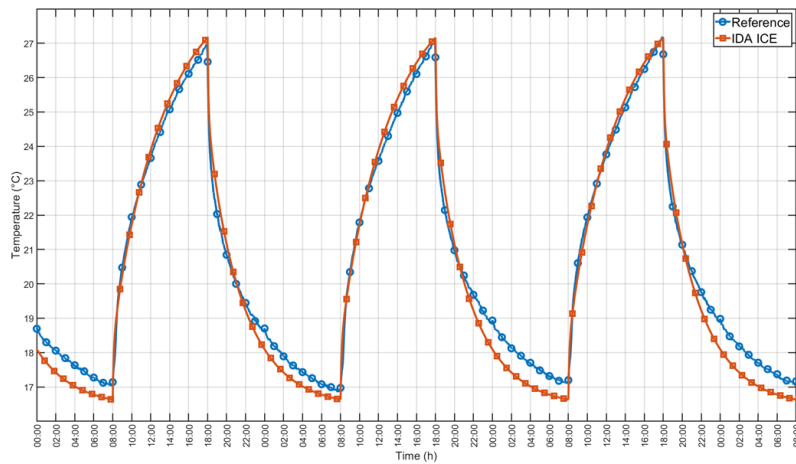


Figure 2.27: Air flow rates providing too much cooling during night.

Table 2.10: Input data for the building body.

| Component | Surface area m^2 | U-value $W/(m^2 \cdot K)$ | Layer | λ $W/(m \cdot K)$ | t mm | C_p $J/(kg \cdot K)$ | ρ kg/m^3 |
|-------------------|-----------------------|------------------------------|------------|------------------------------|-------------|---------------------------|--------------------|
| Walls, ceiling | 44 | 0.22 | Gypsum | 0.22 | 12.5 | 1090 | 970 |
| | | | Air in gap | 0.17 | 48 | 1006 | 1.2 |
| | | | Aluminium | 218 | 1 | 900 | 2700 |
| | | | Polyuretan | 0.022 | 100 | 1400 | 30 |
| | | | Aluminium | 218 | 1 | 900 | 2700 |
| Floor | 13.5 | 0.24 | Wood | 0.14 | 13 | 2300 | 500 |
| | | | Aluminium | 218 | 1 | 900 | 2700 |
| | | | Polyuretan | 0.022 | 100 | 1400 | 30 |
| Door | 2 | 0.64 | Aluminium | 218 | 1 | 900 | 2700 |
| Window | 4 | 0.78 | | | | | |

Table 2.11: Input data for the ventilation system.

| Setting | Air flow rate in $m^3/(h \cdot m^2)$ | Air flow rate out $m^3/(h \cdot m^2)$ | Supply air temperature $^{\circ}C$ | Schedule |
|---------|---|--|---------------------------------------|---------------|
| Day | 135 | 135 | 18.8 | 08:00 - 18:00 |
| Night | 230 | 230 | 14.3 | 18:00 - 08:00 |

Heat gains

The heat gains were modelled in IDA-ICE to match its experimental counterparts as closely as possible. For example, in the experiment, external heat gain from the sun through a window was emulated with a heating mat placed a few centimeters from the climate room window with aluminum foil attached to the inside of the window to minimize the heat loss by radiation to the surrounding room. This was replicated in IDA-ICE by placing an electric radiator of the same surface area 5 centimeters from the wall, which was given aluminum foil surface properties in the area behind the radiator.

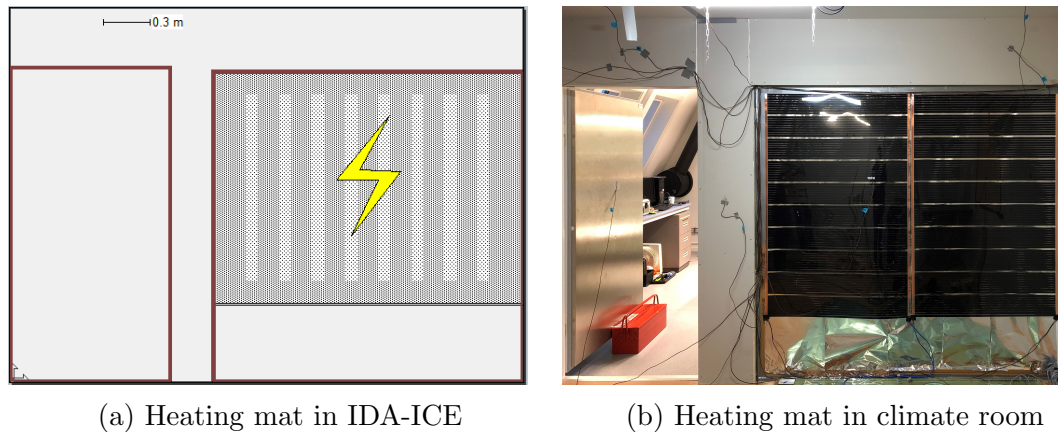


Figure 2.28: Modelling of the heating mat used to emulate solar gain in the experiment

The lights that were placed in the ceiling in the experiment were given the same size, placement and bulb properties in the IDA-ICE model as well. As the rest of the heat gains in the experiment were built with incandescent light bulbs placed inside metal tubes painted with a matte black finish, the internal gains were modelled as electrical equipment with a high emissivity constant. A bulk of $40W$ for extra heat gains were also added to include the measuring equipment, and some heat gain that was observed to come from the electrical panel inside the room. This was based on data from the printed labels on the equipment, and slight adjustments so that the temperature curve would match with the experiment.

Table 2.12: Input data for internal heat gains.

| Component | Size W | IDA-ICE model | Luminous eff. lm/W | Convective fraction [-] | Longwave emissivity [-] | Schedule |
|------------------------|-------------|--|-------------------------|----------------------------|----------------------------|---------------|
| Sun | 200 | Electric radiator of 3 m ² | | | 0.9 | 08:00 - 18:00 |
| Lights | 2 x 28 | Lights | 75.7 | 0.3 | | 08:00 - 18:00 |
| Occupants | 2 x 90 | Electrical equipment | | | 0.9 | 08:00 - 18:00 |
| Computers | 2 x 60 | Electrical equipment | | | 0.9 | 08:00 - 18:00 |
| Measuring equipment | 40 | Electrical equipment | | | 0.9 | 24h |

Validating the climate room model before addition of PCM spackle

Figure 2.29 shows the simulated results versus the experimental results of the reference experiment, and it can be seen that the curves closely match. IDA-ICE calculates mean air temperature in the room, and to compare the results an average room temperature in the reference experiment was calculated based on temperature readings at different heights as mentioned in chapter 2.1.

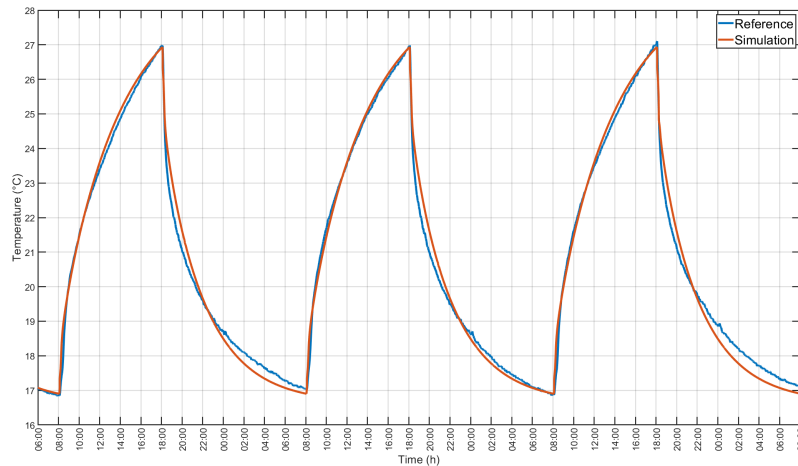


Figure 2.29: Simulated vs. experimental results for the reference experiment.

Validating the PCM spackle model

To validate the PCM spackle model of IDA-ICE, none of the parameters in the reference model was changed. Just like in the true experiment, the PCM spackle was added as a layer to the surfaces of the walls and ceiling in thicknesses of 1.7mm and 2.1mm , respectively. IDA-ICE's PCMwallH module was used to model the PCM spackle material data, where a partial enthalpy method is used to calculate the changing heat capacity of the material with temperature. Enthalpy data was added based on results from the DSC-test of the PCM spackle. Although results have not been presented yet, the guarded hot box experiment provided values for the thermal conductivity of the material. The density of the PCM spackle was provided by Gyproc. The input data used for the PCM layer is shown in table 2.13.

Table 2.13: Properties of PCM layer in IDA ICE

| Property | Value |
|---|--|
| Density, ρ | 970 kg/m^3 |
| Thermal conductivity, λ_{solid} | $0.08\text{W}/(\text{m} \cdot \text{K})$ |
| Thermal conductivity, λ_{liquid} | $0.08\text{W}/(\text{m} \cdot \text{K})$ |
| Heat capacity, C_p | Function of surface temperature (figure 1.1) |

To validate the accuracy of the PCM spackle model, the average room temperature in all corresponding time steps in the experiment will be compared to the simulation. A linear regression analysis was performed where the coefficient of variation of the root mean square error (CV_{RMSE}) and the coefficient of determination (R^2) was calculated after equation 2.5 and 2.6, respectively. The CV_{RMSE} value is a measure of the predictive capabilities of the model, while the R^2 value explains how close the simulated data was to the measured regression line in the analysis.

$$CV_{RMSE} = \frac{1}{y_m} \sqrt{\left(\sum_{i=1}^n \frac{(y_i - \hat{y}_i)^2}{n} \right)} \quad (2.5)$$

$$R^2 = 1 - \frac{(\sum y_i - \hat{y}_i)^2}{(\sum y_i - y_m)^2} \quad (2.6)$$

Where y_m is the mean of measured values, \hat{y}_i the actual measured value, y_i is the simulated value and n is the number of data points.

Optimization of night ventilation strategies for energy savings potential

A work environment with cubicles in an office building situated in Oslo, Norway, was modelled to simulate the PCM spackle in a realistic environment. Although studies have shown that the use of PCM in buildings can give significant energy savings for cooling needs, it's vital to design a strategy where the PCM can release the energy at night which it has absorbed during the hottest part of the day. The aim for this analysis was to couple the use of PCM spackle with different night ventilation (NV) strategies and analyze energy savings potential by varying some key influential parameters for both PCM and NV efficiency. The parameters chosen to vary was NV air flow rates, PCM thickness and NV strategy and control mechanisms.

This chapter will first describe the design of the office building before detailing the NV strategies and analysis setup.

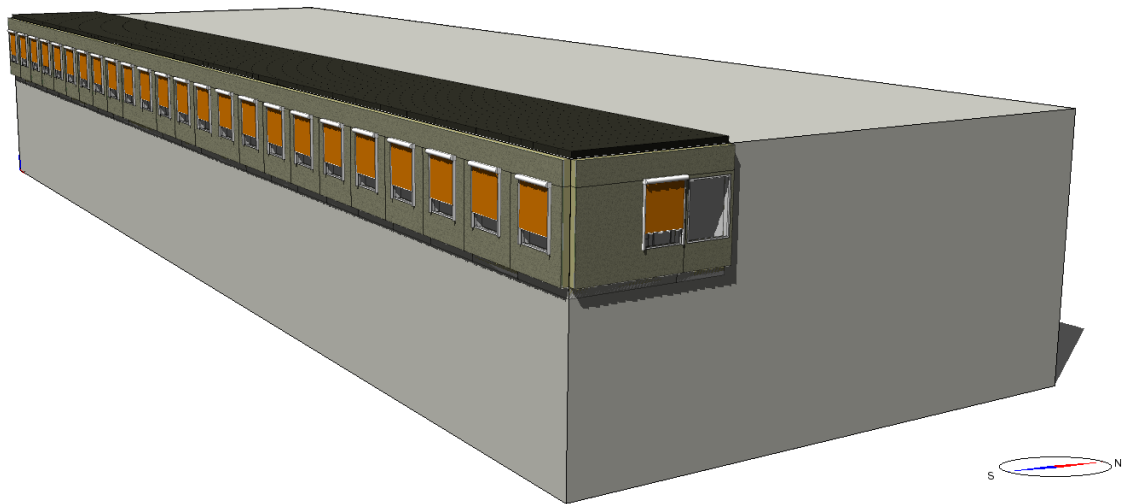


Figure 2.30: Part of an office building fitted with cubicles.

Description of the building and TEK-17 validation

In choice of building design, it was desired to not limit the analysis too much to a particular layout or energy efficiency. A simplistic design was therefore prioritized, and the minimum energy requirements in the Norwegian building code (TEK-17) was chosen as a baseline for the building. In that regard, the building can be said to be a TEK-17 building by design and the results of the analysis can more conveniently be linked to standardised building criteria.

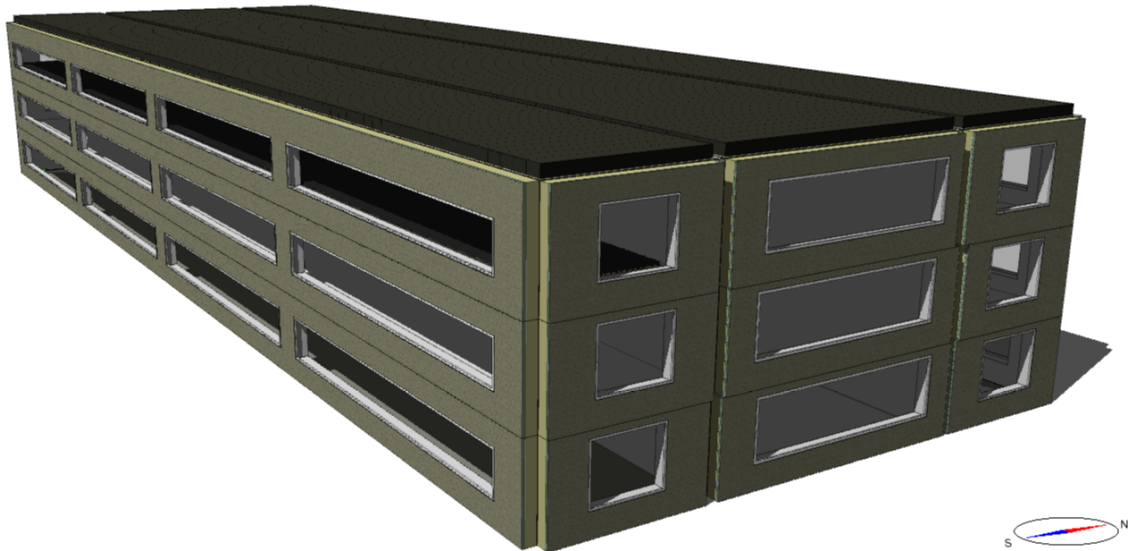


Figure 2.31: The whole office model in use for compliance check.

In performing the compliance check for energy efficiency, a whole model of the building was checked with Simien, which is a dynamic energy simulation software for buildings also having a standardised TEK-17 compliance check module. An IDA-ICE version of the building model which was implemented into Simien is shown in figure 2.31. The compliance check involves controlling the buildings total net energy usage against allowed budgets defined in TEK-17. This is performed using standardized values for climate, indoor set point temperatures, internal heat loads and operating hours from the norwegian standard, NS-3031. These values are not meant to represent realistic use of the particular building, but are a means to standardize all buildings and serve as a common reference point for comparisons.

The building body was designed with common building strategies of today in mind, where the use of prefabricated components are a cost effective solution for building entrepreneurs. Modern buildings in Norway are commonly built with hollow core concrete slabs for roof and floor separators, and lightweight insulated constructions for external and internal walls. Structural support is limited in size to allow for flexibility of change. The intricate build up of these particular construction parts was not prioritized to perfect for the validation, as the important factors for energy efficiency for these construction parts are the heat capacity of the building mass and the thermal resistance of the external shell. This is dominated by the amount of concrete used and insulation thickness. The material data used here are listed in table 2.14.

As the building have a large total window area, external solar shading was needed in order to pass the total net energy demand requirement. Diffusive screens were

Table 2.14: Building materials used in model

| Material | ρ [kg/m^3] | C_p [J/kgK] | λ [W/mK] |
|-----------------------------|---------------------|-------------------|----------------------|
| Insulation | 20 | 750 | 0.036 |
| Concrete | 2300 | 1050 | 1.70 |
| Insulated wooden frame wall | 92 | 2010 | 0.052 |

set to be drawn when solar flux on the particular facade exceeded $100W/m^2$. A building of this size normally have cooling supplied by ventilation, or other complex systems. When this is the case, as noted in NS-3031 annex A, energy usage for cooling should be simulated dynamically. This was done with the IDA-ICE model with a yearly energy simulation in Oslo, Blindern.

All input data used for the compliance check, both in Simien and IDA-ICE are listed in table 2.15. The specific net energy demand of the building proved to be $112.5kWh/(m^2 \cdot year)$ where as the requirement is maximum $115kWh/(m^2 \cdot year)$, as shown in table 2.16. To emphasise again, the real energy usage would be considerably lower due to the conservative and standardised input parameters used for TEK-17 validation.

Table 2.15: Input data for compliance check

| Ext. component | Surface area (total) [m ²] | U-value [W/m ² K] | Construction |
|-------------------------|---|---|---|
| External wall | 1500 (incl. windows) | 0.22 | 200 mm insulated frame wall |
| Roof | 1150 | 0.18 | 200 mm insulation, 250 mm concrete slab |
| Slab on ground | 1150 | 0.18 | 200 mm insulation, 250 mm concrete slab |
| Windows (incl. frame) | 624 | 1.20 | Triple layer with external shading screens. $g_{window} = 0.53, g_{system} = 0.27$ $T_{vis,window} = 0.69, T_{vis,system} = 0.23$ |
| Int. component | Surface area (total) [W/m ² K] | Construction | |
| Floor separator | 2300 | 10 mm floor coating, 250 mm concrete slab | |
| Partitioning walls | 1845 | 48 mm insulated frame wall | |
| Other parameters | Value | Int. heat gain | Size [W/m ²] |
| Infiltration, n50 | 1.5 h ⁻¹ | Occupants | 4 |
| Overall thermal bridges | 0.09 W/m ² K | Equipment | 11 |
| Air flow on hours | 8.9 m ³ /h · m ² | Lights | 8 |
| Air flow off hours | 2 m ³ /h · m ² | | |
| Heat regen. efficiency | 0.89 | | |
| COP,heating | 2.3 | | |
| COP,cooling | 2.5 | | |
| SFP | 1.5 kW/(m ³ /s) | | |
| SPP | 0.5 - 0.6 kW/(l/s) | | |
| Set-point heating | 20 °C | | |
| Set-point cooling | 22 °C | | |
| Hot tap water | 5.0 kWh/(m ² · year) | | |
| Operational hours | 07:00 - 19:00 (12/5/52) | | |

Table 2.16: Net energy budget, TEK-17 validation.

| Post | Description | kWh/(m ² · year) |
|-------------------------------|--------------------------------|-----------------------------|
| 1a | Space heating | 17.3 |
| 1b | Ventilation heating | 3.4 |
| 2 | Hot water | 5.0 |
| 3a | Fans | 16.3 |
| 3b | Pumps | 2.0 |
| 4 | Lights | 25.1 |
| 5 | Equipment | 34.4 |
| 6 | Cooling | 15.3 |
| | Exhaust heat pump, regenerated | -10.1 |
| | Exhaust heat pump, auxillary | 3.8 |
| Total net energy demand | | 112.5 |
| Requirement net energy demand | | 115.0 |

Design of an office cubicles environment for analysis

To save simulation times, it was chosen to only fit one section of the building with a realistic interior. The south facing zone of the 3rd floor was fitted with office cubicles, keeping the different components of the building body the same as the validated model. That includes overall U-values, infiltration, thermal bridges, window properties and the solar shading settings. The windows in this section of the building were divided into smaller sized windows for each cubicle, but the total area was kept the same. Although a slight change in window frame area and more connections for thermal bridges, it was reasoned to not play a major importance.

The floor area of the model was $636m^2$, and all other input data for the model are detailed in annex B.

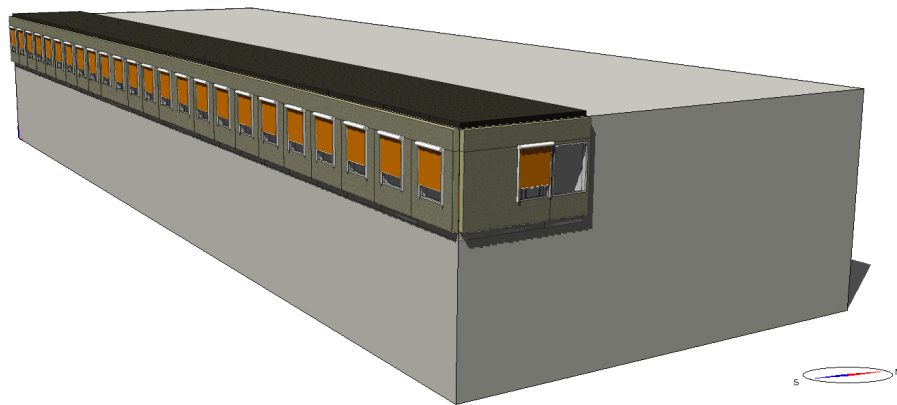
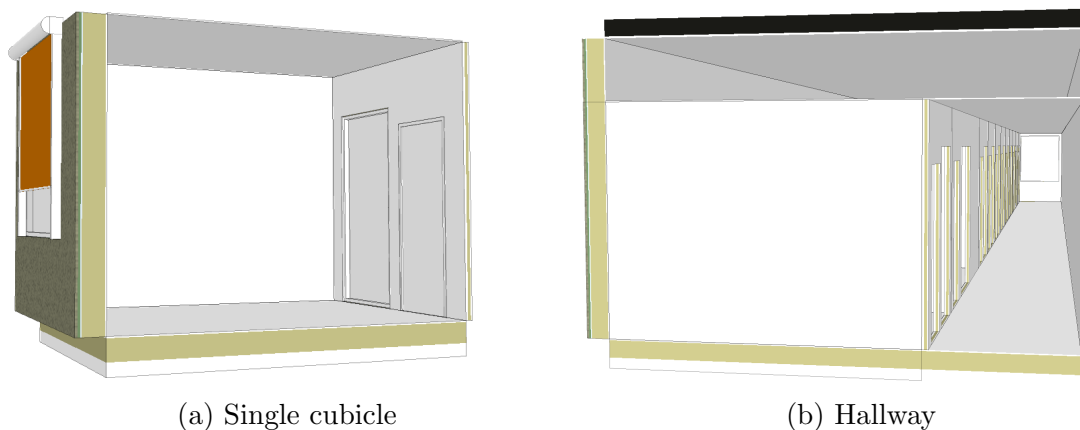


Figure 2.32: Office cubicles fitted to one of the zones in the building

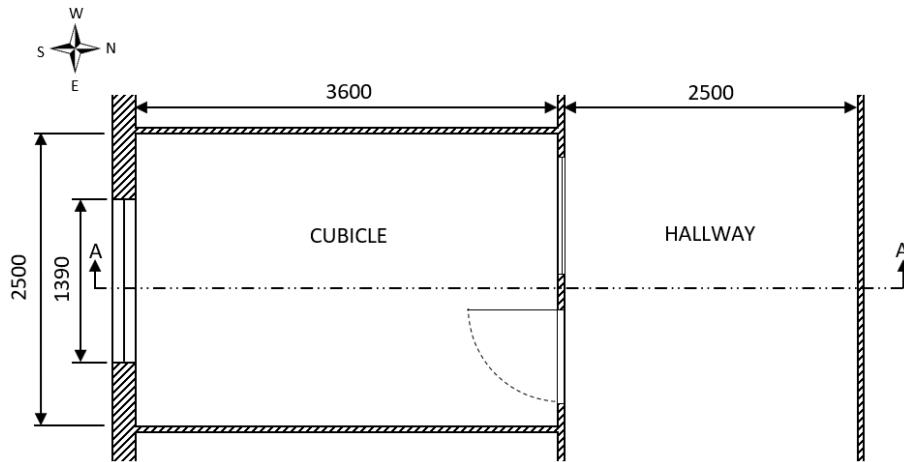
More detail was put into the build up of the construction parts as to model the heat transfer more accurately. All cubicles were of the same design as shown in figure 2.33 and 2.34, where general guidelines from SINTEF Byggforskserien was followed [35].



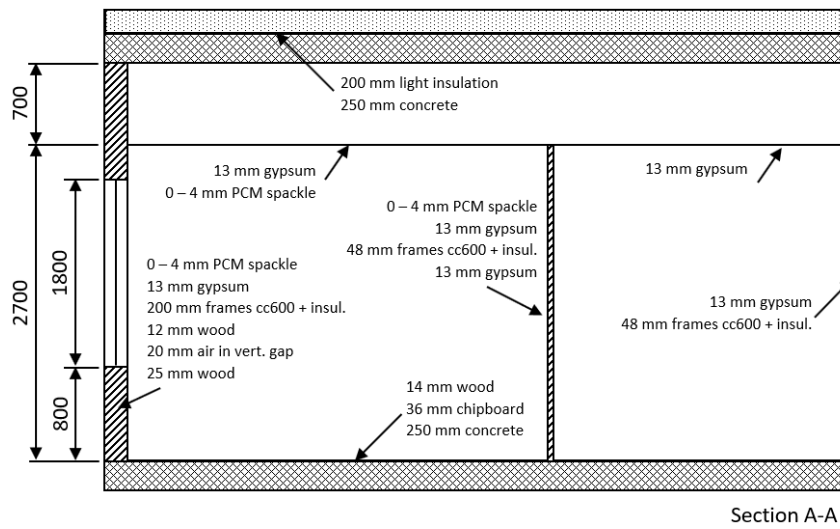
(a) Single cubicle

(b) Hallway

Figure 2.33: IDA-ICE model of a single cubicle, and the corridor



(a) Plan view.



Section A-A

(b) Section view.

Figure 2.34: Design of an office cubicle.

Table 2.17: Materials in use for the model.

| Material | ρ kg/m ³ | C_p J/kgK | λ W/mk |
|-----------------------------|--------------------------|-------------|----------------|
| Light insulation | 20 | 750 | 0.036 |
| Concrete | 2300 | 1050 | 1.70 |
| Insulated wooden frame wall | 92 | 2010 | 0.052 |
| Gypsum board | 970 | 1090 | 0.22 |
| Chipboard | 1000 | 1300 | 0.13 |
| Wood | 500 | 2300 | 0.14 |

Design of night ventilation strategies

As mentioned in chapter 1.2, several researchers have identified natural NV strategies to show great potential in utilizing both PCM's and the thermal inertia in the rest of the building. As not all buildings can utilize pure natural ventilation efficiently, it was also desired to explore a hybrid NV strategy and compare the benefits of the two strategies. When starting to build the control mechanisms for the strategies, it was soon found to be a complex matter where several parameters affected the outcome of results. Some further analysis of research on the field was done to better utilize the influential parameters more efficiently.

Geros et al. [36] revealed three key parameters affecting the efficiency of strategies by experimental measurements in three office buildings in Greece, namely the indoor-outdoor air temperature differential, the useful air flow rate applied during night time and the thermal capacity of the building. Their results showed that during night, the lower the outside air temperature, and the higher the air flow rate is supplied to the building, efficiency of the NV increased. Additionally, the importance of thermal mass was clearly observable in the experiments as by increasing the buildings thermal inertia in cooperation with effective NV it produced a lower temperature development and delay in the peak indoor air temperature.

PCM, as aforementioned, is in essence used to increase the thermal mass of the building, but pose challenges in low thermal conductivity. Several researchers have studied the combination of NV strategies with the characteristics of PCM to further expand on important parameters. Solgi et al. [18] verified Geros et al. conclusions in an experimental study that the key parameters for NV efficiency are the airflow rate, differential indoor-outdoor temperature and the thickness of the PCM layer, which is equivalent to an increase in thermal mass. Evola et al. [37][38] did simulations and experimental work on PCM wallboards installed in lightweight buildings, and found the air flow rate to be effective but reach a point of diminishing returns between 4 and 8 ACH. However, the supply air strategy or temperatures was not detailed in the reports. Zhou et al. [39] simulated the effect of natural NV in a multilayered building with PCM and concluded that the air change hours (ACH) should be as high as possible, where up to 40 ACH was tested. Whenever hybrid NV strategies are used, most studies report a critical value of air-flow rates where the energy savings are starting to drop due to fan usage [18].

An important and complicated factor is the control mechanism for the NV strategy. Wang et al. [40] analyzed three different control schemes in a similar climate and office building as in this report. It was found that the most efficient strategy was the one which ventilated the office space excessively, where the NV control was not deactivated until the surface temperatures dropped below the outdoor air temperatures. Otherwise it was concluded that a strategy which prolonged the operational hours as long as possible, from 21:00 - 07:00 had second best effect. Roach et al. [41] explored a custom control which aimed at using NV until a certain set point temperature inside the building was reached. 13, 15, 17 and 19 °C was tested, and it was found that the strategy reaching the lowest indoor temperature was best, but led to problems with overcooling in regards to thermal comfort when the working hours started. They concluded that 15°C could be the optimum set point temperature, but further research would be needed.

Upon researching more studies on control schemes, it's noticed that no one-fits-all solution exists. Researchers explore different ideas based on the particular

climate and building conditions of study. There is also a lack in recommendations in national standards on the details of NV control mechanisms.

The key parameters that will be explored are listed in table 2.18. 2 and 4 mm thicknesses of the PCM spackle will be investigated, and will be applied to all inner walls and ceiling surfaces in the office cubicles. Preliminary simulations found the results to very dependent on the air flow rates, and it was decided to adjust this parameter in small increments up to 5 ACH. Also, the control strategies would aim at having long operational hours.

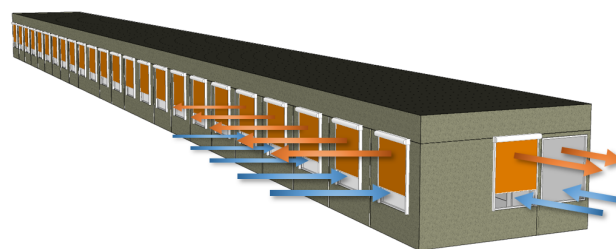
Table 2.18: Night ventilation parameters under investigation.

| Parameter | Varying values |
|-------------------------|------------------------|
| NV air flow rate | 0.5, 1, 2, 3, 4, 5 ACH |
| PCM thickness | 2 mm, 4 mm |
| NV strategy and control | Natural, hybrid |

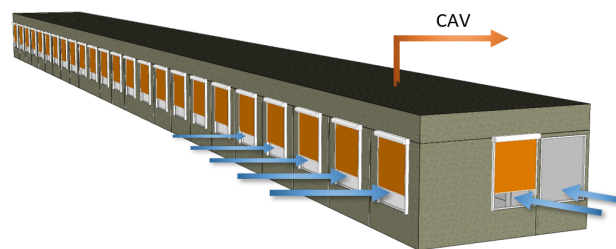
Natural and hybrid night ventilation strategies

The aim of the strategies was to create simple NV mechanisms where the key parameters aforementioned could be explored, and also tackle some of the challenges reported with some original ideas. The aim was not to explore designs such as e.g. cross ventilation or stack flow, but rather to produce certain air flow rates inside the building and analyze energy usage. How those air flows most efficiently can be achieved for other buildings are heavily dependent on building layout and possibilities, and was therefore not investigated.

In the natural NV strategy, each cubicle was ventilated with a single sided window opening and the corridor had window openings in each end. In the hybrid strategy, windows were opened by a small degree to let air in while the exhaust fan of the ventilation system extracted air from the building.



(a) Natural night ventilation strategy.



(b) Hybrid night ventilation strategy.

Figure 2.35: Essential functioning of the two strategies.

Some choices are similar for both the strategies. A mechanism for controlling the minimum allowed indoor air temperature was needed as the mentioned problem of over cooling and thermal comfort posed by Roach et al.[41] was also observed in preliminary testing. In the natural strategy, automatic window openers (PI regulators) would control the opening degree of the windows if a minimum set point temperature was reached, while a thermostat for the exhaust fan would turn the fan on and off in the hybrid strategy. Roach suggested $15^{\circ}C$ as a set point value, but this was found still to be rather on the cold side.

Also, in the studies researched it was noted a lack of consideration for condensation on internal surfaces. This could be a problem wherever air is trapped in enclosures, such as inside electrical equipment, closets and et cetera. If the surface of the enclosure is cooled and the air inside is slow to ventilate, condensation could occur on the inner surfaces. A minimum allowed temperature of $16^{\circ}C$ was chosen as this should be a safe set point. A Mollier diagram shows that for condensation to occur, the air will have to be $31^{\circ}C$ with relative humidity (RH) of 40%, or $26^{\circ}C$ with RH of 50%. Having indoor air with higher RH than this during the summer in Norway normally means that the building have excessive moisture addition to the air or that the building have poor overall air change rate, which would not be the case if NV strategies like this are used.

The overall operational hours of NV was set to 21:00 - 07:00, while the work day started at 08:00. With $16^{\circ}C$ as set point, over cooling could however still occur on some days. A solution to the problem was to raise the set point to $19^{\circ}C$ for the last hour of NV operation, 06:00 - 07:00. It was found that passive heat sources, mainly excessive heat in thermal mass, most often could provide valuable passive acclimation of the space. Also, the ventilation system aided a little bit by providing $19^{\circ}C$ air at low air flow rates from 07:00. As a measure of failure to acclimate the space, electrical heating was activated at 08:00 when the occupants entered the building with a set point temperature of $19^{\circ}C$.

Hybrid night ventilation control

When the NV strategy was activated, the supply air fan was switched off while the windows in the building opened to 10% at the same time. A custom created control macro for the exhaust fan is shown in figure 2.36. Thermostats with the set point temperatures aforementioned can be seen running on separate schedules (21:00 - 06:00 & 06:00 - 07:00), where switches forwards the thermostat signal to the AHU if the schedule is active. 1°C hysteresis centralized around the current set point temperature was used for the thermostats. The measuring signal for the thermostats is connected to a representative cubicle in the middle of the building.

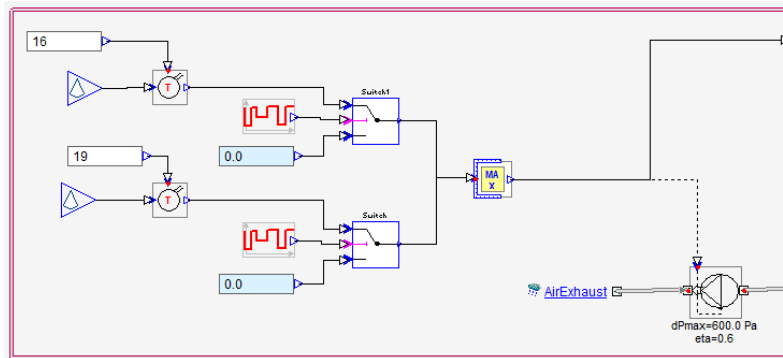


Figure 2.36: Control macro of air handling unit for hybrid night ventilation.

Figure 2.37 shows how the airflows manifests in the model during a simulated case with hybrid NV. It can be seen that air is entering the windows without any air returning. The larger arrows pointing upwards in each office cubicle and the hallway represents the air extracted by the CAV ventilation. The smaller arrows inside the building represents air flows between zones due to internal infiltration.

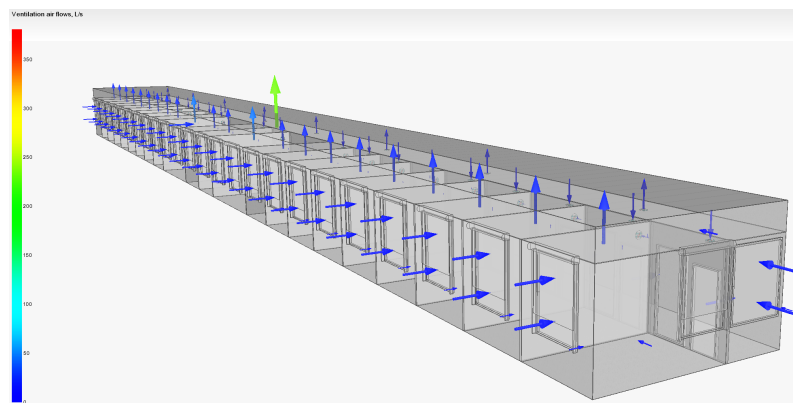


Figure 2.37: Air flows in the model with hybrid night ventilation.

Natural night ventilation control

In this strategy, the air flow rates are determined by the effective opening area of the windows, a displacement factor, $C_d = 0.65$ and the total indoor-outdoor air pressure differential. The control macro follows the same principals as in the hybrid strategy, but the opening degree of the windows are instead gradually closed by proportional integral (PI) regulators to limit the air flows if the minimum set point temperature is reached. If the set point is not reached, a static opening degree to achieve the desired air flow rate is rather in use.

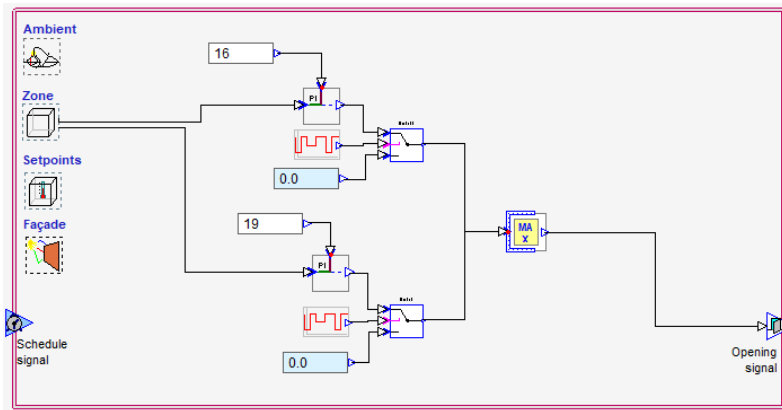


Figure 2.38: Control macro of the window opening signal for natural night ventilation.

Figure 2.39 shows the air flows during a simulated case, and it can be seen that each window allows for two way passage of air. It can also be seen by the colorization of the arrows that slightly more air enters the windows of the cubicles than are exiting, which in turn leads to more air being discharged through the windows in the corridor.

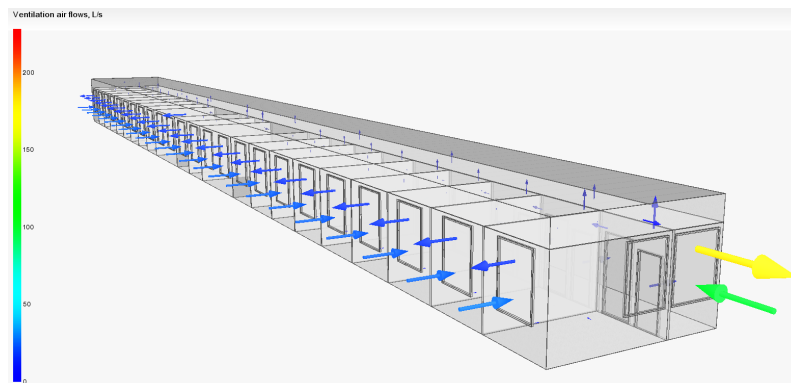


Figure 2.39: Air flows in the model with natural night ventilation.

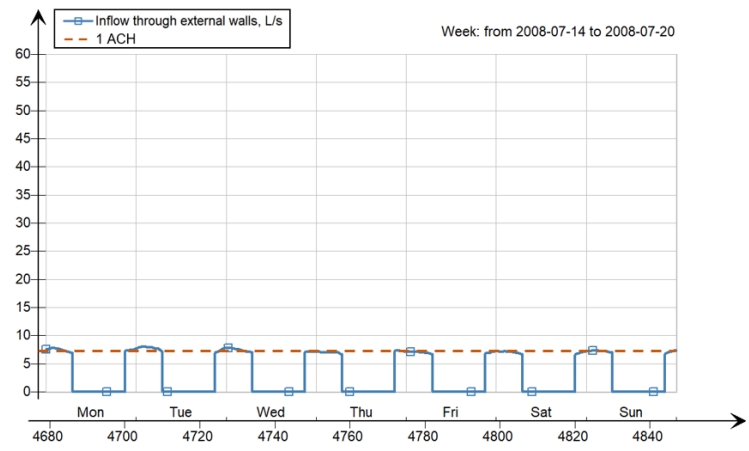
Controlling the air flow rates with the strategies

The air flow rates were easy to control with the hybrid NV strategy, as the fan dictated the amount of air extracted from the building. As the air flows with natural NV strategy were of a dynamic nature, it was aimed at rather having average air flow rates by fine tuning the opening degree of the windows. While the opening degree was found to be the most effective factor in controlling the air flows, the temperature difference between inside and outside caused some variations throughout each night which are shown in figure 2.40.

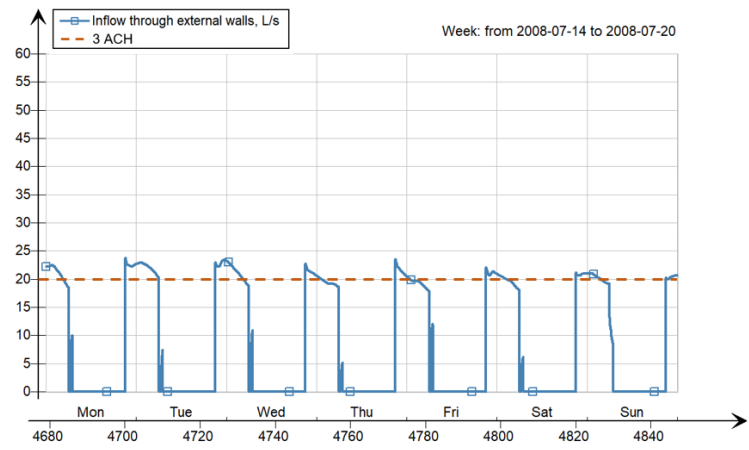
In table 2.19, it's shown how the opening percentage of the windows corresponded to the average air flow rates in the zones. The corridor needed a larger effective area of the windows to be opened to maintain the same air flow rate since the zone is much larger in volume compared to its window sizes. When comparing the natural and hybrid NV strategies in test simulations, the results showed close to identical indoor conditions for similar air flow rates which indicated accurate approximation of average air flows. However, the end results will rather be presented in terms of opening percentage of the windows to not confuse that constant air flow rates were the case for the natural NV strategy.

Table 2.19: Amount of window openings for natural ventilation strategy

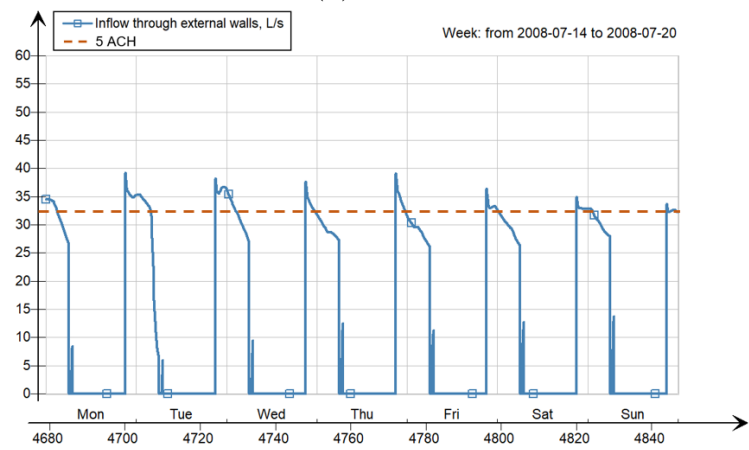
| Average air flow rate | | Effective window opening area | |
|-----------------------|-----------------------|-------------------------------|----------|
| [ACH] | [$m^3/h \cdot m^2$] | Cubicle | Corridor |
| ~0.5 | ~1.4 | 14 % | 30 % |
| ~1 | ~2.7 | 20 % | 40 % |
| ~2 | ~5.4 | 26 % | 55 % |
| ~3 | ~8.1 | 32 % | 70 % |
| ~4 | ~10.8 | 36 % | 77.5 % |
| ~5 | ~13.5 | 40 % | 85 % |



(a) 1 ACH



(b) 3 ACH



(c) 5 ACH

Figure 2.40: Different air flow rates that were targeted for the office cubicles for the natural ventilation strategy.

Analysis

Climate and simulation period

The location is subject to a temperate cold climate, and has a Köppen-Geiger classification: Dfb [42]. An EPW climate file with data from a weather station at Blindern was applied to the model, and the summer months of June, July and August in 2008 was picked as the simulation period. The year of 2008 was chosen as the region experienced a hot summer exceeding normal conditions, although not being too extreme. This choice was to be in agreement with the motivation driving new cooling technologies and the climate prospects of today which estimates a warmer climate in the years to come. Figure 2.41 shows the outdoor air temperature throughout the simulation period.

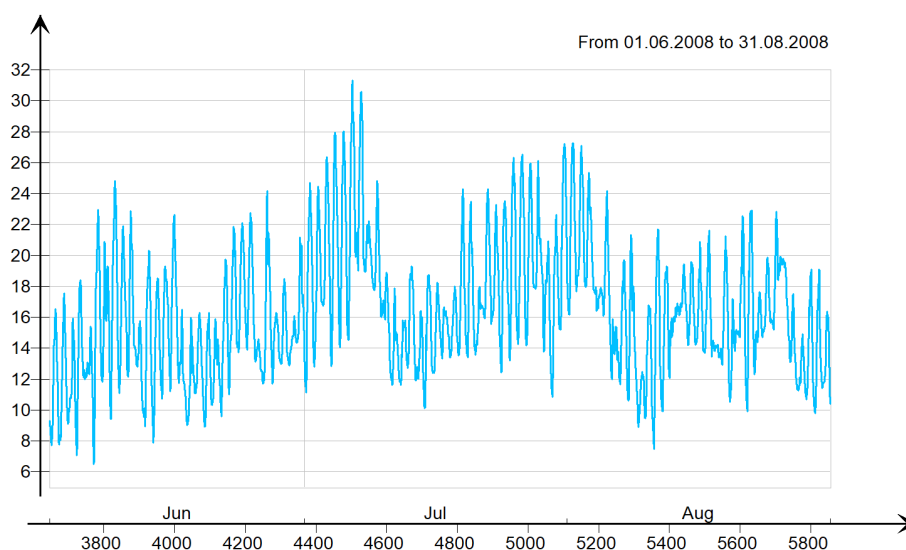


Figure 2.41: Outdoor air temperature through the simulation period.

Simulation cases

Table 2.20 shows the cases that were simulated along with the parameters that were varied. The reference case was only simulated one time, as no parameters were varied. When the PCM spackle was varied at different thicknesses for the other strategies, it was applied to the surface of the gypsum boards in every office cubicle. That includes all surfaces except for the floors, windows and doors. 0 mm means that no PCM spackle was applied, and only the gypsum boards were exposed to the air.

Table 2.20: Simulation cases

| Simulation case | PCM spackle <i>mm</i> | Night ventilation air flow rate <i>ACH</i> | $m^3/(h \cdot m^2)$ |
|-----------------|--------------------------|---|--------------------------------|
| Reference case | No PCM | CAV off | CAV off |
| Natural NV | 0, 2, 4 | 0.5, 1, 2, 3, 4, 5 | 1.4, 2.7, 5.4, 8.1, 10.8, 13.5 |
| Hybrid NV | 0, 2, 4 | 0,5, 1, 2, 3, 4, 5 | 1.4, 2.7, 5.3, 8.1, 10.8, 13.5 |

The ventilation schedule are shown in table 2.21. The internal heat gains were unchanged for each simulation case, and are shown in table 2.22 while some important parameters changed from the TEK-17 validation model are shown in table 2.23.

Table 2.21: Ventilation schedule for the simulation cases

| Weekdays | | | | |
|-----------------------------|--|--|---------------|---------------------|
| Simulation case | 07:00 - 08:00 | 08:00 - 18:00 | 18:00 - 21:00 | 21:00 - 07:00 |
| Reference | CAV off hrs. | CAV on | CAV off hrs. | CAV off hrs |
| Natural NV | CAV off hrs. | CAV on | CAV off hrs. | Natural ventilation |
| Hybrid NV | CAV off hrs. | CAV on | CAV off hrs. | Hybrid ventilation |
| Weekends | | | | |
| Simulation case | 07:00 - 21:00 | 21:00 - 07:00 | | |
| Reference | CAV off hrs. | CAV off hrs. | | |
| Natural NV | CAV off hrs. | Natural ventilation | | |
| Hybrid NV | CAV off hrs. | Hybrid ventilation | | |
| Ventilation settings | | | | |
| Ventilation case | Air flow rate cubicle | Air flow rate corridor | Supply temp | |
| CAV on | 2 <i>ACH</i> / 5.4 $m^3/(h \cdot m^2)$ | 0.9 <i>ACH</i> / 2.5 $m^3/(h \cdot m^2)$ | 19 °C | |
| CAV off hrs. | 0.3 <i>ACH</i> / 0.7 $m^3/(h \cdot m^2)$ | 0.3 <i>ACH</i> / 0.7 $m^3/(h \cdot m^2)$ | 19 °C | |
| Natural ventilation | Varying 0.5 - 5 <i>ACH</i> | Varying 0.5 - 5 <i>ACH</i> | Outdoor air | |
| Hybrid ventilation | Varying 0.5 - 5 <i>ACH</i> | Varying 0.5 - 5 <i>ACH</i> | Outdoor air | |

Table 2.22: Internal heat gains schedule.

| Space | Internal heat load | Size | Schedule |
|----------|--------------------|---------|---------------|
| Cubicle | 1x Occupant | 1.2 Met | 08:00 - 18:00 |
| | 1x Light | 60 W | 08:00 - 18:00 |
| | 1x Computer | 60 W | 08:00 - 18:00 |
| Corridor | 8x Light | 102 W | 08:00 - 18:00 |

Table 2.23: Changed parameters from TEK-17 validation model.

| Parameter | Value |
|------------------|------------------------------|
| Heating setpoint | 19°C (deactivated during NV) |
| Cooling setpoint | 26°C (operative temperature) |
| SFP_{sup} | 1.5 kWh/(m^3/s) |
| SFP_{exh} | 1.0 kWh/(m^3/s) |
| COP_{all} | 1 |

Calculation of energy savings

All energy systems in the model, including the air handling unit (AHU), plant and local heating/cooling units were given a coefficient of performance (COP) of 1 in order to be an ideal system where the true energy usage is not camouflaged by COP's.

Local ideal cooling units with unlimited capacity were put in place in each office cubicle, but with a slight system smoothing value. The Norwegian working environment act and the building code TEK-17 limits the indoor operative temperature

allowed for light work environments to 19-26 °C with 50 hours of exceeding temperatures allowed. It was decided to disregard the over temperature hours (OTH) due to its complications, and have the local cooling units operate constantly on 26°C operative temperature set point.

To not confuse the purpose of the strategy, the local cooling units were just a tool to reveal the surplus energy that needed to be removed or stopped from entering the office cubicles to not exceed thermal comfort criteria in the official regulations. There is already some cooling load in effect in the building with the solar shading and the supply air temperatures of 19°C, as the building needed to pass the minimum energy efficiency requirements in the building code. How the building entrepreneur wants to solve the problem of OTH are a case of where COP's can be best utilized for the particular building, how much daylight and outlook from windows should be blocked by extra solar shading, cost efficiency of solutions and et cetera. The ideal cooling unit with a COP of 1 allow the numbers to be comparable to all alternative solutions, both passive and active systems.

Local cooling energy saved

As the NV strategies and the PCM spackle are affecting the local heat exchange in each cubicle, the first analysis will look at how much energy is spent locally for mechanical cooling. Equation 2.8 was calculated for the whole building for the whole simulation period, which reveals the energy saved for cooling in relation to the reference case.

$$E_{saved} = \frac{E_{localcooling} - E_{localcooling,reference}}{E_{localcooling,reference}} \cdot 100 \text{ [%]} \quad (2.7)$$

Total energy saved

To get a fuller picture of how the NV strategies and the PCM spackle are affecting the total energy consumption of the building, all energy posts that are changing due to the strategies are regarded. Both the natural and the hybrid NV strategy are affecting energy spent by the air handling unit's (AHU) fans. Additionally in comparison with the reference case, some extra energy benefits or deficits from the heat regenerator in the AHU was also included. This is due to heat recovery or cold recovery based on the air temperature that is extracted from the building, and if the AHU needs to heat or cool the outside air to supply 19°C air to the building. This was found in practice to only shift the results $\pm 1\%$.

$$E_{saved} = 1 - \frac{E_{localcooling} + E_{fans} + \Delta E_{AHUregen.}}{E_{localcooling,reference} + E_{fans,reference}} \cdot 100 \text{ [%]} \quad (2.8)$$

Where $\Delta E_{AHUregen} = (E_{AHUheating} - E_{AHUheating,ref}) + (E_{AHUcooling} - E_{AHUcooling,ref})$

Solidification of the PCM

To investigate the solidification of the PCM spackle, temperatures were recorded at the inner side of the PCM layer in IDA-ICE. This was reasoned to be a more reliable measure for the PCM layer as a whole than the surface temperature. If solidification occurs at this point, surely it has also occurred in the rest of the material. As a criteria for solidification, temperatures dropping below 20°C were set as a threshold, the same as the onset melt temperature (fig 1.1). This was done separately for each surface in a representative cubicle, and an area weighted average was derived to represent the total PCM spackle in the cubicle.

Figure 2.42 show the PCM module in IDA-ICE which is the PCM layer that is applied to the wall and ceiling constructions, where point A is the surface exposed to the room. The temperatures were recorded at point B.

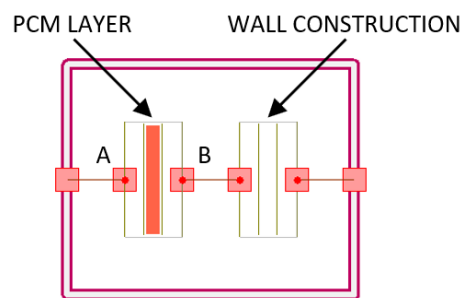
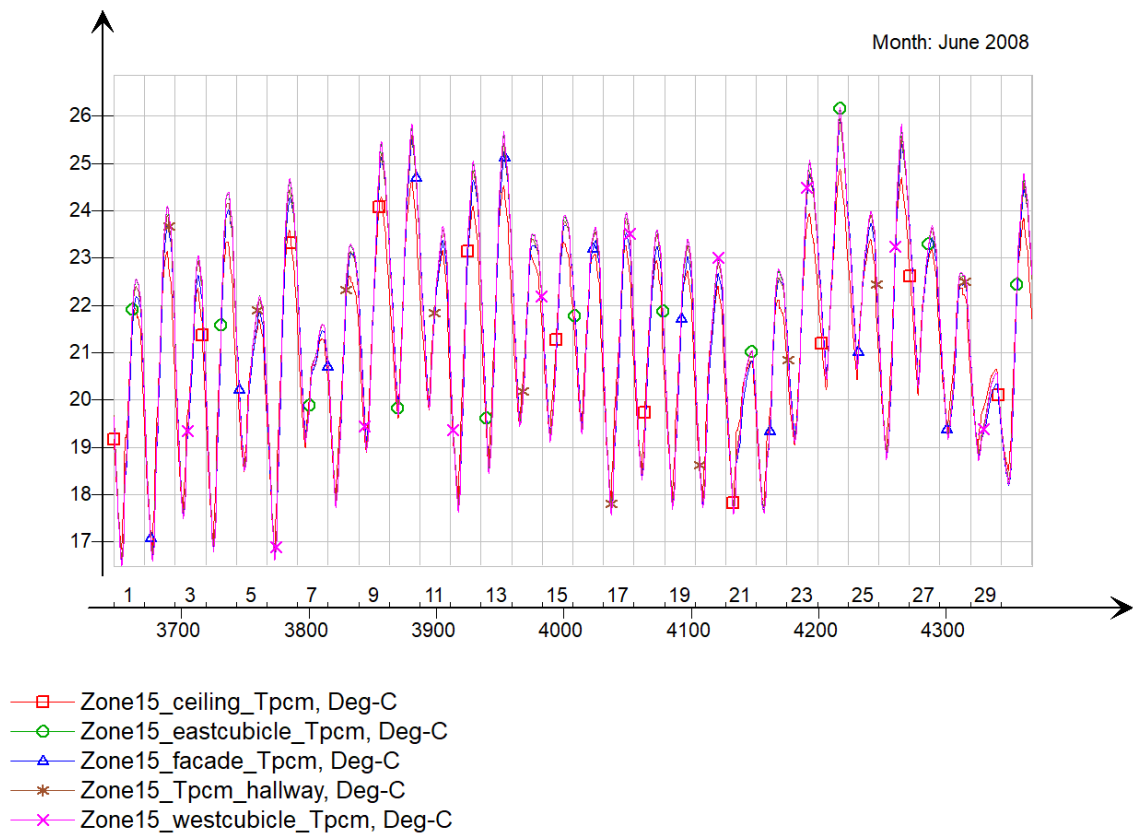


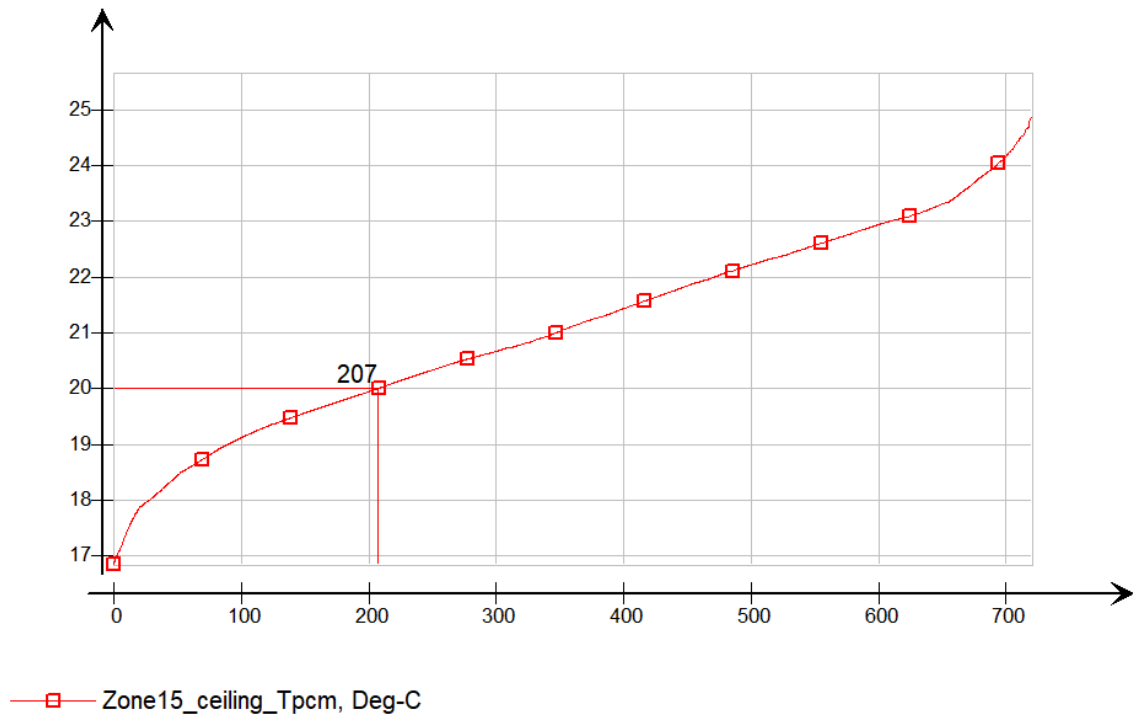
Figure 2.42: PCMWallH module in IDA-ICE.

It was analyzed how much time the PCM spackle spends in solid state on a monthly ratio basis. This was done by dividing the amount of hours in a month where the temperatures of the PCM spackle were below 20°C by the total amount of hours in the respective month. An example of the data gathering is shown in figure 2.43, where it can be seen in 2.43b that duration diagrams were used for each surface to have IDA-ICE calculate the amount of time.

One important limitation to this method is that it will be more accurate to calculate the solidification rate on a daily average, as the use of PCM's is a phenomenon of daily cycles. However, as this will be used for a comparative analysis between 2 mm and 4 mm thicknesses of the PCM spackle it can provide sufficient insight.



(a) All recordings of PCM temperatures.



(b) Duration diagram where IDA-ICE calculates amount of hours spent below 20°C.

Figure 2.43: Example of data gathering of PCM temperatures for the month of June.

Chapter 3

Results and discussion

3.1 Climate room experiment

An experiment was performed where a climate room emulated an office cubicle for two persons in Oslo. The PCM spackle was applied to the walls and ceiling surfaces at 1.7mm and 2.1mm thicknesses on average, respectively.

Figure 3.1 show 5 daily cycles of the experiment. It can be seen that stable conditions was achieved for the experiment, only having slight daily deviations in high and low peak temperatures of $\approx \pm 0.3^\circ\text{C}$ for each of the cases. The minor daily instability is due to the supply air temperatures and air flows having slight daily variances. The success of achieving sufficiently stable conditions was important for the results to serve as support for the validation of the IDA-ICE model.

For the remainder of this section, the fourth daily cycle will be analysed as the best match between starting conditions and supply air temperatures for both cases throughout the day were achieved.

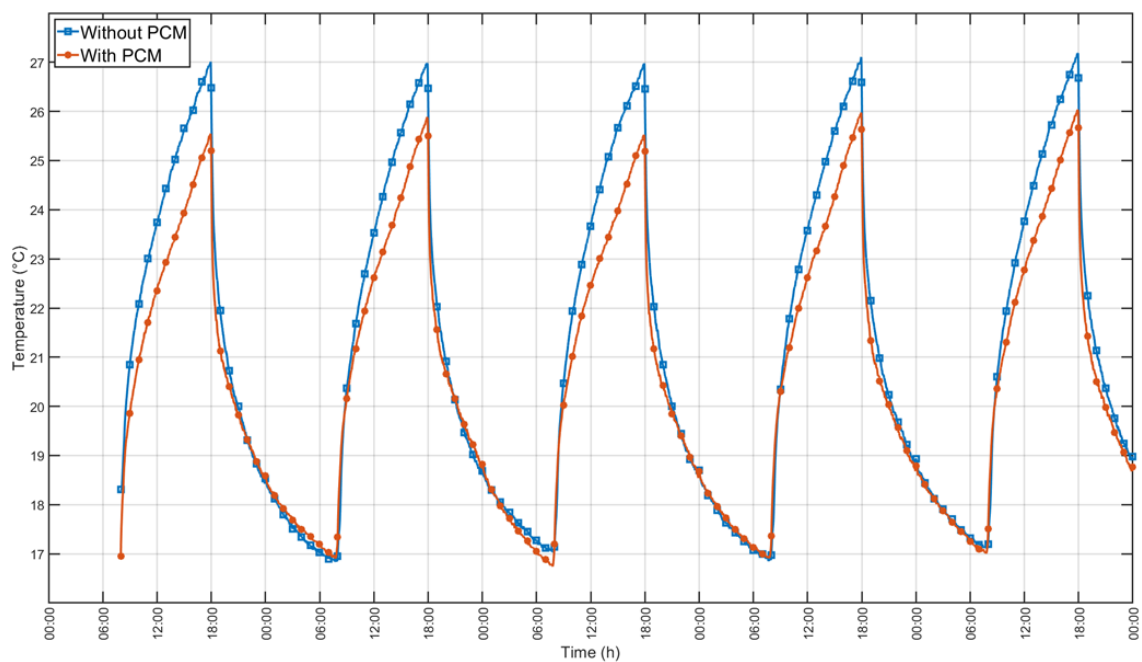
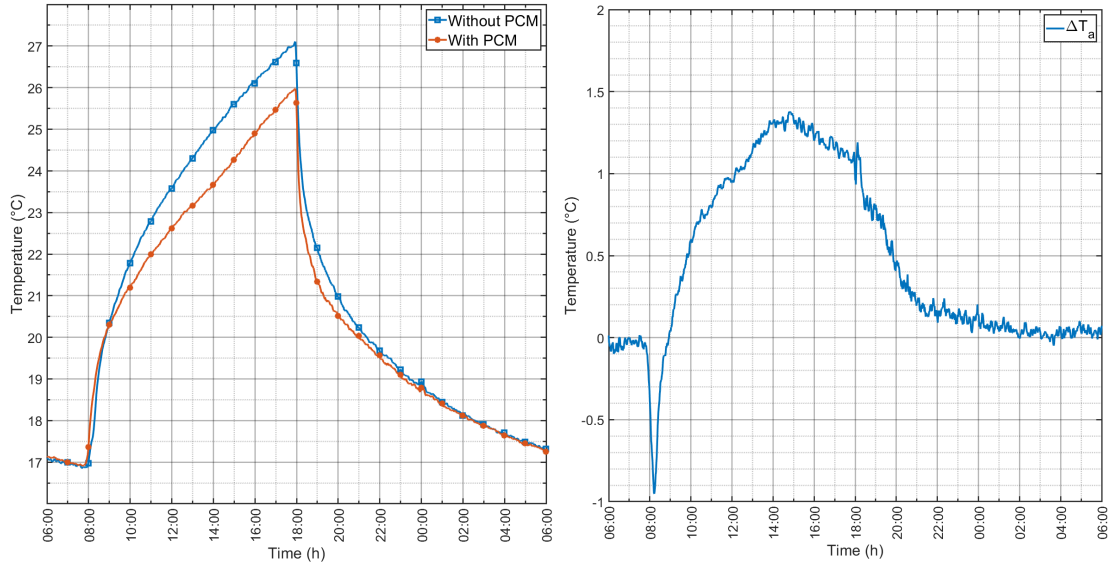


Figure 3.1: Average air temperatures for the experiment.

Air temperatures

Figure 3.2 shows the average air temperatures in the climate room for the fourth daily cycle of both cases. The temperatures are a weighted average consisting of temperature readings at 0.1, 0.6, 1.1 and 2.1 meters above floor level.



(a) Temperature profiles throughout the day. (b) ΔT of the air temperature with and without PCM spackle.

Figure 3.2: Average air temperatures with and without the PCM spackle.

In figure 3.2a it can be seen that the PCM spackle cause for a temperature reduction throughout the day, before cooling load is applied at 18:00. The magnitudes of the temperature reduction are more easily observed in figure 3.2b, where the temperature difference between the two cases are plotted for each time step. It can be seen that the PCM spackle reduces the peak indoor air temperature at 18:00 by approximately $1.1^{\circ}C$, while the highest temperature reduction of $1.3^{\circ}C$ occurs at 14:00 when the room temperature is $23.5^{\circ}C$. The cooling effect from the PCM spackle can be noticed from 09:00, when the room temperature is $20.4^{\circ}C$.

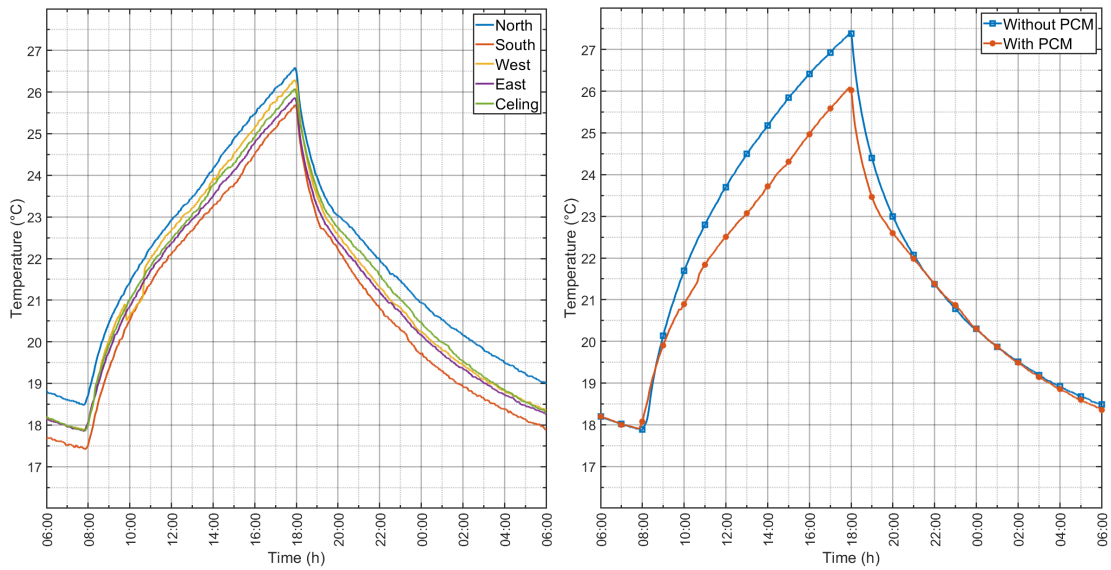
Comparing the air temperature reduction to experimental results from similar studies by Schoessig et al. [22] and Voelker et al.[23], the PCM spackling of this experiment seems to work more potently. The mentioned studies observed a higher temperature reduction, but at much larger thicknesses.

Surface temperatures

Inspecting the surface temperatures gives more insight to the behaviour of the PCM spackle. In figure 3.3, average surface temperatures are plotted both for each individual surface and as a total area weighted average that is compared to the reference experiment. In the calculations, the surface measurements for the door and heating foil on the south surface are excluded. Also, the center thermocouple in the ceiling is left out due to it being placed directly above the ventilation diffuser.

It can be seen in figure 3.3a that satisfying phase change cycles occurred on all surfaces that the PCM spackle was applied to. If the onset melt temperature of $20^{\circ}C$ is held as a threshold, it can be inferred that proper solidification was reached

as all surfaces temperatures dropped below $\approx 18.5^{\circ}\text{C}$ at the end of night ventilation cooling.



(a) Average surface temperature for the PCM spackle at each individual surface where it was applied. (b) Area weighted average for all surface face temperatures with and without PCM spackle.

Figure 3.3: Average surface temperatures.

By inspecting figure 3.3b and 3.4 it can be seen that the cooling effect from the PCM spackle is noticeable around 08:45, which corresponds to an average surface temperature of $\approx 19.5^{\circ}\text{C}$. It can also be seen that the maximum temperature reduction starts between 13:00 and 14:00 and has an absolute peak before starting to decline shortly after 15:00. This corresponds with average surface temperatures of $\approx 23.5^{\circ}\text{C}$ and $\approx 24.5^{\circ}\text{C}$, respectively. The data fits very well with the onset melt temperature of 20°C and peak melting temperature of 24°C that was provided from the DSC test of the material.

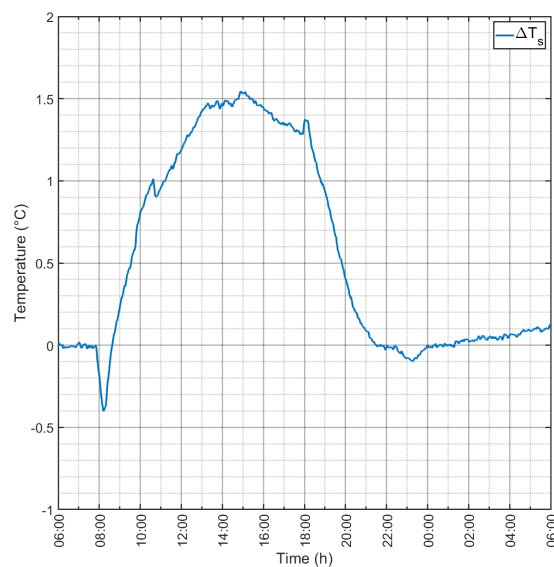


Figure 3.4: ΔT of the surface temperature with and without PCM spackle.

As mentioned in chapter 1.2, having a melting temperature which suits the environment where the PCM is used has been identified in numerous research as the key design parameter for successful application. The results from the experiment show that this is indeed the case for the PCM spackle as the thermal comfort range posed by regulations in Norway is $19 - 26^{\circ}\text{C}$. Although this could have been expected from the material data, it is important to show that the material functions as intended in a real case application.

Moreover, at the thicknesses that was applied of the material, the results show that the heat gains of a typical office cubicle environment utilizes the latent heat storage potential of the PCM well as the surface temperatures started below the onset melt temperature and reached $\approx 26^{\circ}\text{C}$ which is the upper end of the phase change (fig. 1.1). This is true as long as sufficient cooling can be applied.

The night ventilation supply air temperature was measured to be 14.3°C on average, but there was some uncertainty related to the actual air flow rate as this was not recorded during the experiments. Based on the initial setup of the ventilation system and calibration of a simulation model of the experiment, $\approx 230\text{m}^3/(\text{h} \cdot \text{m}^2)$ or $\approx 7\text{ACH}$ was estimated. The result show that this was abundant to solidify the PCM, but this must also be regarded as a powerful cooling load as research have found effective results at lower air flow rates, higher supply temperatures and shorter operational hours of the night ventilation. More conservative night ventilation could be explored in further experimental studies of the PCM spackle, and it can be interesting to investigate if the ingenuity of the thin layer applications and direct exposure to the air can be beneficially exploited.

3.2 Determination of thermal conductivity

The thermal conductivity was measured for a 1 m^2 square specimen of the PCM spackle applied to a gypsum board. Three cases were measured, where the aim was to measure the conductivity of the composite spackle material during different phases of the PCM; solid, in phase transition and melted. The experiment cases are shown in table 3.1. Each case was accompanied by a reference case without the PCM spackle applied to calibrate heat losses in the system.

Table 3.1: Experiment cases to be performed of the PCM spackle.

| # | Case | Temperature range |
|---|---------------|--------------------|
| 1 | Solidified | $< 20\text{ C}$ |
| 2 | In transition | $20 - 24\text{ C}$ |
| 3 | Melted | $> 24\text{ C}$ |

Surface temperature of specimen

As detailed in the methodology chapter, some problems with convective heat transfer with the specimen lead to having high temperature variations along the specimen surface. This can be seen in figure 3.5 where the surface temperature of the specimen is presented for all thermocouple readings for one of the cases. It can be seen that the

temperature difference could be as high as $7K$ from top to bottom of the specimen surface.

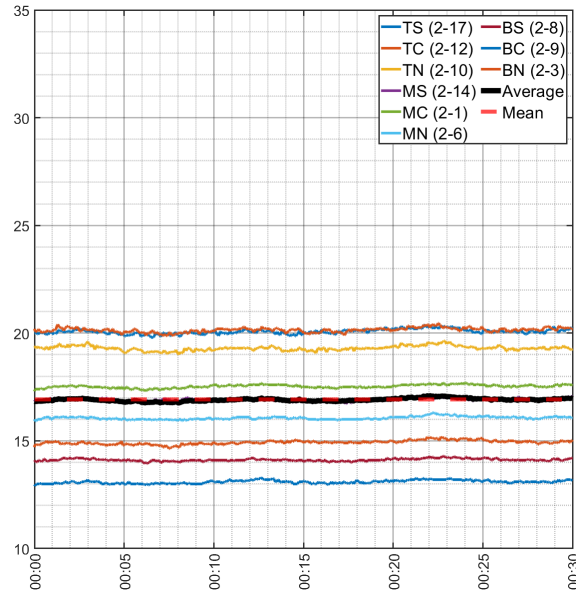
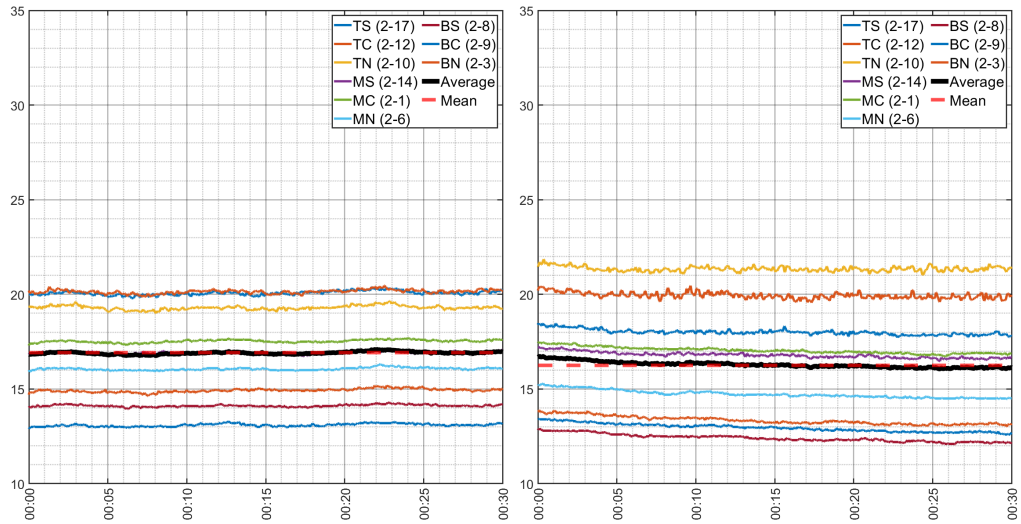


Figure 3.5: Reference test of case 1.

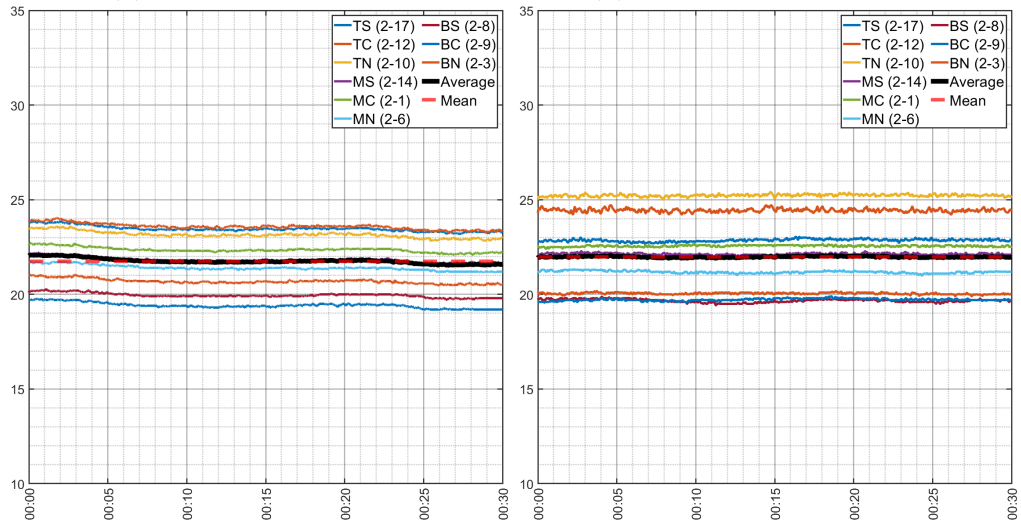
Although high surface temperature variations was experienced, having nine thermocouples on each side of the surface made it possible to calculate a fairly representative average temperature for each side of the specimen. In figure 3.5 it can be seen that the thick black line is an average reading of all thermocouples, while the red dotted line denoted as "mean" in the legend is a time-averaged constant value of the average reading.

Most importantly, figure 3.6 show that a good match in surface temperatures was achieved for each reference and PCM spackle test. It can also be observed that the surface temperatures for each individual thermocouple is more separated in the PCM spackle tests than in the reference tests. Also, the absolute difference between minimum and maximum reading are $\approx 1K$ higher in all three PCM spackle cases compared to their reference case counterparts. This agrees with results from a study on convective heat transfer over a vertical PCM wall which found that the energy transfer with a PCM wall is much more sensitive to low convective heat transfer than that of a wall without PCM [29], but it could also be due to the fact that the heat rate supplied to the metering box was slightly less for the PCM spackle tests.



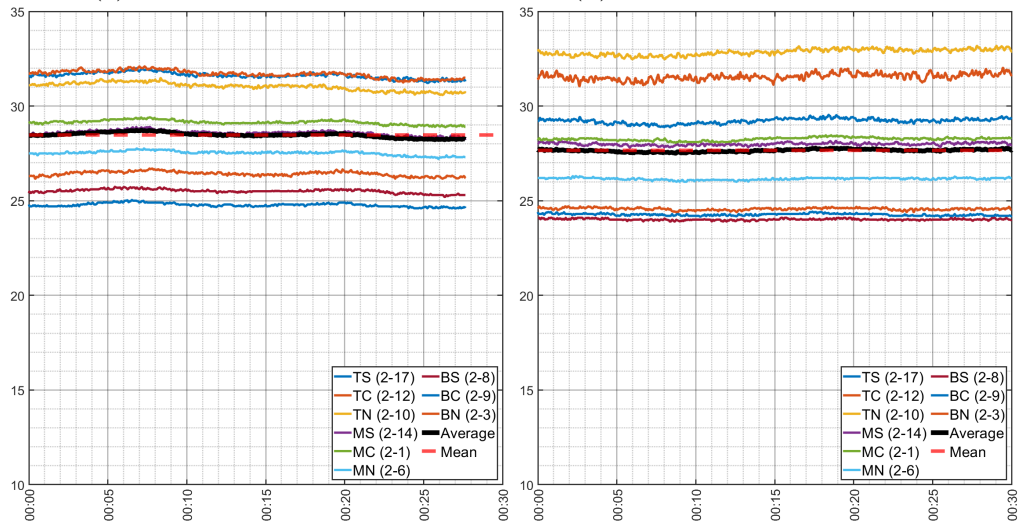
(a) Solidified, reference.

(b) Solidified, PCM spackle.



(c) Transitional, reference.

(d) Transitional, PCM spackle.



(e) Melted, reference.

(f) Melted, PCM spackle.

Figure 3.6: Surface temperatures on the hot side of both the reference and the PCM spackle specimen. Y-axis: surface temperature ($^{\circ}C$), X-axis: time (hh:mm).

Calculation of thermal conductivity

The thermal conductivity of the PCM spackle specimen was calculated as shown in table 3.2. Φ_p is the total power supplied to the metering box for both heat ballast and fans, and ΔT is the surface temperature difference between the hot side and the cold side of the specimen, based on the time-averaged surface temperatures on each side.

Table 3.2: Calculation of thermal conductivity.

| Parameter | Case 1 | Case 2 | Case 3 |
|-----------------------------|--------|--------|--------|
| $\Phi_{p,\text{ref}} [W]$ | 145 | 87 | 145 |
| $\Phi_{p,\text{PCM}} [W]$ | 130 | 78 | 134 |
| $\Delta T_{\text{ref}} [K]$ | 12.17 | 6.97 | 11.91 |
| $\Delta T_{\text{PCM}} [K]$ | 12.80 | 7.89 | 12.66 |
| $k [W/(m^2 \cdot K)]$ | 0.08 | 0.07 | 0.08 |

The results show that the thermal conductivity of the PCM spackle is close to the expected value of $k = 0.1W/(m^2 \cdot K)$ provided by Gyproc based on material composition. The thermal conductivity is shown to be quite stable throughout the temperature range that was tested, although a slight drop from 0.08 to 0.07 W/m²K was observed in the phase transition range of 20 – 24°C. This corresponds to a drop of 12.5% in the thermal conductivity. If this effect is true or due to faults of the experiment is not certain. The implication of this would be slightly lower energy transfer between the material and its surroundings during phase transition.

Very few studies have investigated the conductivity during the phase transitions, but some have reported a similar drop in research of other types of PCM's for building applications although not made much comments on the matter [43],[44]. Chen et al. [45] explained that the understanding of thermal conductivity of PCM's in the midst of phase transition is not established yet. In a work on formulating a heat equation during phase transition, the effect of thermal conductivity drop during phase transition was explained as a response to the thermal diffusivity being lowered which represents how fast heat propagates through the material.

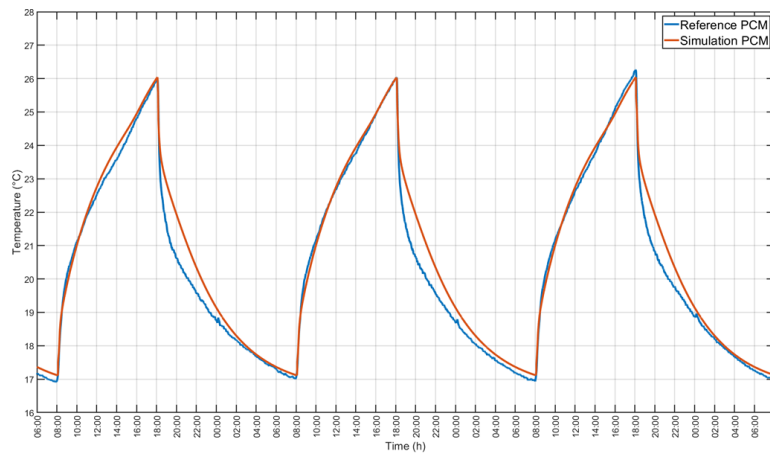
However, the results should not be held as a reliable measure given the uncertainties of the experiment. As the thermal conductivity was found to be intriguingly close to the expected value, it was chosen to use it in further work with the IDA-ICE simulations.

3.3 Numerical simulations

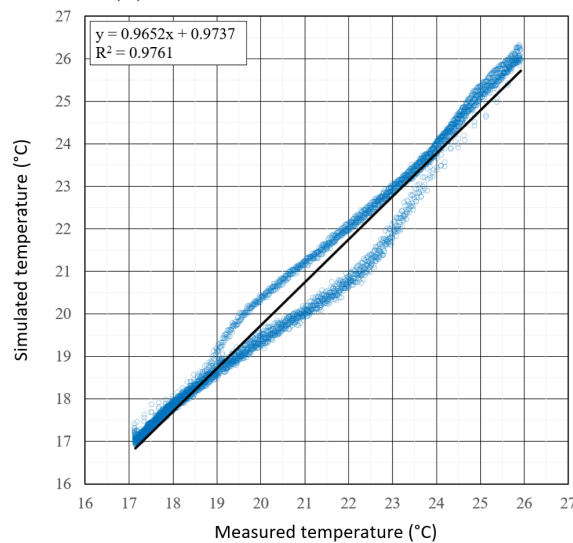
Validation

The climate room experiment was replicated numerically with IDA-ICE to validate the PCM spackle model. Figure 3.7a show the average air temperature during the three last days of the experiment versus simulations. A close match between the curves can be seen, only slightly deviating during the cooling phase. This is due to the effect of hysteresis, where the heat capacity curve in reality is not identical when the material is cooled as when it's heated. This is typically seen in DSC data for microencapsulated PCM's when both curves are presented [46]. As only the heating curve of the material was known, it was also used for the reverse phase transition during cooling in IDA-ICE. This has also been done in similar studies and argued to not be of significant importance for the reliability of the results [38].

However, the results are accurate with $CV_{RMSE} = 1.12\%$ and $R^2 = 0.976$ which indicates a very close match between the results and good predictive capabilities of the model.



(a) Average air temperature.



(b) Regression line for measurements of each time step in simulations and experiment.

Figure 3.7: Experimental vs. simulated results with the PCM spackle.

Optimization of night ventilation strategies for energy savings potential

Two night ventilation (NV) strategies, a natural and a hybrid system were developed and simulated in an office building consisting of single celled cubicles. The energy efficiency of the office building was designed after minimum specifications in the Norwegian building code, and was located in Oslo, Norway (59.94°N 10.72°E , cold temperate climate, Köppen-Geiger: Dfb). The simulation period was the summer months of June, July and August, where diurnal variations in the outdoor temperature are usually in the order of $10 - 15\text{ K}$. The simulation model was an ideal system with COP's of 1, supply ventilation air temperature was constant at 19°C and mechanical cooling was activated locally when operative temperature reached 26°C . For the energy calculations, both strategies were compared to a base case where no NV was activated, only having CAV at reduced air flow rates during night.

The whole building is considered in the energy calculations, but whenever details of the strategies or efficiency of the PCM spackle are investigated, a representative cubicle in the middle of the building is rather in focus. Most often, the case of 3 ACH with the hybrid NV is used as an example as this is a middle ground of the air flow rates simulated.

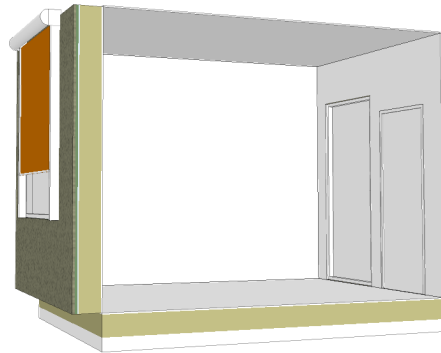


Figure 3.8: Representative office cubicle in the middle of the building. The facade with window is in the south direction.

Functioning of the night ventilation controls

The NV air flow rates of the two strategies were different in nature, where the hybrid strategy caused for constant rates controlled by the exhaust fan, and the natural strategy had dynamic air flows determined by the effective opening area of the windows and the indoor-outdoor air pressure differential. However, in an effort to have some equal comparison basis between the two strategies, the opening degree of the windows were fixed to certain positions in the natural strategy to approximate equal average air flows as in the hybrid case.

The air flow rates were varied by 0.5, 1, 2, 3, 4 and 5 air change hours (ACH) which corresponds to 1.4, 2.7, 5.4, 8.1, 10.8 and 13.5 $m^3/h \cdot m^2$, respectively. In figure 3.9, the operative temperature inside an office cubicle is shown for three weeks; mid-June, mid-July and mid-August. Different air flow rates are compared between the two strategies which show that a good correspondence in the temperature development was achieved. The most important factor in the energy savings calculations is the time that peak operative temperature occurs, which can be seen to be very similar for both strategies.

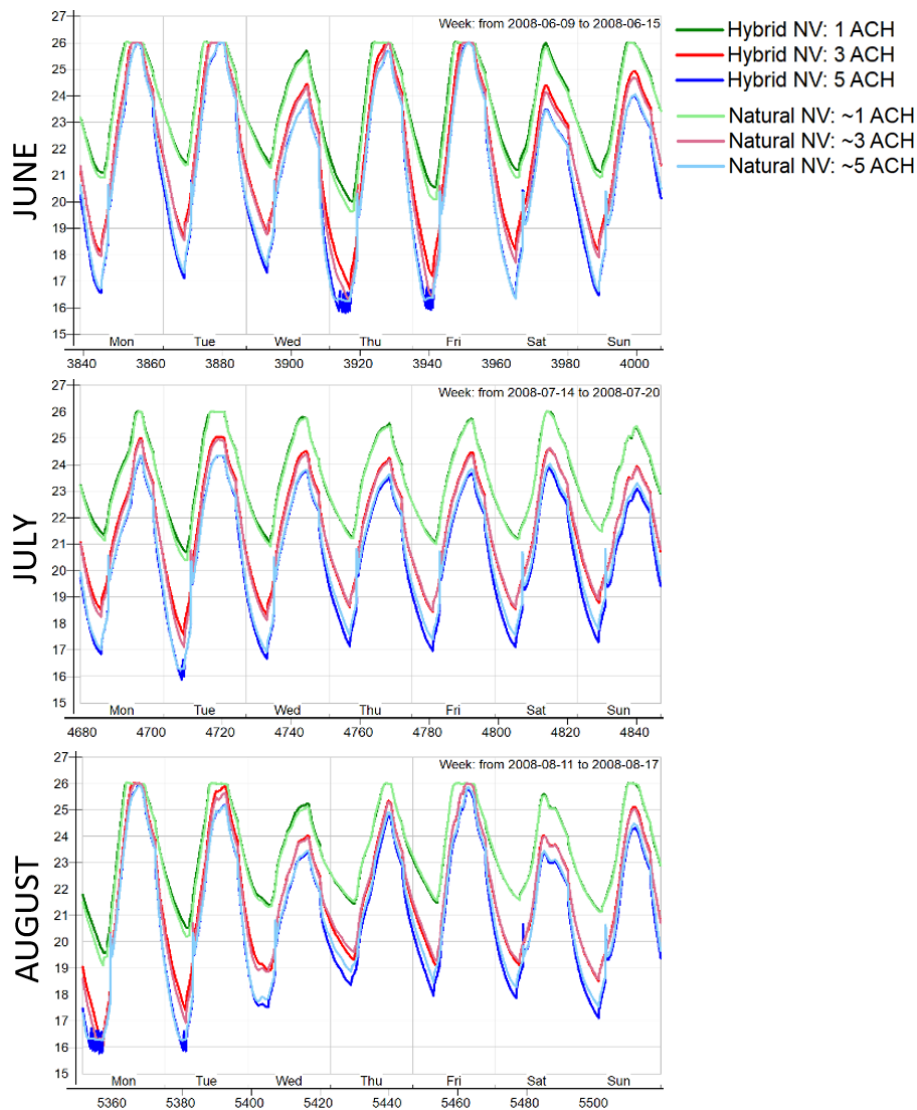


Figure 3.9: Operative temperature comparison between the two strategies.

To avoid over cooling and thermal discomfort by the start of the workday at 08:00, the minimum air temperature set point for the strategies was raised from 16°C to 19°C for the last hour of operation of the strategies (06:00 - 07:00). Further explanation of this was given in the methodology chapter. If the indoor temperature conditions would enable this part of the controls into play, passive heat sources would assist to acclimate the space for up to an additional hour. By 08:00, most often the indoor air held a minimum air temperature of 19°C if not more. As a measure of failure to acclimate the space, electrical heating was activated at 08:00 if the air temperature was below 19°C .

A typical scenario of this occurring can be seen in figure 3.10 between 06:00 - 07:00. For the two cases, it can be seen that the shift in set point temperature at 06:00 causes the air flow rates to adjust accordingly as the two cases were subject to different temperature conditions. From 07:00 - 08:00, the NV strategies was deactivated and the air temperatures was well above 19°C by the start of the work day at 08:00.

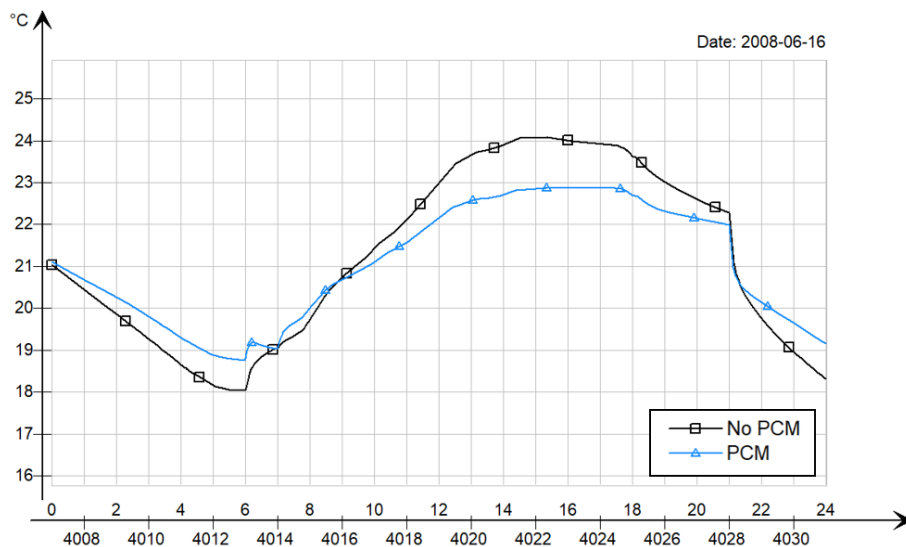


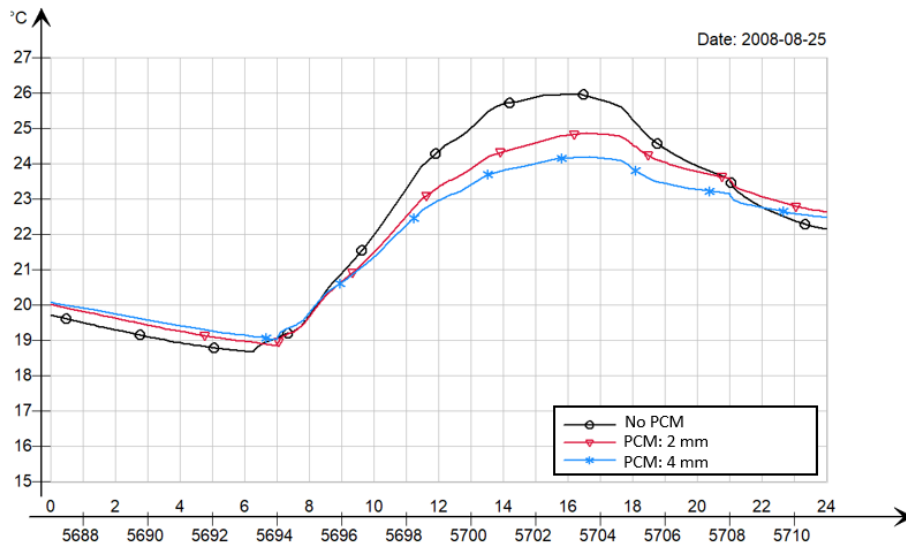
Figure 3.10: Air temperature in a cubicle. Case: 3 ACH, natural NV.

Although being only a minute detail in the NV controls, it was found that the strategy of reducing or cutting off night ventilation one hour early was effective for this particular building. Only negligible amounts of energy for electric space heating was used at 08:00 if thermal comfort criteria was unmet. For air flow rates up to 3 ACH, thermal comfort criteria was always met and no space heating were necessary. From then on, an increasing tendency of energy usage for heating was observed as $0.1 \text{ kWh}/\text{m}^2$ were needed at 3 ACH, increasing to the worst case of $0.5 \text{ kWh}/\text{m}^2$ at 5 ACH for the whole simulated period. Although the amounts are negligible in this case, the effect should be taken into considerations if designing night ventilation strategies intended for high air flows and low indoor air temperatures. Also, passive heat sources might not be a sufficient tool to acclimate spaces for all buildings and scenarios.

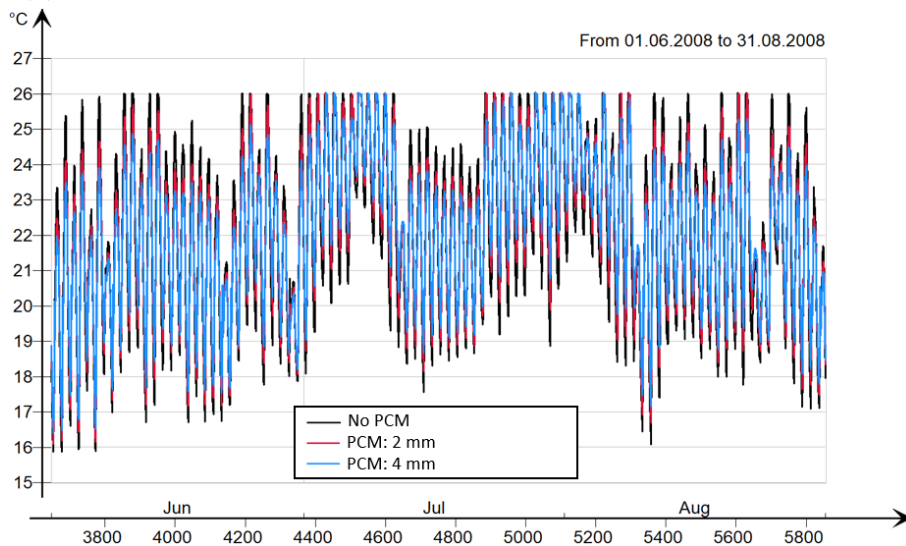
Temperature reduction and peak shift

The inclusion of the PCM spackle decreased the peak indoor operative temperature while also delaying the time of occurrence of the peak. The maximum effect could be observed if the temperature development was not capped by mechanical cooling at 26°C , which is shown in figure 3.11a. Here, the reduction amounts to $\approx 1.1^{\circ}\text{C}$ and $\approx 1.9^{\circ}\text{C}$ for the inclusion of 2 and 4 mm PCM spackle, respectively, and the peak is delayed by ≈ 1 hour for both cases.

The effect was consistent for the whole simulated period, where daily variations in the operative temperature is noticeably attenuated by the PCM spackle. The peak reduction can be seen for the whole period in figure 3.11b by viewing the different colors of the high and low peaks of each day.



(a) Operative temperature: peak reduction and shift for a single day.



(b) Operative temperature: peak reduction for the whole simulated period.

Figure 3.11: Attenuation effect on operative temperature with PCM spackle for the whole simulated period. Case: 3 ACH, hybrid NV.

Cooling load and energy reduction

Due to the attenuation effect on the temperature profile, cooling load needed to maintain thermal comfort can be reduced. When mechanical cooling is activated, all excessive heat in the cubicle must be removed to stop further temperature rise. By delaying the occurrence of peak temperature to later in the day, the heat gains inside the cubicle can be considerably less at the time which reduces the mechanical cooling load that must be applied. Moreover, if the heat gains are intense and the peak delay is short, the mechanical cooling load can still be alleviated as the PCM spackle still absorbs heat from the space. This effect is due to the fact that surface temperatures are usually still climbing after mechanical cooling is activated, and continue to do so until both surface and air temperature equals the set point temperature for cooling. The high heat capacity of the PCM spackle is therefore still useful for some time after cooling load is applied to the space.

The cooling load reduction is shown in figure 3.12 for two examples in a cubicle; one being a day with high heat gain (a,c) and the other being a more typical day where cooling is still needed (b,d). It can be seen that the cooling load reduction is significantly lowered when the PCM spackle is more successful in delaying the peak temperature.

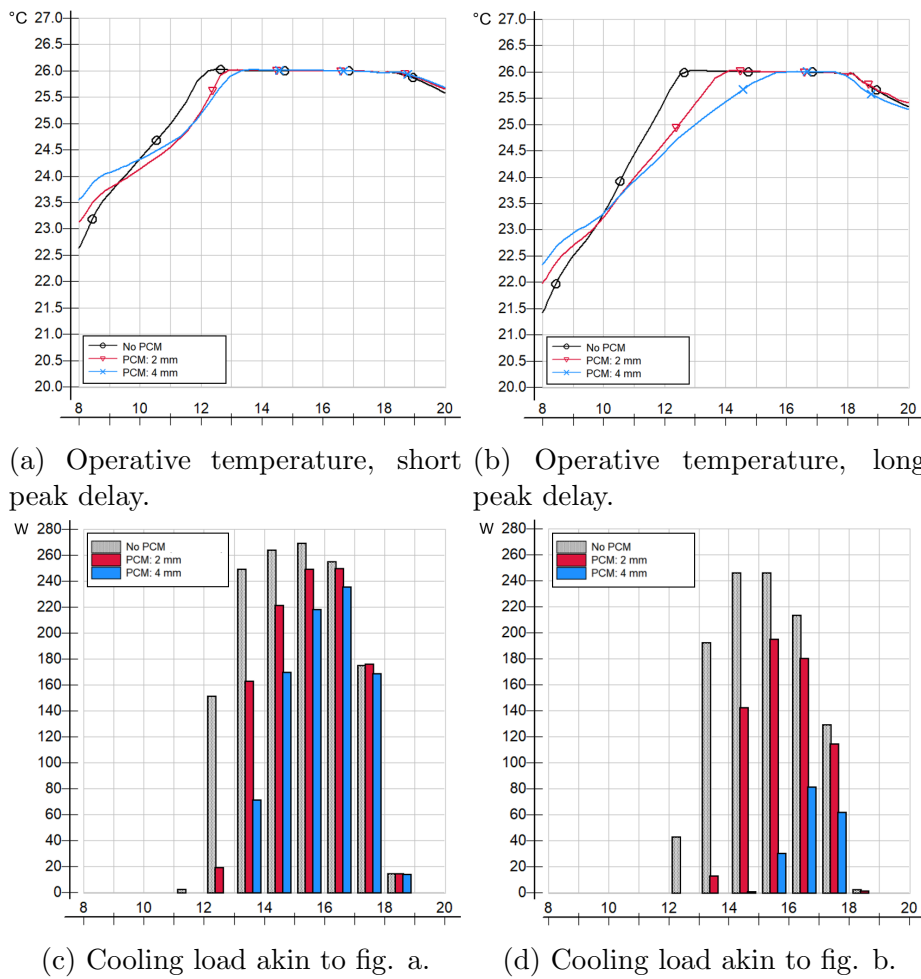


Figure 3.12: Cooling load reduction in a cubicle (hourly average) during a day of high heat gains (a,c) and a typical day (b,d). Case: 3 ACH, hybrid NV.

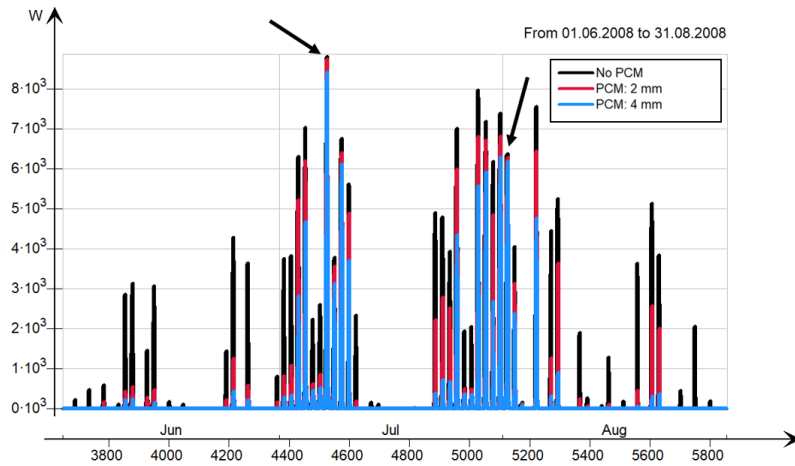


Figure 3.13: Cooling load on a daily basis for the whole simulated period for the entire building. Case: 3 ACH, hybrid NV.

Figure 3.13 shows cooling load in total for the building for the whole simulated period in the case of 3 ACH. The PCM spackle are compared to the night ventilation alone, indicated by the different colors of the lines. Each line represents the peak cooling load for a particular day. Two extreme days (marked by arrows) can be seen where the PCM spackle brings almost no contribution to the lower the cooling load. An inspection of the temperatures on these days showed that the outdoor temperatures were as high as 22°C during the whole night and the indoor temperatures did not drop below 24°C during night ventilation. This led the PCM spackle to not function for the subsequent day. However, these conditions occur rarely in Norway, and for most days the PCM spackle brings remarkable cooling load reduction compared to the night ventilation alone.

Figure 3.14 shows a cooling load duration diagram for the reference case and some of the simulated cases with and without the PCM spackle. Cooling loads in buildings are not sized for the extreme peaks, so if disregarding the few hours closest to the Y-axis in the figure, it can be seen that both the NV and the PCM spackle can lessen the load. It can also be seen a larger separation between the PCM spackle and NV alone for 3 and 5 ACH than with 1 ACH, indicating more effective utilization of the PCM.

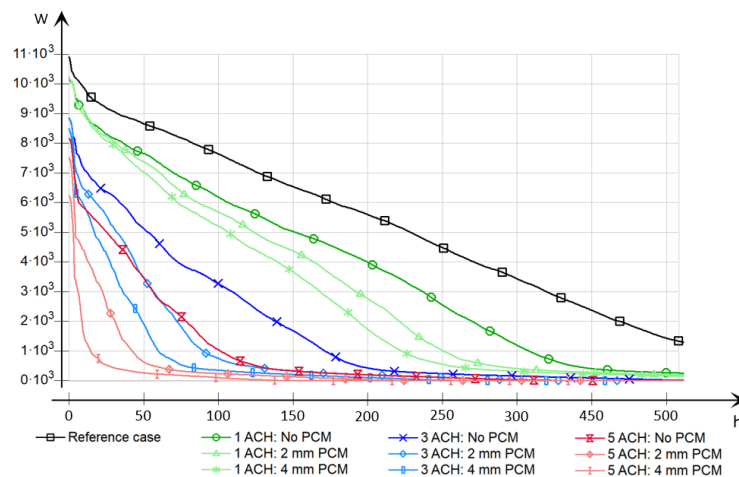


Figure 3.14: Cooling load duration diagram.

As the cooling load can be significantly reduced on the average days with high heat loads, the overall energy consumption for cooling also shows considerable savings. The energy reduction for local cooling is shown in figure 3.15 for the whole simulated period, where both the cases with and without PCM spackle is compared to the base case of no NV. By this comparison, it's easy to distinguish the cooling reduction gained from just NV alone and that of the case when NV is combined with PCM spackle. Note that although the window opening percentages for the natural NV is almost equivalent to the air flow rates of the hybrid NV, it was chosen to not show air flow rates at the x-axis for the natural NV to not claim that constant air flow rates were the case.

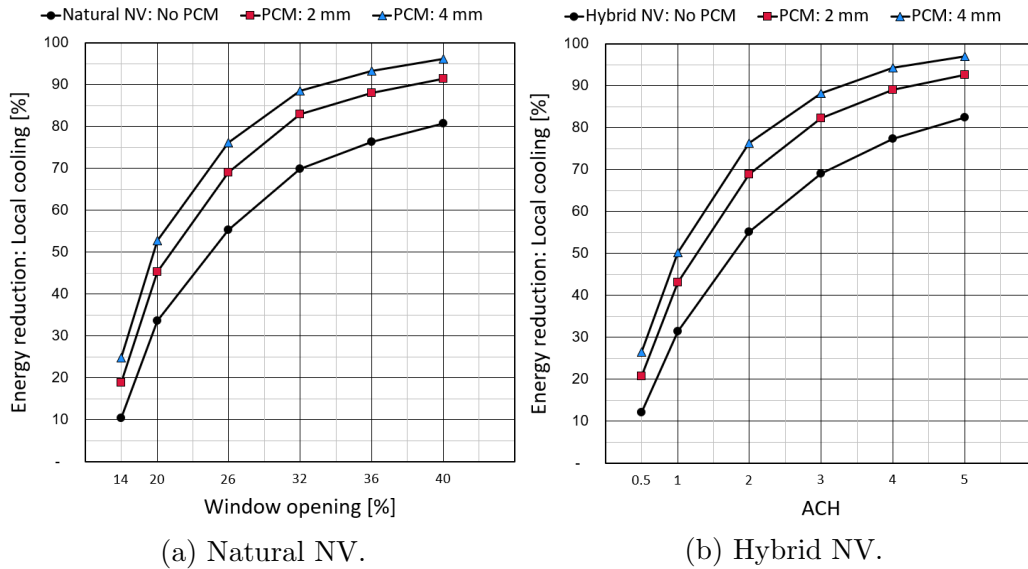


Figure 3.15: Energy reduction for local mechanical cooling for all simulated cases.

First of all, both natural and hybrid strategies show the same tendency in energy reduction for local cooling, which was expected as the air flow rates were close to equal on average. More interestingly, it can be seen that increasing the air flow rates during NV increases the potential for energy savings considerably. As for the case of 5 ACH, $\approx 80\%$ reduction can be gained from NV, further increased up to $\approx 95\%$ coupled with the PCM spackle. The slope of the curves are however decreasing asymptotically towards a saturated value. It can be seen that going above an air flow rate of 3 ACH ($8.1 \text{ m}^3/h \cdot \text{m}^2$), very little additional benefits are gained and this can be considered as an optimum ventilation rate.

Furthermore, it can be seen that the NV alone is the main contributor to the energy savings, but the PCM spackle adds benefits to the savings. At 3 ACH, 2 mm of PCM spackle adds $\approx 14\%$ of energy savings to the night ventilation, while 4 mm adds $\approx 7\%$ on top of that. This show that doubling the amount of PCM spackle from 2 mm to 4 mm yielded reduced benefits as well, indicating that 4 mm might not have been utilized as efficiently as 2 mm.

Moreover, it's interesting that the lowest air flow rates also show that the PCM spackle contribute additionally to the energy savings compared to just NV alone. This indicates that the PCM spackle are in fact beneficially utilized still at low air flow rates.

Although both strategies are equally effective at reducing local cooling demand, an energy calculation was made where all energy posts of the building affected by the strategies were taken into account. This included fan usage, auxiliary power and heat/cold recovery from the air handling unit's (AHU) heat regenerator. The main downside with hybrid NV is the increasing energy usage for fans with increasing air flow rates. With natural ventilation, all fans can be shut off which is an additional bonus. Figure 3.16 shows the results for both strategies. They are both compared to the same base case where the AHU provided balanced air flows of 0.25 ACH ($0.7m^3/h \cdot m^2$) throughout the night. The SFP's were 1,5 and 1,0 $kW/(m^3/s)$ for the supply and exhaust fans, respectively.

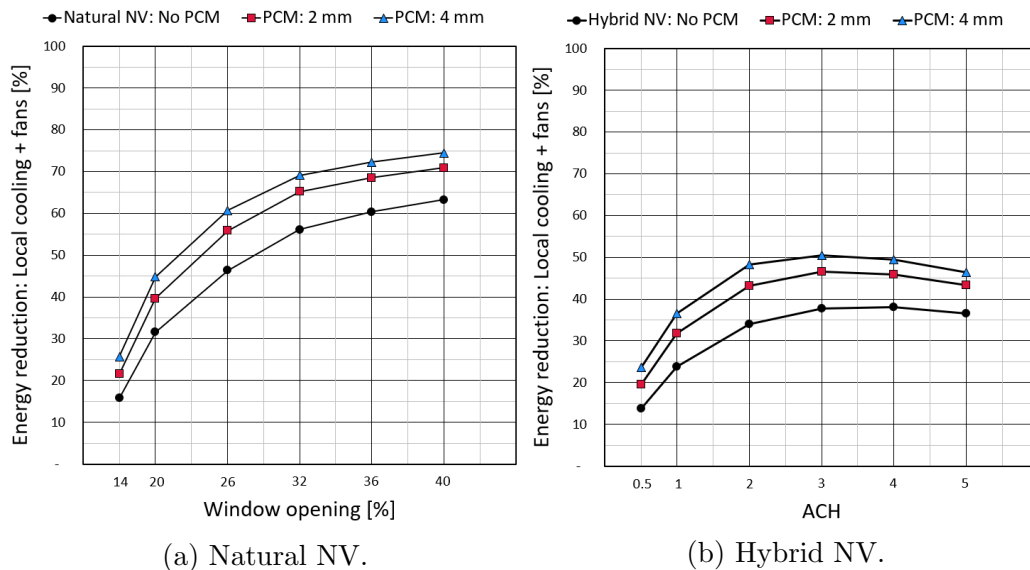


Figure 3.16: Energy reduction for both local cooling and extra energy usage.

The natural NV strategy show the same tendency as before, but as not much energy was spent for the reduced CAV ventilation of the base case at night, the energy savings are lower when fan usage are included into the fraction. This should not be taken into considerations when this strategy is considered as all important energy factors are happening locally in the zones.

The main findings here are that the total energy savings are actually dropping after 3 ACH for the hybrid NV strategy. It can also be seen that it's not worthwhile to increase the airflow rates more than 2 ACH for the hybrid NV, as the total energy savings are becoming saturated more quickly before starting to reduce. By comparing the two cases, it's apparent that the natural NV case provides more energy savings for all air flow rates which should be the preferred strategy if both solutions are feasible for a building.

These calculations show a limitation of hybrid NV systems compared to fully passive systems, but there are more aspects that can be analyzed with the hybrid system. It may be as well as important to reduce the cooling power load for a building even if maximum energy savings are not achieved, where higher air flow rates was shown previously to be very effective.

Solidification

Figure 3.17 show the temperature of the PCM spackle at the individual interior constructions during a week of varying heat gains. It can be seen that the PCM spackle temperature responds well to daily temperature variations although solidification is not reached every day. The odd one out is the ceiling which have noticeably lower high peak temperatures than the rest. This is due to the ceiling having no insulation, only a thin gypsum plate separating the space from a technical shaft above. However, this does not affect the solidification rate, but might indicate that the PCM is utilized less efficiently at surfaces like this as a lower amount of the latent heat of fusion is utilized.

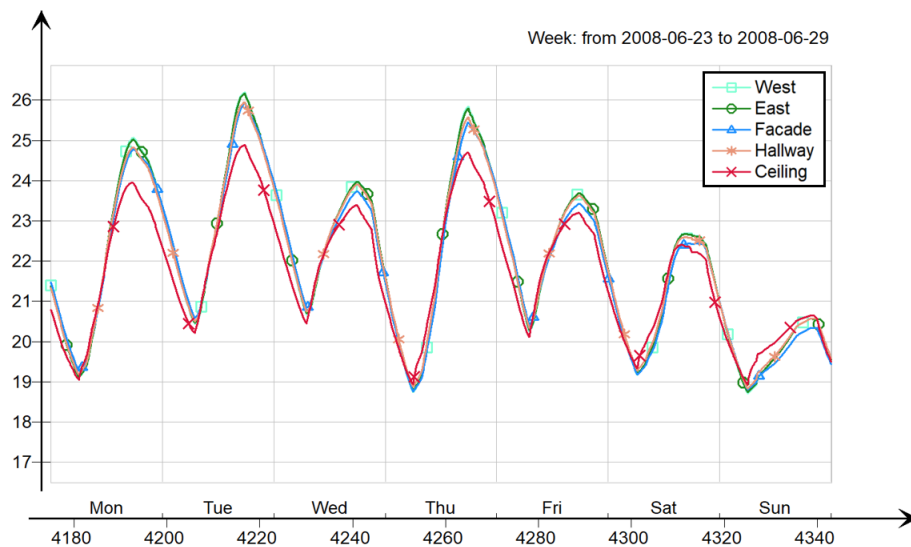


Figure 3.17: PCM spackle temperatures. Case: 3 ACH, hybrid NV. 2 mm PCM.

Taking an area weighted average of all temperatures, the fraction of time spent in solid state on a monthly average was calculated for the simulated cases of 1, 3 and 5 ACH. This is shown in figure 3.18 and the 2 mm and 4 mm layers is compared side by side.

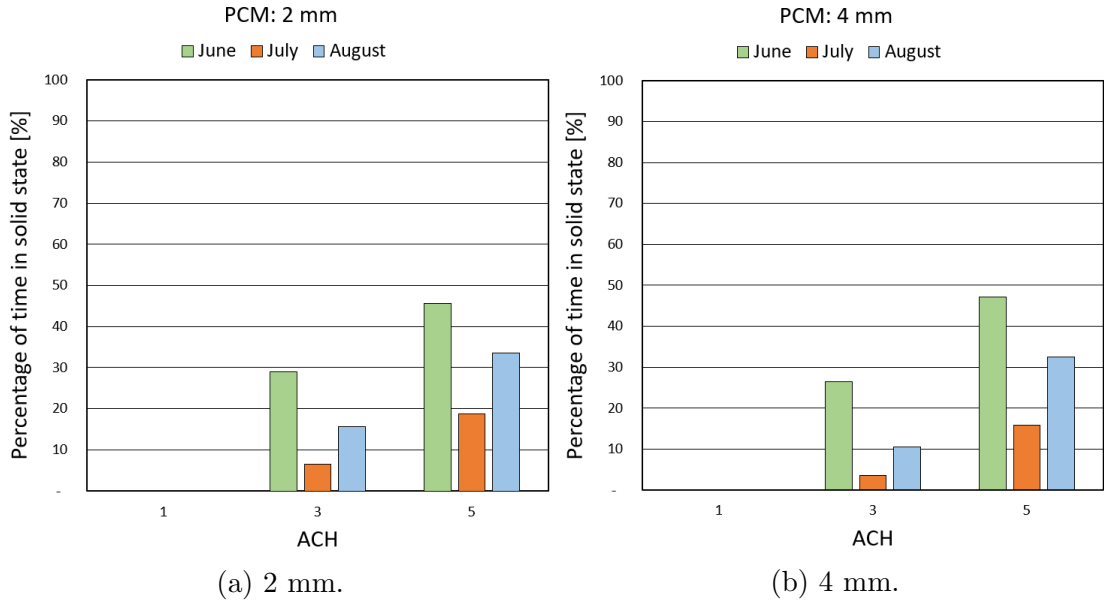


Figure 3.18: Time spent solidified on a monthly average ratio.

It can be seen that the PCM spackle never solidified in the case of 1 ACH, but from 3 ACH and on wards the PCM spackle spent increased time in solid state. The results also show that June is the month with highest solidification rate, while July is the lowest. The operational hours of NV ($21:00 - 07:00$) is only active for $10h/24h = 42\%$ of the time which can be a threshold to compare the results against. Having an average time solidified close to (or even above) this value means that the ventilation flow rates are excessive. In that regard, it can be seen that 5 ACH is indeed ventilating much more than needed for June and August as the time spent solidified is $\approx 45\%$ and $\approx 33\%$, respectively, for both 2 mm and 4 mm. In July, the time solidified is $\approx 19\%$ for 2 mm and $\approx 15\%$ for 4 mm which is more desirable.

Moreover, at 3 ACH (optimal air flow rate in terms of energy savings), it can be seen that the month of June have $\approx 27 - 29\%$ time spent solidified for 2 mm and 4 mm, which is a bit excessive. July have a much lower rate of $\approx 4 - 6\%$. An example of how this knowledge can be utilized beneficially is to shift the air flows to a higher rate in July than in June. This can be a valuable strategy for hybrid NV as high air flow rates were previously shown to be a critical factor.

Furthermore, it can be seen that both the 2 mm and 4 mm of the PCM spackle spent approximately the same time solidified for all cases. This indicates that solidification did not pose an issue when doubling the thickness. This might be a beneficial trait of the PCM spackle, as it is intended for relatively thin layer applications it does not matter much if 2 mm or 4 mm is used in terms of reaching solidification.

Further research can positively investigate this topic closer, as the issue of reaching solidification should not be the only concern for cost effective application of the PCM-spackle. Some hints from the energy savings analysis is that 4 mm only gave $\approx 7\%$ benefit, while 2 mm gave $\approx 14\%$ compared to night ventilation alone. This might indicate that the latent heat of fusion was not satisfactory utilized for the 4 mm case, and an interesting approach can be to analyze the PCM storage efficiency, η_{PCM} posed by Evola in a methodology study of analyzing PCM for effective utilization [37].

Chapter 4

Conclusion

This study set out to investigate how a novel spackle material enhanced with microencapsulated PCM could improve thermal behaviour and cooling energy performance in office buildings in Norway during the summer. This was analyzed both experimentally and with numerical simulations. The studied application of the material was in the range of $\approx 2-4$ mm on walls and ceiling surfaces in office cubicles. The results showed that although being applied only in thin layers it gave a significant boost to the thermal inertia of the environment, slowing down and reducing the indoor temperature development throughout the hot period of the day. This leads to better thermal comfort of the occupants by reducing the operative temperature, and also reducing the cooling load and energy consumption needed to maintain thermal comfort requirements in buildings.

In the experiment, 1.7 and 2.1 mm of the PCM spackle was applied to gypsum boards on the walls and ceiling, respectively, in a climate room. When the maximum air temperature of the reference experiment reached 27.1°C before cooling load was applied, the PCM spackle caused for a reduction of 1.1 K at the same time of day. A maximum air temperature reduction of 1.3 K occurred early afternoon during peak melt of the PCM. By inspecting the surface temperatures, it was observed that melting started around $\approx 19.5^{\circ}\text{C}$ and had a peak performance between $\approx 23.5 - 24.5^{\circ}\text{C}$, indicating the start of melting and peak melting of the PCM. This makes the PCM spackle fit well with both the thermal comfort range and normal indoor temperature conditions during the summer season in Norway, which has been identified by researchers to be one of the most important factors for achieving positive impact of PCM's in building applications.

The PCM spackle was modelled in IDA-ICE and validated against the experimental results with $R^2 = 0.976^{\circ}\text{C}$ and $CV_{RMSE} = 1.12\%$ which indicated good accuracy of the PCM-wall model. An office building with multiple single celled cubicles was modelled to analyze the PCM spackle in a larger scale environment and dynamic climate conditions. The summer months of June, July and August was simulated in Oslo, Norway. A natural and a hybrid night ventilation strategy was designed and investigated together with the PCM spackle to find how these can be utilized together for the best potential for energy savings.

It was found that the PCM spackle at 2 mm and 4 mm application in each cubicle could contribute to 14% and 21% additional energy savings for local cooling, respectively. These numbers were in addition to the very effective night ventilation strategies which boosted the total energy savings to 70 – 95% from 2 – 5 *ACH*.

However, going beyond 3 ACH gave diminishing returns in energy savings and it was determined to be the optimal air flow rate for night ventilation. When considering the total change in delivered energy to the building, it was found that energy savings started to decrease from 3 ACH and on wards for the hybrid night ventilation due to ever increasing energy consumption by fans with higher air flow rates.

Moreover, the PCM spackle at the respective thicknesses could also cause for a $\approx 1.1 - 1.9K$ reduction in the operative temperature, and ≈ 1 hour delay of the peak temperature in comparison to the night ventilation alone. This effect showed the potential for the PCM spackle to significantly reduce the cooling power load needed to maintain thermal comfort criteria in comparison to just the night ventilation alone.

Furthermore, by investigating the solidification on a monthly average ratio it was found that the PCM spackle spent an excessive amount of time solidified at 5 ACH in June and August. At the optimal air flow rate of 3 ACH, it was found that the month of June still had excessive solidification ratio of 27 – 29%, while July only had an average ratio of 4 – 6% for 2 mm and 4 mm, respectively. It was also found that both 2 mm and 4 mm spent approximately the same amount of time solidified for all air flow rates, indicating that reaching solidification was not an issue when the amount of PCM spackle was doubled.

Overall, this study found that both PCM technology and night ventilation strategies can contribute significantly to reduce the cooling demand for buildings with office cubicles environments in Norway.

Further work

- The PCM spackle can be investigated in buildings geared towards passive house and NZEB standards as these thermal environments are known to have challenges with high indoor temperatures during the summer season. Also residential buildings can be investigated as other regards must be taken in designing night ventilation strategies.
- The experiment showed the night ventilation of 7 ACH to be abundant. Further research can be done investigating more conservative strategies for cooling the PCM spackle. Experimental work can be advantageous as the complex behaviour of convection is difficult to simulate.
- Investigations of efficient latent heat utilization can be interesting to correctly size the amount of PCM spackle for it's intended thermal environment. This can be beneficial in terms of finding the most cost effective applications.
- There is currently a lack of investment appraisal analysis of PCM's ready for the market. This can be important to convince and motivate the use of the materials, and further drive development in PCM technology. A simple payback period analysis based on energy reduction and investment costs can be interesting.

References

- [1] UN. “Paris agreement”. In: (2015). URL: http://unfccc.int/files/essential_background/convention/application/pdf/english_paris_agreement.pdf (visited on 12/17/2019).
- [2] European Commission. *A clean planet for all. A European strategic long-term vision for a prosperous, modern, competitive and climate neutral economy*. 2018.
- [3] European Commission. *Final Report of the High-Level Panel of the European Decarbonisation Pathways Initiative*. 2018. URL: <http://doi:10.2777/636> (visited on 06/02/2020).
- [4] IEA. *Global Status Report for Buildings and Construction 2019*. 2019. URL: <https://www.iea.org/reports/global-status-report-for-buildings-and-construction-2019> (visited on 12/16/2019).
- [5] IEA. *World Energy Outlook 2019, 'Cooling'*. 2019. URL: <https://www.iea.org/fuels-and-technologies/cooling> (visited on 12/16/2019).
- [6] IEA. *The Future of Cooling*. 2018. URL: <https://www.iea.org/reports/the-future-of-cooling> (visited on 12/16/2019).
- [7] Ruben Baetens, Bjørn Petter Jelle, and Arild Gustavsen. “Phase change materials for building applications: a state-of-the-art review”. In: *Energy and buildings* 42.9 (2010), pp. 1361–1368. DOI: <https://doi.org/10.1016/j.enbuild.2010.03.026>.
- [8] Hussein Akeiber, Payam Nejat, Muhd Zaimi Abd. Majid, et al. “A review on phase change material (PCM) for sustainable passive cooling in building envelopes”. en. In: *Renewable and Sustainable Energy Reviews* 60 (July 2016), pp. 1470–1497. ISSN: 1364-0321. DOI: [10.1016/j.rser.2016.03.036](https://doi.org/10.1016/j.rser.2016.03.036). URL: <http://www.sciencedirect.com/science/article/pii/S1364032116002719> (visited on 05/27/2020).
- [9] C. A. Balaras. “The role of thermal mass on the cooling load of buildings. An overview of computational methods”. en. In: *Energy and Buildings* 24.1 (Jan. 1996), pp. 1–10. ISSN: 0378-7788. DOI: [10.1016/0378-7788\(95\)00956-6](https://doi.org/10.1016/0378-7788(95)00956-6). URL: <http://www.sciencedirect.com/science/article/pii/0378778895009566> (visited on 05/27/2020).
- [10] Simen Edsjø Kalnæs and Bjørn Petter Jelle. “Phase change materials and products for building applications: A state-of-the-art review and future research opportunities”. en. In: *Energy and Buildings* 94 (May 2015), pp. 150–176. ISSN: 03787788. DOI: [10.1016/j.enbuild.2015.02.023](https://doi.org/10.1016/j.enbuild.2015.02.023). URL: <https://linkinghub.elsevier.com/retrieve/pii/S0378778815001188> (visited on 05/27/2020).

- [11] N. Soares, J. J. Costa, A. R. Gaspar, et al. “Review of passive PCM latent heat thermal energy storage systems towards buildings’ energy efficiency”. en. In: *Energy and Buildings* 59 (Apr. 2013), pp. 82–103. ISSN: 0378-7788. DOI: [10.1016/j.enbuild.2012.12.042](https://doi.org/10.1016/j.enbuild.2012.12.042). URL: <http://www.sciencedirect.com/science/article/pii/S0378778813000157> (visited on 05/27/2020).
- [12] Adeel Waqas and Zia Ud Din. “Phase change material (PCM) storage for free cooling of buildings—A review”. en. In: *Renewable and Sustainable Energy Reviews* 18 (Feb. 2013), pp. 607–625. ISSN: 13640321. DOI: [10.1016/j.rser.2012.10.034](https://doi.org/10.1016/j.rser.2012.10.034). URL: <https://linkinghub.elsevier.com/retrieve/pii/S136403211200576X> (visited on 05/27/2020).
- [13] Farah Souayfane, Farouk Fardoun, and Pascal-Henry Biwole. “Phase change materials (PCM) for cooling applications in buildings: A review”. en. In: *Energy and Buildings* 129 (Oct. 2016), pp. 396–431. ISSN: 0378-7788. DOI: [10.1016/j.enbuild.2016.04.006](https://doi.org/10.1016/j.enbuild.2016.04.006). URL: <http://www.sciencedirect.com/science/article/pii/S0378778816302419> (visited on 05/27/2020).
- [14] E. Osterman, V.V. Tyagi, V. Butala, et al. “Review of PCM based cooling technologies for buildings”. en. In: *Energy and Buildings* 49 (June 2012), pp. 37–49. ISSN: 03787788. DOI: [10.1016/j.enbuild.2012.03.022](https://doi.org/10.1016/j.enbuild.2012.03.022). URL: <https://linkinghub.elsevier.com/retrieve/pii/S0378778812001703> (visited on 05/27/2020).
- [15] Vincenc Butala and Uroš Stritih. “Experimental investigation of PCM cold storage”. en. In: *Energy and Buildings* 41.3 (Mar. 2009), pp. 354–359. ISSN: 0378-7788. DOI: [10.1016/j.enbuild.2008.10.008](https://doi.org/10.1016/j.enbuild.2008.10.008). URL: <http://www.sciencedirect.com/science/article/pii/S0378778808002351> (visited on 05/27/2020).
- [16] Ebrahim Solgi, Zahra Hamedani, Ruwan Fernando, et al. “A literature review of night ventilation strategies in buildings”. en. In: *Energy and Buildings* 173 (Aug. 2018), pp. 337–352. ISSN: 0378-7788. DOI: [10.1016/j.enbuild.2018.05.052](https://doi.org/10.1016/j.enbuild.2018.05.052). URL: <http://www.sciencedirect.com/science/article/pii/S0378778818307850> (visited on 04/08/2020).
- [17] V. Antony Aroul Raj and R. Velraj. “Review on free cooling of buildings using phase change materials”. en. In: *Renewable and Sustainable Energy Reviews* 14.9 (Dec. 2010), pp. 2819–2829. ISSN: 1364-0321. DOI: [10.1016/j.rser.2010.07.004](https://doi.org/10.1016/j.rser.2010.07.004). URL: <http://www.sciencedirect.com/science/article/pii/S136403211000184X> (visited on 05/27/2020).
- [18] Ebrahim Solgi. “Experimental and numerical investigations of phase change material and night ventilation characteristics in buildings”. Dissertation. Queensland, Australia: Griffith University, 2019.
- [19] Yeliz Konuklu, Milan Ostry, Halime O. Paksoy, et al. “Review on using microencapsulated phase change materials (PCM) in building applications”. en. In: *Energy and Buildings*. SI: IEA-ECES Annex 31 Special Issue on Thermal Energy Storage 106 (Nov. 2015), pp. 134–155. ISSN: 0378-7788. DOI: [10.1016/j.enbuild.2015.07.019](https://doi.org/10.1016/j.enbuild.2015.07.019). URL: <http://www.sciencedirect.com/science/article/pii/S037877881530133X> (visited on 05/28/2020).

- [20] Xu Han, Yong Li, Li Yuan, et al. “Experimental study on effect of microencapsulated phase change coating on indoor temperature response and energy consumption”. en. In: *Advances in Mechanical Engineering* 9.6 (June 2017), p. 168781401770390. ISSN: 1687-8140, 1687-8140. DOI: [10.1177/1687814017703901](https://doi.org/10.1177/1687814017703901). URL: <http://journals.sagepub.com/doi/10.1177/1687814017703901> (visited on 06/02/2020).
- [21] Xuezheng Wang, Lecheng Zhang, Yi-Hsien Yu, et al. “Nano-encapsulated PCM via Pickering Emulsification”. en. In: *Scientific Reports* 5.1 (Oct. 2015), p. 13357. ISSN: 2045-2322. DOI: [10.1038/srep13357](https://doi.org/10.1038/srep13357). URL: <http://www.nature.com/articles/srep13357> (visited on 06/14/2020).
- [22] P. Schossig, H. -M. Henning, S. Gschwander, et al. “Micro-encapsulated phase-change materials integrated into construction materials”. en. In: *Solar Energy Materials and Solar Cells*. EuroSun2004 89.2 (Nov. 2005), pp. 297–306. ISSN: 0927-0248. DOI: [10.1016/j.solmat.2005.01.017](https://doi.org/10.1016/j.solmat.2005.01.017). URL: <http://www.sciencedirect.com/science/article/pii/S0927024805000796> (visited on 06/13/2020).
- [23] Conrad Voelker, Oliver Kornadt, and Milan Ostry. “Temperature reduction due to the application of phase change materials”. en. In: *Energy and Buildings* 40.5 (Jan. 2008), pp. 937–944. ISSN: 0378-7788. DOI: [10.1016/j.enbuild.2007.07.008](https://doi.org/10.1016/j.enbuild.2007.07.008). URL: <http://www.sciencedirect.com/science/article/pii/S0378778807002034> (visited on 05/27/2020).
- [24] Refrigerating and Air-Conditioning Engineers American Society of Heating. *2017 ASHRAE handbook: Fundamentals : SI edition*. English. OCLC: 1030302297. Atlanta, GA: ASHRAE, 2017, ©2017, 2017. ISBN: 978-1-939200-58-7 978-1-939200-57-0.
- [25] Ron Lenk and Carol Lenk. *Practical lighting design with LEDs*. English. OCLC: 1021102823. 2017. ISBN: 978-1-119-16532-3 978-1-119-16534-7 978-1-119-16531-6. URL: <https://onlinelibrary.wiley.com/doi/book/10.1002/9781119165347> (visited on 05/16/2020).
- [26] Lauren Cole, Lindsay R. Hoggatt, Jamie A. Sterrenberg, et al. “A Transient Experiment to Determine the Heat Transfer Characteristics of a 100 W Incandescent Light Bulb, Operating at 48 W”. In: *Fluid Mechanics and Heat Transfer: Inexpensive Demonstrations and Laboratory Exercises* (2018). Publisher: CRC Press, p. 179.
- [27] Zhiwei Lian, Yan Zhang, and Seong-Ryong Park. “Radiant heat gain from indoor heat sources”. en. In: *Heat and Mass Transfer* 42.9 (July 2006), pp. 795–801. ISSN: 1432-1181. DOI: [10.1007/s00231-005-0040-3](https://doi.org/10.1007/s00231-005-0040-3). URL: <https://doi.org/10.1007/s00231-005-0040-3> (visited on 05/16/2020).
- [28] ISO. *ISO 8990:1994 Thermal insulation — Determination of steady-state thermal transmission properties — Calibrated and guarded hot box*. ISO 8990:1994. Library Catalog: www.iso.org. URL: <https://www.iso.org/cms/render/live/en/sites/isoorg/contents/data/standard/01/65/16519.html> (visited on 04/01/2020).

- [29] Damien David, Frédéric Kuznik, and Jean-Jacques Roux. “Numerical study of the influence of the convective heat transfer on the dynamical behaviour of a phase change material wall”. en. In: *Applied Thermal Engineering* 31.16 (Nov. 2011), pp. 3117–3124. ISSN: 13594311. DOI: [10.1016/j.applthermaleng.2011.04.001](https://doi.org/10.1016/j.applthermaleng.2011.04.001). URL: <https://linkinghub.elsevier.com/retrieve/pii/S135943111100189X> (visited on 05/25/2020).
- [30] Drury B. Crawley, Jon W. Hand, Michaël Kummert, et al. “Contrasting the capabilities of building energy performance simulation programs”. en. In: *Building and Environment*. Part Special: Building Performance Simulation 43.4 (Apr. 2008), pp. 661–673. ISSN: 0360-1323. DOI: [10.1016/j.buildenv.2006.10.027](https://doi.org/10.1016/j.buildenv.2006.10.027). URL: <http://www.sciencedirect.com/science/article/pii/S0360132306003234> (visited on 05/30/2020).
- [31] Cristina Cornaro, Marco Pierro, Daniele Roncarati, et al. “Validation of a PCM simulation tool in IDA ICE dynamic building simulation software using experimental data from Solar Test Boxes”. In: Feb. 2017.
- [32] Stian Wirak. “Modeling and validation of passive techniques for stabilizing indoor environment in buildings - A case study of the Viking Ship Museum in Norway”. eng. Accepted: 2018-09-17T14:01:05Z Publisher: NTNU. MA thesis. Trondheim, Norway: NTNU, 2018. URL: <https://ntnuopen.ntnu.no/ntnu-xmlui/handle/11250/2563035> (visited on 05/30/2020).
- [33] Jens Pfafferoth, Sebastian Herkel, and Martina Jäschke. “Design of passive cooling by night ventilation: evaluation of a parametric model and building simulation with measurements”. en. In: *Energy and Buildings* 35.11 (Dec. 2003), pp. 1129–1143. ISSN: 0378-7788. DOI: [10.1016/j.enbuild.2003.09.005](https://doi.org/10.1016/j.enbuild.2003.09.005). URL: <http://www.sciencedirect.com/science/article/pii/S0378778803000975> (visited on 05/29/2020).
- [34] *8.6.1 ASHRAE Guideline 14-2014 - Knovel*. URL: https://app.knovel.com/web/view/khtml/show.v/rcid:kpASHRAEVC/cid:kt011Z7UE1/viewerType:khtml//root_slug:ashrae-handbook-heating/url_slug:ashrae-guideline-14-2014?b-q=ashrae%20guideline%2014-2014&sort_on=default&b-subscription=true&b-group-by=true&page=17&b-sort-on=default&b-content-type=all_references&include_synonyms=no&view=collapsed&zoom=1&q=ashrae%20guideline%2014-2014 (visited on 06/11/2020).
- [35] SINTEF. *344.110 Tilpasningsdyktige kontorbygninger - Byggforskserien*. URL: https://www.byggforsk.no/dokument/3223/tilpasningsdyktige_kontorbygninger#i4 (visited on 06/11/2020).
- [36] V Geros, M Santamouris, A Tsangrasoulis, et al. “Experimental evaluation of night ventilation phenomena”. en. In: *Energy and Buildings* 29.2 (Jan. 1999), pp. 141–154. ISSN: 0378-7788. DOI: [10.1016/S0378-7788\(98\)00056-5](https://doi.org/10.1016/S0378-7788(98)00056-5). URL: <http://www.sciencedirect.com/science/article/pii/S0378778898000565> (visited on 05/30/2020).
- [37] G. Evola, L. Marletta, and F. Sicurella. “A methodology for investigating the effectiveness of PCM wallboards for summer thermal comfort in buildings”. en. In: *Building and Environment* 59 (Jan. 2013), pp. 517–527. ISSN: 0360-1323. DOI: [10.1016/j.buildenv.2012.09.021](https://doi.org/10.1016/j.buildenv.2012.09.021). URL: <http://www.sciencedirect.com/science/article/pii/S0360132312002636> (visited on 05/28/2020).

- [38] Gianpiero Evola and Luigi Marletta. “The Effectiveness of PCM Wallboards for the Energy Refurbishment of Lightweight Buildings”. en. In: *Energy Procedia*. 6th International Conference on Sustainability in Energy and Buildings, SEB-14 62 (Jan. 2014), pp. 13–21. ISSN: 1876-6102. DOI: [10.1016/j.egypro.2014.12.362](https://doi.org/10.1016/j.egypro.2014.12.362). URL: <http://www.sciencedirect.com/science/article/pii/S1876610214033931> (visited on 06/04/2020).
- [39] Guobing Zhou, Yongping Yang, Xin Wang, et al. “Numerical analysis of effect of shape-stabilized phase change material plates in a building combined with night ventilation”. en. In: *Applied Energy* 86.1 (Jan. 2009), pp. 52–59. ISSN: 0306-2619. DOI: [10.1016/j.apenergy.2008.03.020](https://doi.org/10.1016/j.apenergy.2008.03.020). URL: <http://www.sciencedirect.com/science/article/pii/S0306261908000949> (visited on 05/28/2020).
- [40] Zhaojun Wang, Lingli Yi, and Fusheng Gao. “Night ventilation control strategies in office buildings”. en. In: *Solar Energy* 83.10 (Oct. 2009), pp. 1902–1913. ISSN: 0038-092X. DOI: [10.1016/j.solener.2009.07.003](https://doi.org/10.1016/j.solener.2009.07.003). URL: <http://www.sciencedirect.com/science/article/pii/S0038092X09001595> (visited on 05/29/2020).
- [41] P. Roach, F. Bruno, and M. Belusko. “Modelling the cooling energy of night ventilation and economiser strategies on façade selection of commercial buildings”. en. In: *Energy and Buildings* 66 (Nov. 2013), pp. 562–570. ISSN: 0378-7788. DOI: [10.1016/j.enbuild.2013.06.034](https://doi.org/10.1016/j.enbuild.2013.06.034). URL: <http://www.sciencedirect.com/science/article/pii/S0378778813003836> (visited on 05/28/2020).
- [42] Markus Kottek, Jürgen Grieser, Christoph Beck, et al. “World Map of the Köppen-Geiger climate classification updated”. In: *Meteorologische Zeitschrift* 15.3 (2006). Place: Stuttgart, Germany Publisher: Schweizerbart Science Publishers, pp. 259–263. DOI: [10.1127/0941-2948/2006/0130](https://doi.org/10.1127/0941-2948/2006/0130). URL: <http://dx.doi.org/10.1127/0941-2948/2006/0130>.
- [43] Qibin Li, Yinsheng Yu, Yilun Liu, et al. “Thermal Properties of the Mixed n-Octadecane/Cu Nanoparticle Nanofluids during Phase Transition: A Molecular Dynamics Study”. en. In: *Materials* 10.1 (Jan. 2017), p. 38. ISSN: 1996-1944. DOI: [10.3390/ma10010038](https://doi.org/10.3390/ma10010038). URL: <http://www.mdpi.com/1996-1944/10/1/38> (visited on 05/26/2020).
- [44] Sana Sari-Bey, Magali Fois, Igor Krupa, et al. “Thermal characterization of polymer matrix composites containing microencapsulated paraffin in solid or liquid state”. en. In: *Energy Conversion and Management* 78 (Feb. 2014), pp. 796–804. ISSN: 01968904. DOI: [10.1016/j.enconman.2013.11.014](https://doi.org/10.1016/j.enconman.2013.11.014). URL: <https://linkinghub.elsevier.com/retrieve/pii/S0196890413007358> (visited on 05/26/2020).
- [45] Hongyi Chen, Zhongmou Yue, Dudi Ren, et al. “Thermal Conductivity during Phase Transitions”. en. In: *Advanced Materials* (Dec. 2018), p. 1806518. ISSN: 0935-9648, 1521-4095. DOI: [10.1002/adma.201806518](https://doi.org/10.1002/adma.201806518). URL: <https://onlinelibrary.wiley.com/doi/abs/10.1002/adma.201806518> (visited on 05/26/2020).

- [46] M. N. A. Hawlader, M. S. Uddin, and Mya Mya Khin. “Microencapsulated PCM thermal-energy storage system”. en. In: *Applied Energy*. Energex 2002 - New and Renewable Sources of Energy - Topic I 74.1 (Jan. 2003), pp. 195–202. ISSN: 0306-2619. DOI: [10.1016/S0306-2619\(02\)00146-0](https://doi.org/10.1016/S0306-2619(02)00146-0). URL: <http://www.sciencedirect.com/science/article/pii/S0306261902001460> (visited on 05/28/2020).

Appendix A

Experiment

Sensor placements and details: climate room experiment

Air sensors

Figure A.1 and A.2 show the layout for all measuring points except for surface temperatures.

A measuring jig placed in the middle of the ventilation diffuser and the northern wall held sensors in position for measurement of air temperatures and other thermal comfort linked parameters at heights of $0.1m$, $0.6m$ and $1.1m$ from the floor. Ventilation supply and exhaust air temperatures were measured by placing thermocouples inside the ducts, in the center from the duct walls. Omnidirectional air velocity meters were placed at the west and east surface to verify that the ventilation diffuser could provide sufficient air flow over the wall surfaces.

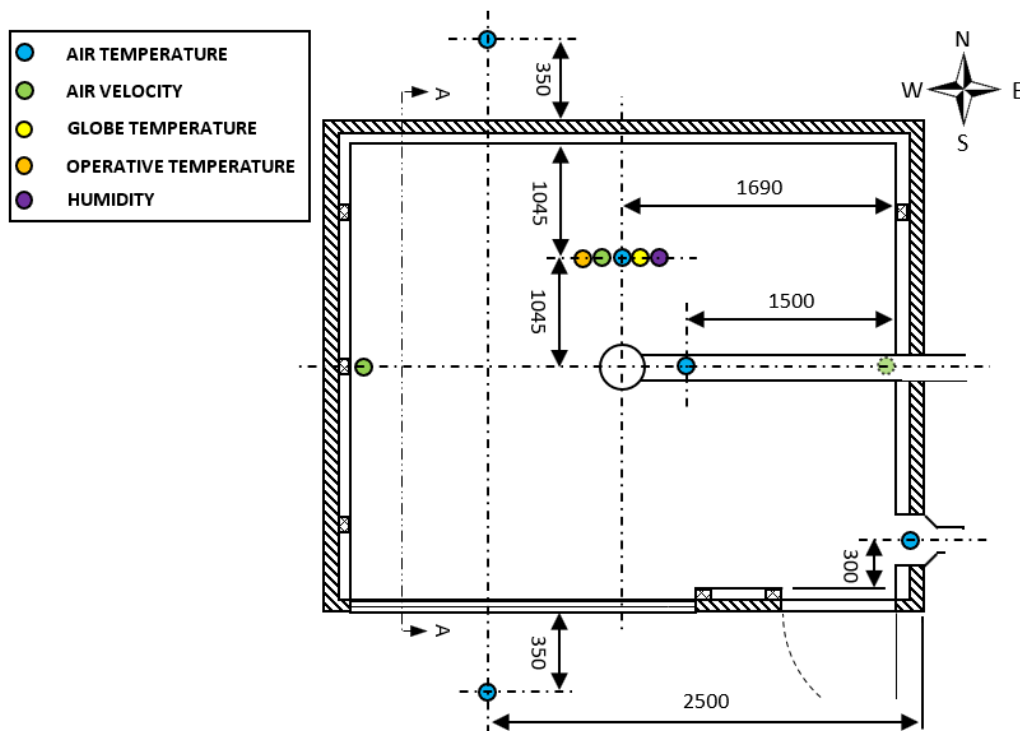


Figure A.1: Air based sensors in climate room experiment. Plan view.

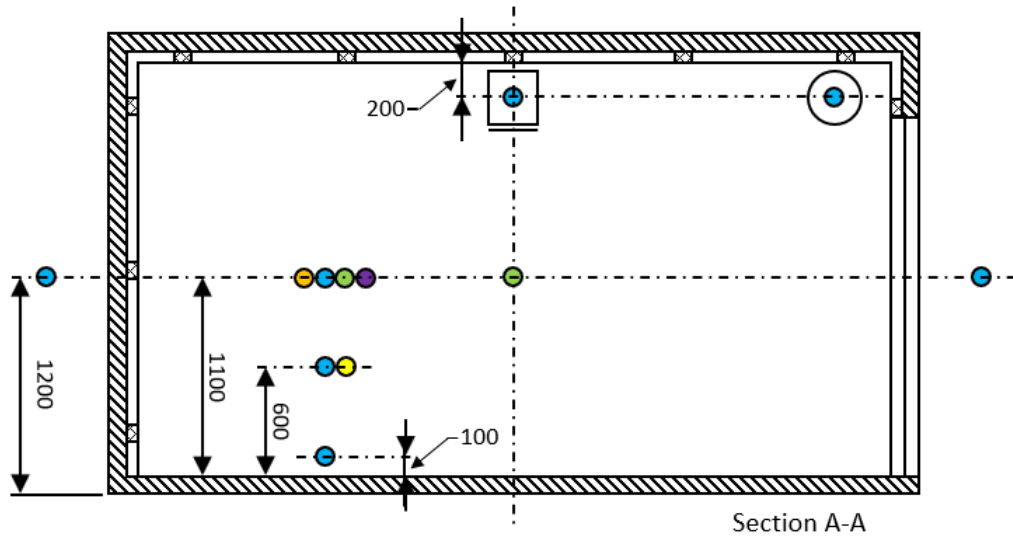
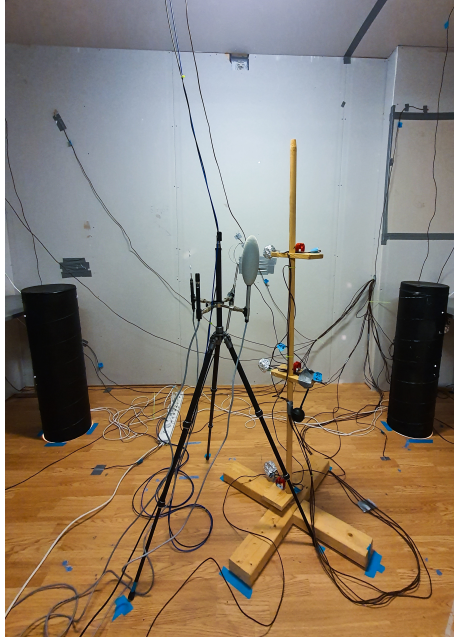
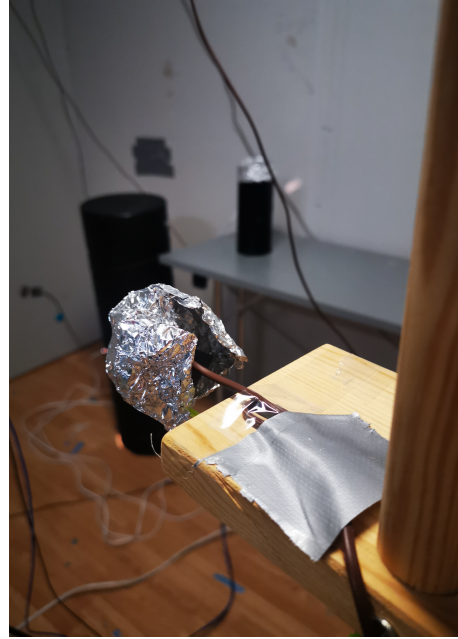


Figure A.2: Air based sensors in climate room experiment. Section view.

Figure A.3a show the measuring jig, where figure A.3b show that the thermocouples for air temperatures were placed inside bowls of aluminum foil to shield against thermal radiation. Figure A.3c show a thermocouple placed inside a ventilation duct, where it was strived to maintain its position away from the duct walls. Figure A.3d show that the air velocity meters were placed at a 3.5cm distance from the wall surface.



(a) Measurement jig.



(b) Radiative shield.



(c) Supply air temperature.



(d) Air velocity at wall surface.

Figure A.3: Details of measurements.

Surface temperatures

Five thermocouples were placed in a symmetric grid on each surface, having one measuring point in the center. The measuring points in the corners are drawn 50cm in from the edges. All surfaces follow the pattern shown in figure A.4, except for the floor and the south wall. At the floor, the corner points were drawn 90cm in from the edges to not be placed too close to the heat loads.

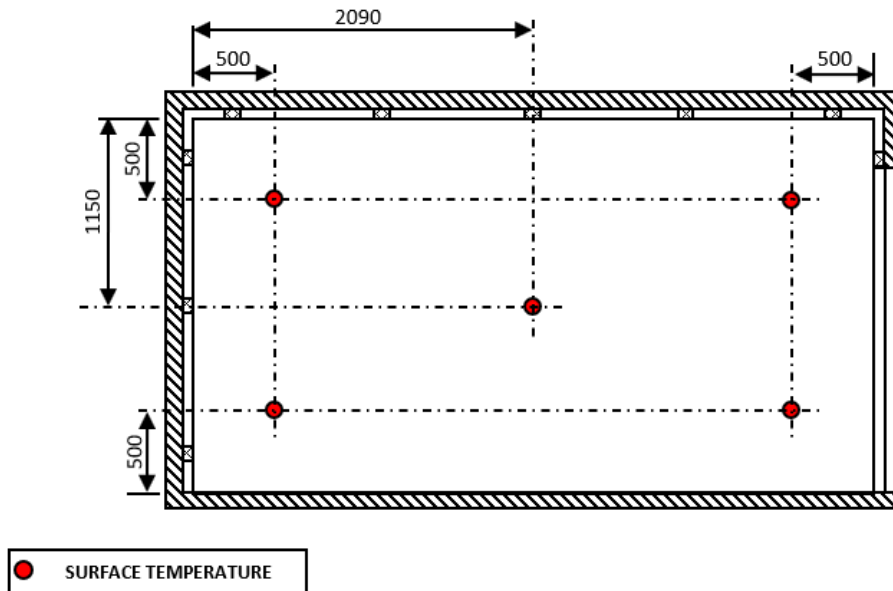


Figure A.4: Surface temperatures for west wall. Section view.

The southern wall had a different layout altogether due to the door and the heat foil, as shown in figure A.5. One thermocouple was placed centrally on the heating foil.

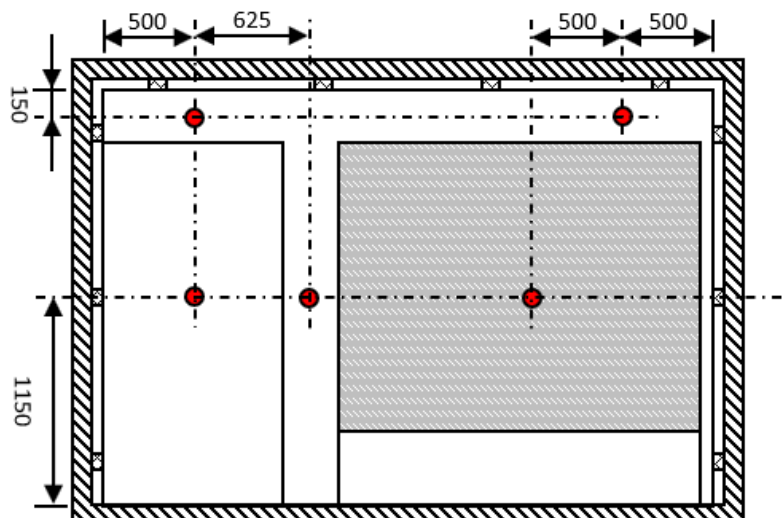


Figure A.5: Surface temperatures for south wall. Section view.

The thermocouples were attached to the surfaces like shown in figure A.6. The wires were pressed against the surface.

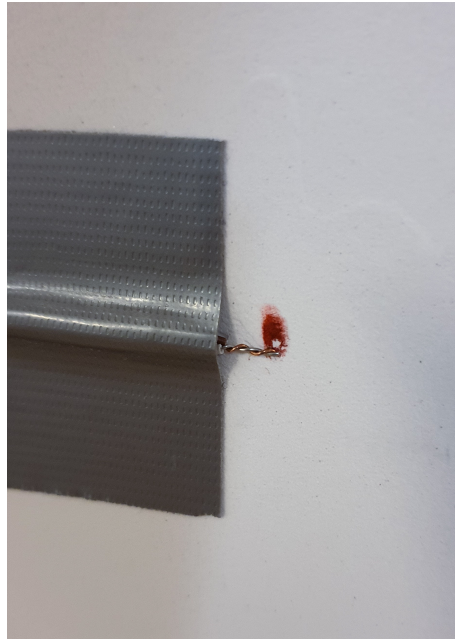


Figure A.6: Thermocouple placing for surface measurements.

Sensor placements and details: guarded hot box experiment

Specimen

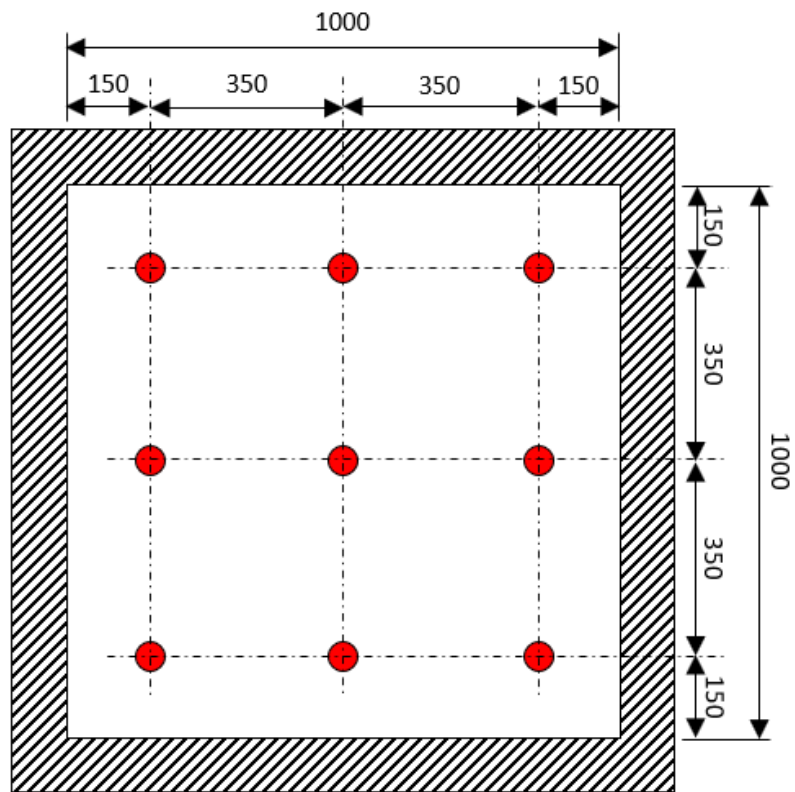


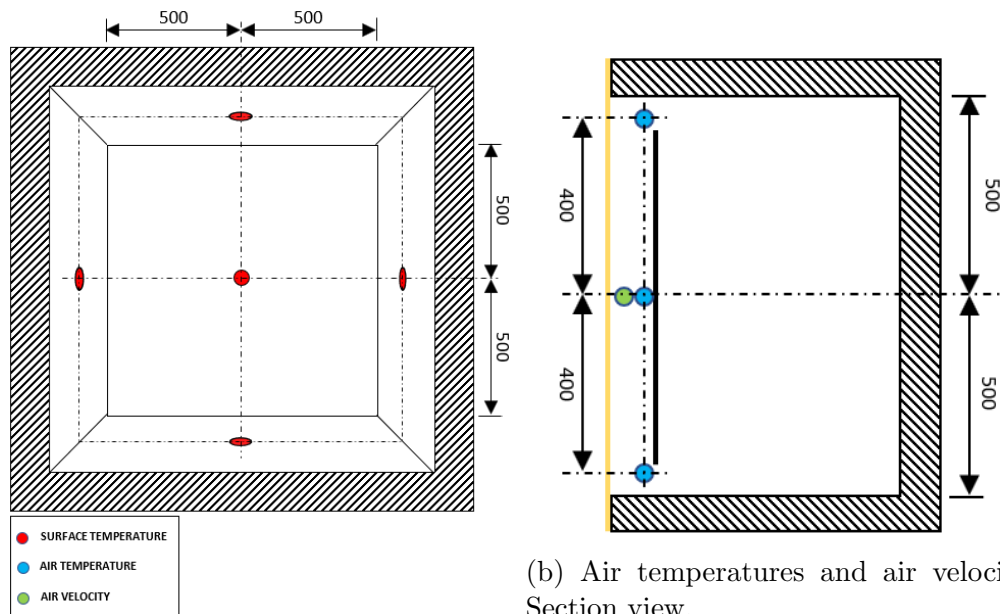
Figure A.7: Placement of thermocouples on the specimen surface. Section view.

Metering box

Surface and air temperatures were logged in the metering box, as well as air velocity across the specimen surface. Figure A.8a show that each surface of the metering box had a centrally placed measuring point. Similarly, the outside surface of the box had an identical setup of measuring points. The purpose of this was to calculate the heat loss by conduction through the meter box in case it was needed.

Figure A.8b show how the air stream across the specimen surface was measured. The purpose of these measurements was to calculate heat transfer by convection if needed. The air temperature was measured at three levels, the inlet, center, and outlet of the air stream, at the specimen side of the guard plate. The air velocity was measured at center position of the specimen surface. The air temperatures measuring points were placed centrally in the north - south direction, but at different heights from top to bottom.

The anemometer was placed approximately 3.5cm from the specimen surface, while the thermocouples in the air stream were placed approximately 5cm from the surface.



(a) Surface temperatures. Section view.

(b) Air temperatures and air velocity. Section view.

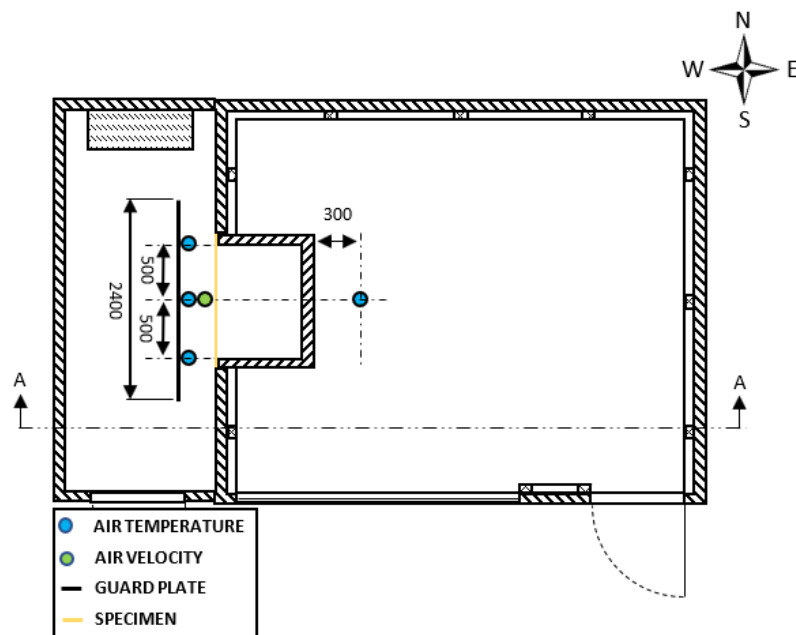
Figure A.8: Sensor placements in the metering box.

Cold box and guard box

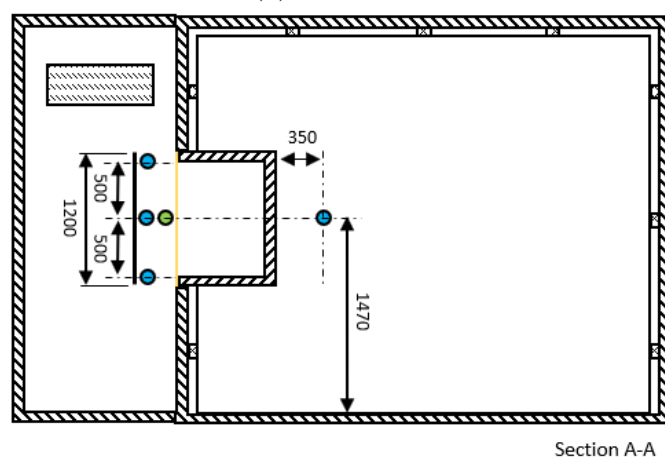
Air temperatures at different positions were measured in the cold box and the guard box room as shown in figure A.9.

In the cold box, five measuring points were used for air temperatures between the guard plate and the specimen. The measuring points forms a square cross with its center aligned with the center of the specimen. Air velocity was measured centrally on the surface of the specimen. The purpose of these points were to calculate the convective heat transfer between the specimen and the cold room if needed.

In the guard box, only one measurement point of the air temperature was in place, placed centrally 30cm from the metering box. The purpose of this measurement was to monitor the room temperature during the experiments.



(a) Plan view.




(b) Section view.

Figure A.9: Measurement points in the cold box and guard box rooms.

Appendix B

Simulations

| | | | |
|---|-----------------------------|--------------------------|---------------------------------------|
|  | | Input data Report | |
| Project | | Building | |
| Customer | | Model floor area | 636.0 m ² |
| Created by | Andreas Aamodt | Model volume | 1084.4 m ³ |
| Location | Blindern-Oslo | Model ground area | 0.0 m ² |
| Climate file | NOR_Oslo_Blindern_1992-2014 | Model envelope area | 558.7 m ² |
| Case | cubicles run3 BASE CASE | Window/Envelope | 12.6 % |
| Simulated | 02.06.2020 22:55:12 | Average U-value | 0.4103 W/(m ² K) |
| | | Envelope area per Volume | 0.5153 m ² /m ³ |

Wind driven infiltration airflow rate 451.429 l/s at 50,000 Pa

| Building envelope | Area [m ²] | U [W/(m ² K)] | U*A [W/K] | % of total |
|---|------------------------|--------------------------|---------------|---------------|
| Walls above ground | 170.62 | 0.22 | 37.54 | 16.38 |
| Rendered l/w concrete wall 250 | 53.91 | 0.22 | 11.86 | 5.17 |
| Rendered l/w concrete wall 250 PCM | 116.71 | 0.22 | 25.68 | 11.20 |
| Walls below ground | 0.00 | 0.00 | 0.00 | 0.00 |
| Roof | 318.00 | 0.18 | 57.24 | 24.97 |
| Concrete joist roof | 318.00 | 0.18 | 57.24 | 24.97 |
| Floor towards ground | 0.00 | 0.00 | 0.00 | 0.00 |
| Floor towards amb. air | 0.00 | 0.00 | 0.00 | 0.00 |
| Windows | 70.13 | 1.20 | 84.17 | 36.72 |
| Triple with suspended low-e film (argon) (WIN7) | 70.13 | 1.20 | 84.17 | 36.72 |
| Doors | 0.00 | 0.00 | 0.00 | 0.00 |
| Thermal bridges | | | 50.29 | 21.94 |
| Total | 558.75 | 0.41 | 229.24 | 100.00 |

| Thermal bridges | Area or Length | Avg. Heat conductivity | Total [W/K] |
|--|-----------------------|----------------------------|-------------|
| External wall / internal slab | 211.80 m | 0.000 W/(m K) | 0.000 |
| External wall / internal wall | 131.02 m | 0.000 W/(m K) | 0.000 |
| External wall / external wall | 6.82 m | 0.000 W/(m K) | 0.000 |
| External windows perimeter | 178.72 m | 0.000 W/(m K) | 0.000 |
| External doors perimeter | 0.00 m | 0.000 W/(K m) | 0.000 |
| Roof / external walls | 70.60 m | 0.000 W/(m K) | 0.000 |
| External slab / external walls | 0.00 m | 0.000 W/(K m) | 0.000 |
| Balcony floor / external walls | 0.00 m | 0.000 W/(K m) | 0.000 |
| External slab / internal walls | 0.00 m | 0.000 W/(K m) | 0.000 |
| Roof / internal walls | 60.00 m | 0.000 W/(m K) | 0.000 |
| External walls, inner corner | 0.00 m | 0.000 W/(K m) | 0.000 |
| Roof / external walls, inner corner | 0.00 m | 0.000 W/(K m) | 0.000 |
| External slab / external walls, inner corner | 0.00 m | 0.000 W/(K m) | 0.000 |
| Total envelope (incl. roof and ground) | 558.75 m ² | 0.090 W/(m ² K) | 50.287 |
| Extra losses | - | - | -0.000 |
| Sum | - | - | 50.287 |

| Windows | Area [m ²] | U Glass [W/(m ² K)] | U Frame [W/(m ² K)] | U Total [W/(m ² K)] | U*A [W/K] | Shading factor g |
|---------|------------------------|--------------------------------|--------------------------------|--------------------------------|-----------|------------------|
| E | 5.04 | 1.13 | 1.86 | 1.20 | 6.05 | 0.53 |
| S | 60.05 | 1.13 | 1.86 | 1.20 | 72.08 | 0.53 |
| W | 5.04 | 1.13 | 1.86 | 1.20 | 6.05 | 0.53 |
| Total | 70.13 | 1.13 | 1.86 | 1.20 | 84.17 | 0.53 |

| Air handling unit | Pressure head supply/exhaust [Pa/Pa] | Fan efficiency supply/exhaust [-/-] | System SFP [kW/(m ³ /s)] | Heat exchanger temp. ratio/min exhaust temp. [-/°C] |
|-------------------|--------------------------------------|-------------------------------------|-------------------------------------|---|
| AHU | 900.00/600.00 | 0.60/0.60 | 1.50/1.00 | 0.90/1.00 |

| DHW use | L/per occupant and day | No. of persons | Total, [l/s] |
|---------|------------------------|----------------|--------------|
| | 0.000 | 24.000 | 0.000 |